Chapter 5

(Results and Discussion)

5.1 PART-I : SERIES-I

5.1.1 Chemistry

5.1.1.1 Synthesis of Series I (SD 1-17): Substituted 1,3,4-oxadiazole-2-thione linked benzylpiperazine derivatives

Synthesis of the designed compounds **SD1-17** was achieved by following a 3-4 steps protocol depicted in (The compounds **SD 1-17 were synthesized as per the reaction sequence presented in Scheme 1**Benzoic acids **(A1-17)** were used as the starting materials for the reaction and reacted with N-hydroxybenzotriazole (HOBT) in the presence of 1-ethyl-3-(3-dimethylaminopropyl)carbodiimide (EDC) in acetonitrile to produce the corresponding benzoic acid esters. These esters were then subsequently reacted *in situ* with hydrazine hydrate at ice-cold (0–5 °C) to room temperature conditions producing the corresponding benzohydrazide **(B1-17)**. The formation of intermediates (**B1-17)** was initially confirmed by FT-IR which showed the presence of two stretching bands of -NH at 3260-3135 and 3147-3078 cm^{-1} and a single stretching band of $-NH_2$ at 3426-33 cm^{-1}. The structure of the intermediates **(B1-17)** was also confirmed by ^1H NMR, which showed the presence of one –NH proton around 10-9 ppm and two $-NH_2$ protons at 5-4 ppm. The intermediates **(B1-17)** were further reacted with carbon disulfide (CS_2) under a basic environment (KOH) in DMF to get secondary intermediates (**C1-17)**. The FT-IR spectrum of which demonstrated the presence of the C=S stretching band at 1270-1220 cm^{-1}. The chemical structure of the intermediates was further validated by ^1H NMR spectroscopy which showed the presence of –SH proton at 12-11 ppm. The final compounds **SD1-17** were prepared using the Mannich reaction where secondary intermediates (**C1-17)** in hot ethanolic solution were reacted with formaldehyde (HCHO) and BP. The structure of the final compounds was confirmed by the FT-IR which showed the presence of C=S at 1270-1220 cm^{-1} and

methylene (–CH_2) group at 2950-2850 cm^{-1}. The secondary intermediates (**C1-17)** exist in -SH and –C=S tautomeric forms which finally convert into –C=S after losing an acidic proton from the 3–NH of the 1,3,4-oxadiazole-2-thiol ring. The ^{1}H NMR spectra of the compounds have also shown the presence of two -CH_2 protons between 5-3 ppm. The structure of the final compounds **(SD1-17)** was confirmed by the ^{13}C NMR spectra which have shown the presence of two carbon signals of methylene (-CH_2) around 70-60 ppm and two piperazine carbon signals at 60-50 ppm. The percentage purity of the final compounds was also estimated through the HPLC which showed purity > 95%. The HRMS spectra of the final compounds have also demonstrated the presence of the corresponding masses.

5.1.1.2 Characterization of the synthesized compounds (Series I SD 1-17)

5.1.1.2.1 3-((4-benzylpiperazin-1-yl)methyl)-5-(4-chlorophenyl)-1,3,4-oxadiazole-2(3H)-thione (SD-1)

Yellow solid, Yield 72%, mp 226–228 °C; TLC (EtOAc: Hexane, 80:20 v/v); R_f = 0.54. FT-IR (Alpha ATR, ν cm^{-1}): 3045 (Ar-CH), 2954 (CH methylene) 1280 (C=S), 1656 (C–N); ^{1}H NMR (500 MHz, $CDCl_3$) δ 7.97 – 7.93 (m, 2H), 7.60 – 7.50 (m, 3H), 7.26 (dd, *J* = 8.2, 5.6 Hz, 2H), 6.99 (dd, *J* = 12.1, 5.1 Hz, 2H), 5.11 (s, 2H), 3.47 (s, 2H), 2.91 (t, *J* = 4.6 Hz, 4H), 2.48 (s, 4H). ^{13}C NMR (126 MHz, $CDCl_3$) δ 178.28, 162.99, 161.05, 158.93, 133.68, 133.66, 132.38, 130.61, 130.55, 129.16, 126.52, 122.44, 115.10, 114.93, 70.33, 62.15, 52.83, 50.21; HRMS $[M + 1]^+$ Calculated 400.1125, Found 400.1139; HPLC purity: 96.55 %; Retention time: 3.8 min.

5.1.1.2.2 *3-((4-benzylpiperazin-1-yl)methyl)-5-(4-nitrophenyl)-1,3,4-oxadiazole-2(3H)-thione (SD-2)*

White solid, Yield 75%, mp 219–221 °C; TLC (EtOAc: Hexane, 80:20 v/v); R_f = 0.60. FT-IR (Alpha ATR, ν cm^{-1}): 3134 (Ar-CH), 2937 (CH methylene) 1218 (C=S), 1658

(C–N); ^{1}H NMR (500 MHz, DMSO-d_6) δ 8.56 (d, J = 7.06 Hz, 2H), 7.94-792 (t, J = 6.01 Hz, 2H), 7.91 – 7.61 (m, 5H), 5.11 (s, 2H), 5.09 (s, 2H), 3.12 (s, 4H), 2.99 (s, 4H). ^{13}C NMR (126 MHz, DMSO-d_6) δ 159.07, 138.37, 133.12, 131.74, 130.05, 129.63, 126.72, 126.68, 90.99, 71.96, 69.84, 45.46, 43.39; HRMS $[M + 1]^+$ Calculated 411.1365, Found 411.1352; HPLC purity: 97.32 %. Retention time: 3.6 min.

5.1.1.2.3 ***3-((4-benzylpiperazin-1-yl)methyl)-5-(4-(trifluoromethoxy)phenyl)-1,3,4-oxadiazole-2(3H)-thione (SD-3)***

Light yellow solid, Yield 71%, mp 224–226 °C; TLC (EtOAc: Hexane, 80:20 v/v); R_f = 0.61. FT-IR (Alpha ATR, ν cm^{-1}): 3066 (Ar-CH), 2941 (CH methylene) 1264 (C=S), 1639 (C–N); ^{1}H NMR (500 MHz, $CDCl_3$) δ 7.99 (d, J = 7.9 Hz, 2H), 7.60 – 7.53 (m, 2H), 7.40 (d, J = 7.5 Hz, 3H), 7.18 (dd, J = 7.9, 6.4 Hz, 2H), 5.11 (d, J = 1.7 Hz, 2H), 4.24 (s, 2H), 2.92 (s, 4H), 2.46 (s, 4H). ^{13}C NMR (126 MHz, $CDCl_3$) δ 178.38, 158.97, 142.57, 132.38, 129.19, 128.50, 127.89, 126.97, 126.58, 122.55, 76.15, 70.35, 51.77, 50.50; HRMS $[M + 1]^+$ Calculated 450.1337, Found 450.1316; HPLC purity: 96.77 %. Retention time: 3.2 min.

5.1.1.2.4 ***3-(4-((4-benzylpiperazin-1-yl)methyl)-5-thioxo-4,5-dihydro-1,3,4-oxadiazol-2-yl)benzonitrile (SD-4)***

White solid, Yield 76%, mp 220–222 °C; TLC (EtOAc: Hexane, 80:20 v/v); R_f = 0.58. FT-IR (Alpha ATR, ν cm^{-1}): 3086(Ar-CH), 2814 (CH methylene) 1288 (C=S), 1651 (C–N); ^{1}H NMR (500 MHz, DMSO-d_6) δ 8.28 (s, 1H), 8.18 (d, J = 7.9 Hz, 1H), 8.07 (d, J = 7.0 Hz, 1H), 7.83 – 7.75 (m, 1H), 7.42 – 7.20 (m, 5H),5.06 (s, 2H), 3.51 (s, 2H), 2.80 (s, 4H), 2.44 (s, 4H). ^{13}C NMR (126 MHz, DMSO-d_6) δ 131.18, 129.44, 128.65, 127.58, 118.23, 114.00, 113.07, 70.44, 62.20, 52.74, 49.71; HRMS $[M + 1]^+$ Calculated 391.1467, Found 391.2856; HPLC purity: 98.22 %. Retention time: 4.9 min.

5.1.1.2.5 3-((4-benzylpiperazin-1-yl)methyl)-5-(2-nitrophenyl)-1,3,4-oxadiazole-2(3H)-thione (SD-5)

Light yellow solid, Yield 72%, mp 221–223 °C; TLC (EtOAc: Hexane, 80:20 v/v); R_f = 0.55. FT-IR (Alpha ATR, ν cm^{-1}): 3078 (Ar-CH), 2954 (CH methylene) 1252 (C=S), 1643 (C–N); ^{1}H NMR (500 MHz, $CDCl_3$) δ 7.99 – 7.89 (m, 2H), 7.62 – 7.49 (m, 3H), 6.95 – 6.82 (m, 4H), 5.16 (s, 2H), 3.76 (d, *J* = 1.6 Hz, 2H), 3.10 (d, *J* = 4.3 Hz, 4H), 3.07 – 3.02 (m, 4H). ^{13}C NMR (126 MHz, $CDCl_3$) δ 178.32, 159.06, 154.11, 145.63, 132.43, 129.19, 126.56, 122.42, 118.65, 114.48, 70.30, 55.57, 50.87, 50.40; HRMS $[M + 1]^+$ Calculated 411.1365, Found 411.1338; HPLC purity: 96.85%. Retention time: 4.1 min.

5.1.1.2.6 ***3-((4-benzylpiperazin-1-yl)methyl)-5-phenyl-1,3,4-oxadiazole-2(3H)-thione (SD-6)***

White solid, Yield 78%, mp 218–220 °C; TLC (EtOAc: Hexane, 80:20 v/v); R_f = 0.60. FT-IR (Alpha ATR, ν cm^{-1}): 3051 (Ar-CH), 2811(CH methylene) 1231 (C=S), 1651 (C–N); ^{1}H NMR (500 MHz, $CDCl_3$) δ 7.95 (d, *J* = 7.4 Hz, 2H), 7.55 (ddd, *J* = 10.5 Hz, 3H), 7.33 – 7.23 (m, 5H), 5.11 (s, 2H), 3.52 (s, 2H), 2.92 (s, 4H), 2.51 (s, 4H). ^{13}C NMR (126 MHz, $CDCl_3$) δ 178.27, 158.94, 137.81, 132.38, 129.21, 129.17, 128.25, 127.14, 126.53, 122.43, 70.33, 63.00, 52.90, 50.19; HRMS $[M + 1]^+$ Calculated 366.1514, Found 366.3757; HPLC purity: 99.04 %. Retention time: 3.7 min.

5.1.1.2.7 ***3-((4-benzylpiperazin-1-yl)methyl)-5-(3-chlorophenyl)-1,3,4-oxadiazole-2(3H)-thione (SD-7)***

Orange solid, Yield 69%, mp 226–228 °C; TLC (EtOAc: Hexane, 80:20 v/v); R_f = 0.51. FT-IR (Alpha ATR, ν cm^{-1}): 3118 (Ar-CH), 2837 (CH methylene) 1268 (C=S), 1680 (C–N); ^{1}H NMR (500 MHz, DMSO-d_6) δ 8.26 (s, 1H), 7.88 (dt, *J* = 7.43, 2.6 Hz, 1H), 7.48 (dt, *J* = 7.4, 3.2 Hz, 1H), 7.42 (t, *J* = 7.4 Hz, 1H), 7.32-7.27 (m, 5H), 5.16 (s, 2H),

3.41 (s, 2H), 2.68 (s, 4H), 2.59 (s, 4H).^{13}C NMR (126 MHz, DMSO-d_6) δ 164.92, 161.36, 134.80, 133.86, 132.52, 132.33, 130.16, 129.41, 127.73, 126.68, 64.84, 61. 89, 50.91, 48.14; HRMS [M + 1]$^+$ Calculated 400.1125, Found 400.1102; HPLC purity: 96.33 %. Retention time: 3.6 min.

5.1.1.2.8 ***3-((4-benzylpiperazin-1-yl)methyl)-5-(4-(trifluoromethyl)phenyl)-1,3,4-oxadiazole-2(3H)-thione (SD-8)***

Light yellow solid, Yield 70%, mp 225–227 °C; TLC (EtOAc: Hexane, 80:20 v/v); R_f = 0.54. FT-IR (Alpha ATR, ν cm^{-1}): 3066 (Ar-CH), 2847 (CH methylene) 1259 (C=S), 1668 (C–N); ^{1}H NMR (500 MHz, DMSO) δ 7.91 (s, 2H), 7.55 – 7.53 (m, 5H), 7.48 (s, 2H), 5.57 (s, 2H), 5.19 (s, 2H), 2.80 (s, 4H), 2.39 (s, 4H). ^{13}C NMR (126 MHz, DMSO) δ 168.57, 152.24, 148.65, 131.34, 131.07, 129.25, 128.80, 127.36, 125.63, 116.20, 69.47, 62.48, 52.96, 50.35; HRMS [M + 1]$^+$ Calculated 434.1388, Found 434.1361; HPLC purity: 95.89 %. Retention time: 4.2 min.

5.1.1.2.9 ***3-((4-benzylpiperazin-1-yl)methyl)-5-(2,4-dichlorophenyl)-1,3,4-oxadiazole-2(3H)-thione (SD-9)***

White solid, Yield 72%, mp 227–229 °C; TLC (EtOAc: Hexane, 80:20 v/v); R_f = 0.61. FT-IR (Alpha ATR, ν cm^{-1}): 3109 (Ar-CH), 2856 (CH methylene) 1242 (C=S), 1649 (C–N); ^{1}H NMR (500 MHz, $CDCl_3$) δ 7.95 (dt, *J* = 3.9, 2.5 Hz, 2H), 7.85-7.49 (m, 3H), 7.21 – 7.10 (m, 3H), 5.11 (s, 2H), 3.47 (d, *J* = 5.1, 2H), 2.91 (s, 4H), 2.48 (s, Hz, 4H). ^{13}C NMR (126 MHz, $CDCl_3$) δ 176.65, 159.77, 154.10, 140.43, 140.05, 132.73, 132.53, 132.34, 129.25, 129.21, 126.52, 126.45, 122.12, 65.52, 61.01, 60.97, 58.66, 56.83; HRMS [M + 1]$^+$ Calculated 434.0735, Found 434.0752; HPLC purity: 96.86 %. Retention time: 3.7 min.

5.1.1.2.10 ***3-((4-benzylpiperazin-1-yl)methyl)-5-(4-hydroxyphenyl)-1,3,4-oxadiazole-2(3H)-thione (SD-10)***

Light yellow solid, Yield 58%, mp 214–216 °C; TLC (EtOAc: Hexane, 80:20 v/v); R_f = 0.42. FT-IR (Alpha ATR, ν cm^{-1}): 3098 (Ar-CH), 2953 (CH methylene) 1268 (C=S), 1644 (C–N); ^{1}H NMR (500 MHz, $CDCl_3$) δ 10.22 (s, 1H), 8.04 – 7.86 (m, 2H), 7.60 – 7.49 (m, 3H), 7.38 – 7.22 (m, 4H), 5.30 (s, 2H), 3.53 (s, 2H), 2.97 (s, 4H), 2.52 (s, 4H). ^{13}C NMR (126 MHz, $CDCl_3$) δ 163.71, 161.83, 148.24, 137.96, 130.98, 130.83, 130.56, 129.24, 128.83, 128.62, 128.22, 127.09, 121.14, 69.54, 63.12, 53.07, 50.51; HRMS [M + 1]$^+$ Calculated 382.1463, Found 382.1454; HPLC purity: 97.55 %. Retention time: 4.0 min.

5.1.1.2.11 ***5-(4-aminophenyl)-3-((4-benzylpiperazin-1-yl)methyl)-1,3,4-oxadiazole-2(3H)-thione (SD-11)***

White solid, Yield 60%, mp 220–222 °C; TLC (EtOAc: Hexane, 80:20 v/v); R_f = 0.44. FT-IR (Alpha ATR, ν cm^{-1}): 3129 (Ar-CH), 2864 (CH methylene) 1232 (C=S), 1661 (C–N); ^{1}H NMR (500 MHz, $CDCl_3$) δ 7.92 – 7.82 (m, 2H), 7.45 (dd, *J* = 9.2, 3.1 Hz, 3H), 7.29 (m, *J* = 7.0 Hz, 3H), 5.74 (s, 2H), 5.25 (s, 2H), 3.54 (s, 3H), 2.98 (s, 4H), 2.58 (s, 4H). ^{13}C NMR (126 MHz, $CDCl_3$) δ 164.57, 164.49, 156.73, 156.63, 148.72, 148.10, 129.68, 128.77, 128.73, 128.65, 128.59, 128.37, 127.48, 121.87, 121.80, 72.79, 69.24, 52.78, 50.00; HRMS [M + 1]$^+$ Calculated 381.1623, Found 381.1604; HPLC purity: 95.46 %. Retention time: 3.6 min.

5.1.1.2.12 3-((4-benzylpiperazin-1-yl)methyl)-5-(3-methoxyphenyl)-1,3,4-oxadiazole-2(3H)-thione (SD-12)

Light orange solid, Yield 76%, mp 228–230 °C; TLC (EtOAc: Hexane, 80:20 v/v); R_f = 0.62. FT-IR (Alpha ATR, ν cm^{-1}): 3018 (Ar-CH), 2926 (CH methylene) 1244 (C=S), 1660 (C–N); ^{1}H NMR (500 MHz, $CDCl_3$) δ 7.97 – 7.91 (m, 2H), 7.61 – 7.47 (m, 3H),

7.15 (dd, *J* = 7.9, 2.8 Hz, 4H), 5.11 (s, 2H), 3.48 (s, 2H), 2.91 (s, 4H), 2.50 (s, 4H), 2.34 (s, 3H). ^{13}C NMR (126 MHz, $CDCl_3$) δ 178.27, 158.91, 136.70, 134.77, 132.35, 129.16, 129.15, 128.91, 126.52, 122.46, 77.31, 77.05, 76.80, 70.35, 62.74, 52.87, 50.23, 21.08; HRMS $[M + 1]^+$ Calculated 396.1620, Found 396.1609; HPLC purity: 96.14 %, Retention time: 3.2 min.

5.1.1.2.13 3-((4-benzylpiperazin-1-yl)methyl)-5-(4-methoxyphenyl)-1,3,4-oxadiazole-2(3H)-thione (SD-13)

White solid, Yield 71%, mp 227–229 °C; TLC (EtOAc: Hexane, 80:20 v/v); R_f = 0.62. FT-IR (Alpha ATR, ν cm^{-1}): 3034 (Ar-CH), 2966 (CH methylene) 1288(C=S), 1669 (C–N); ^{1}H NMR (500 MHz, DMSO-d_6) δ 7.84 (dd, *J* = 8.8, 5.4 Hz, 2H), 7.30 – 7.22 (m, 5H), 7.24 – 7.14 (dd, *J* = 8.8, 6.1 Hz, 2H), 5.02 (s, 1H), 3.86 (d, *J* = 3.5 Hz, 3H), 3.47 (s, 2H), 2.78 (s, 4H), 2.40 (s, 4H). ^{13}C NMR (126 MHz, DMSO-d_6) δ 138.31, 131.98, 129.30, 129.12, 128.62, 127.44, 115.40, 70.21, 62.33, 61.80, 56.06, 52.81, 49.95; HRMS $[M + 1]^+$ Calculated 396.1620, Found 396.1631; HPLC purity: 96.67 %, Retention time: 3.8 min.

5.1.1.2.14 3-((4-benzylpiperazin-1-yl)methyl)-5-(4-chloro-3-nitrophenyl)-1,3,4-oxadiazole-2(3H)-thione (SD-14)

White solid, Yield 68%, mp 230–232 °C; TLC (EtOAc: Hexane, 80:20 v/v); R_f = 0.64. FT-IR (Alpha ATR, ν cm^{-1}): 3121 (Ar-CH), 2956 (CH methylene) 1238 (C=S), 1672 (C=N); ^{1}H NMR (500 MHz, $CDCl_3$) δ 8.16 (d, *J* = 36.7 Hz, 2H), 7.83 (s, 1H), 7.66 (s, 1H), 7.31 (d, *J* = 4.3 Hz, 4H), 5.11 (s, 2H), 3.63 (s, 2H), 2.96 (s, 4H), 2.61 (s, 4H). ^{13}C NMR (126 MHz, $CDCl_3$) δ 136.62, 135.23, 130.24, 129.83, 129.44, 129.13, 128.55, 128.40, 127.54, 70.47, 62.71, 52.64, 49.82; HRMS $[M + 1]^+$ Calculated 445.0675, Found 445.0986; HPLC purity: 97.12 %. Retention time: 4.1 min.

5.1.1.2.15 3-((4-benzylpiperazin-1-yl)methyl)-5-(2,4-dinitrophenyl)-1,3,4-oxadiazole-2(3H)-thione (SD-15)

Creamy white solid, Yield 75%, mp 227–229 °C; TLC (EtOAc: Hexane, 80:20 v/v); R_f = 0.60. FT-IR (Alpha ATR, ν cm^{-1}): 3094 (Ar-CH), 2967 (CH methylene) 1281 (C=S), 1682 (C=N); ^{1}H NMR (500 MHz, $CDCl_3$) δ 8.96 (s, 1H), 7.58 (s, 1H), 7.39 (s, 1H), 7.29 (d, *J* = 2.8 Hz, 3H), 7.27 – 7.22 (m, 2H), 5.36 (s, 2H), 3.50 (s, 2H), 2.94 (s, 4H), 2.52 (s, 4H). ^{13}C NMR (126 MHz, $CDCl_3$) δ 162.40, 153.51, 150.80, 143.08, 137.98, 135.23, 129.20, 128.21, 127.10, 69.42, 63.03, 52.94, 50.51; HRMS $[M + 1]^+$ Calculated 456.1216, Found 456.1227; HPLC purity: 96.84 %. Retention time: 3.4 min.

5.1.1.2.16 3-((4-benzylpiperazin-1-yl)methyl)-5-(2-bromophenyl)-1,3,4-oxadiazole-2(3H)-thione (SD-16)

Light yellow solid, Yield 70%, mp 226–228 °C; TLC (EtOAc: Hexane, 80:20 v/v); R_f = 0.62. FT-IR (Alpha ATR, ν cm^{-1}): 3065 (Ar-CH), 2938 (CH methylene) 1256 (C=S), 1640 (C=N); ^{1}H NMR (500 MHz, $CDCl_3$) δ 7.96 (dd, *J* = 8.1, 5.6 Hz, 2H), 7.52 – 7.48 (m, 2H), 7.31 (d, *J* = 4.4 Hz, 4H), 7.15 (s, 1H), 5.30 (s, 2H), 3.52 (s, 2H), 2.97 (s, 4H), 2.53 (s, 4H). ^{13}C NMR (126 MHz, $CDCl_3$) δ 164.73, 147.42, 139.24, 130.73, 129.30, 128.77, 128.51, 128.21, 127.10, 123.51, 69.54, 63.10, 53.06, 50.44; HRMS $[M + 1]^+$ Calculated 444.0619, Found 444.0624; HPLC purity: 95.54 %, Retention time: 3.7 min.

5.1.1.2.17 3-((4-benzylpiperazin-1-yl)methyl)-5-(2,4-dihydroxyphenyl)-1,3,4-oxadiazole-2(3H)-thione (SD-17)

Yellow solid, Yield 67 %, mp 219–221 °C; TLC (EtOAc: Hexane, 80:20 v/v); R_f = 0.48. FT-IR (Alpha ATR, ν cm^{-1}): 3126 (Ar-CH), 2927 (CH methylene) 1245 (C=S), 1650 (C=N); ^{1}H NMR (500 MHz, DMSO) δ 9.56 (s, 2H), 8.62 – 8.53 (t, *J* = 7.1 Hz, 1H), 8.09 – 8.08 (d, *J* = 5.6 Hz, 1H), 7.69 – 7.60 (m, 1H), 7.34-7.31 (d, *J* = 9.7 Hz, 5H), 5.05 (s, 2H), 3.67 (s, 2H), 2.84 (s, 4H), 2.58 (d, *J* = 4.52 Hz, 4H). ^{13}C NMR (126 MHz,

$CDCl_3$) δ 178.27, 158.91, 136.70, 134.77, 132.35, 129.16, 129.15, 128.91, 126.52, 122.46, 70.35, 62.74, 52.87, 50.23; HRMS $[M + 1]^+$ Calculated 398.1413, Found 398.1428; HPLC purity: 95.12 %, Retention time: 4.2 min.

5.1.2 Biological evaluation

5.1.2.1 Pharmacology (In vitro studies)

5.1.2.1.1 Cholinesterase (hAChE and hBChE) inhibition assay

The *in vitro* inhibitory potential of the compounds **(SD1-17)** was estimated using Ellman's colorimetric method. Most of the synthesized compounds have shown good to moderate while a few showed poor hAChE inhibitory activity. The representative compound of the series **SD-6** that contains an unsubstituted phenyl ring on 1.3.4-oxadiazole-2-thione showed good hAChE inhibitory (IC_{50} = 0.907 ± 0.011 μM) activity as compared to rest of the molecules of the series. As described in Table 5. 1, the compounds like **SD-1** (Cl), **SD-2** (-NO_2), **SD-3** (-OCF_3), **SD-8** (-CF_3), **SD-10** (–OH), and **SD-11** (-NH_2) containing an EWGs at the 4th position of the phenyl ring have shown moderate hAChE inhibitory activity. The introduction of EWG at the 3rd position of the phenyl ring as in compound **SD-4** (–C≡N) and **SD-7** (3-Cl) has shown good hAChE inhibition. Among them, the compound containing the 3–C≡N group showed better activity than the 3-Cl group compound. The introduction of di-substituted EWGs at the phenyl ring of the compounds like **SD-9** (2,4-di Cl), **SD-15** (2,4-di NO_2), **SD-17** (2,4-di OH), and substitution of EWG at 2nd position in compounds **SD-5** (2-NO_2), and **SD-16** (2-Br) have shown moderate to poor hAChE inhibitory activity. However, the 3, 4–di substituted EWG containing compound **SD-14** (4-Cl, 3-NO_2) and EDG at the 3rd and 4th positions of phenyl ring **SD-12** (3-OCH_3) and **SD-13** (4-OCH_3) have shown moderate hAChE inhibition. Peripheral BChE inhibition could also be a therapeutic strategy for halting AD progression [Muñoz-Ruiz et al. 2005]. The dual AChE and

BChE inhibition could be advantageous in AD as disease-modifying therapy rather than symptomatic relief [Greig et al. 2001]. To investigate the dual cholinesterase (ChE) inhibitory profile of the synthesized compounds, an *in vitro* hBChE inhibitory colorimetric assay method was performed. The *in vitro* hBChE assay results (Table 5. 1) showed that the compounds **SD-4** and **SD-6** were the representative hBChE inhibitors among the series. Two more compounds **SD-8** and **SD-14** of the series have also demonstrated good hBChE inhibitory potential while the other compounds of the series were less potent (IC_{50} >10 μM) against the enzyme. The *in vitro* hAChE and hBChE inhibitory potential of the compounds **(SD-1-17)** was measured and compared with the standard drugs donepezil (hAChE; IC_{50} = 0.054 ± 0.006 μM and hBChE; IC_{50} = 2.557 ± 0.038 μM) and rivastigmine (hAChE; IC_{50} = 1.701 ± 0.024 μM and hBChE, IC_{50} = 1.312 ± 0.013 μM).

The *in vitro* findings suggested that the unsubstituted phenyl ring at 1.3.4-oxadiazole-2-thione is more favorable for dual hAChE and hBChE inhibition, while substituted EWGs at the 4-position of the phenyl ring have shown moderate hAChE and poor hBChE inhibitory activity (>10 μM) as compared to the unsubstituted compound. The 3-substituted phenyl ring with EWGs may also be favorable for the hAChE and hBChE inhibitory activity. EDGs at the 3 and 4-position of the phenyl ring have resulted in diminished hAChE and hBChE activity. However, 3,4-di substituted compounds at the phenyl ring have shown better hAChE and hBChE activity than the 2,4-di substituted compounds (Table 5. 1).

Table 5. 1 *In vitro* ChE, and hBACE-1 inhibitory activity of the synthesized compounds

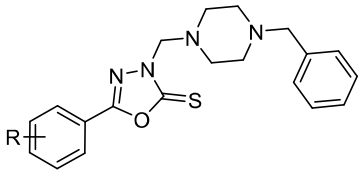

(SD1-17)

Compound Code	R	IC_{50} ±SEM (µM)[a]			Selectivity Index[b] hBChE/hAChE
		hAChE	hBChE	hBACE-1	
SD-1	4-Cl	1.255 ± 0.019	>10	0.943 ± 0.018	nd
SD-2	4-NO_2	1.107 ± 0.008	>10	0.811 ± 0.023	nd
SD-3	4-OCF_3	1.335 ± 0.012	>10	1.113 ± 0.016	nd
SD-4	3-CN	1.077 ± 0.009	1.653 ± 0.019	0.651 ± 0.014	1.534
SD-5	2- NO_2	1.885 ± 0.031	>10	1.172 ± 0.021	nd
SD-6	H	0.907 ± 0.011	1.579 ± 0.037	0.753 ± 0.018	1.703
SD-7	3-Cl	1.424 ± 0.022	>10	0.885 ± 0.013	nd
SD-8	4-CF_3	1.316 ± 0.018	2.416 ± 0.041	0.701 ± 0.019	1.835
SD-9	2, 4-di Cl	2.115 ± 0.037	>10	1.414 ± 0.031	nd
SD-10	4-OH	1.224 ± 0.013	>10	>5	nd
SD-11	4-NH_2	1.218 ± 0.027	>10	>5	nd
SD-12	3-OCH_3	1.937 ± 0.024	>10	1.214± 0.016	nd
SD-13	4-OCH_3	1.531 ± 0.028	>10	1.358 ± 0.012	nd
SD-14	4-Cl, 3-NO_2	1.136 ± 0.018	1.943 ± 0.033	0.806 ± 0.011	1.710
SD-15	2,4-diNO_2	1.419 ± 0.023	>10	1.447 ± 0.022	nd
SD-16	2-Br	2.408 ± 0.027	>10	1.801 ± 0.029	nd
SD-17	2,4-di OH	1.792 ± 0.015	>10	2.154 ± 0.034	nd

Donepezil	--	0.054 ± 0.006	2.557 ± 0.038	1.413 ± 0.017	47.351
Rivastigmine	--	1.701 ± 0.024	1.312 ± 0.013	nd	0.771

nd = The *in vitro* activity or selectivity of the compounds not performed.
[a] The *in vitro* activity of the compounds is represented as IC_{50} ± SEM of three individual experiments (n = 3);
[b] Selectivity index for hAChE = IC_{50} of hBChE/IC_{50} of hAChE;
hAChE inhibition- good (≤ 1.0 µM), moderate (between 1.0-2.0 µM), and poor (> 2.0 µM)
hBChE inhibition:- good (≤ 1.5.0 µM), moderate (between 1.5 2.5 µM), and poor (> 3 µM)
hBACE-1 inhibition:- good (1.5.0 µM), moderate (between 1.5-2.5 µM), and poor (>2.5 µM)

5.1.2.1.2 hAChE Enzyme kinetics

The enzyme kinetics study of the most active compound **SD-6** against hAChE was performed to examine the type of inhibition. Three different concentrations of compound **SD-6** were tested against six different concentrations of the substrates (Acetylthiocholine iodide (ATCI)) along with a fixed enzyme concentration. The Lineweaver-Burk double reciprocal plot was used to calculate the type of inhibition by plotting increasing substrate concentration on the *x-axis* and their respective reaction velocities on the *y-axis*.

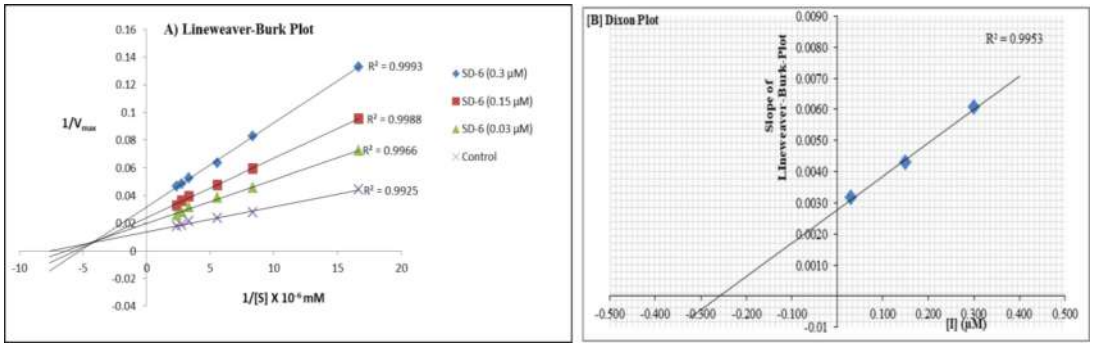

Figure 5. 1 Enzyme kinetics results of compound **SD-6** against hAChE; A) Lineweaver-Burk Plot showing mixed type non-competitive inhibition; B) Dixon plot showing Ki on intersecting point of the negative *x*-axis.

The Lineweaver-Burk plot for compound **SD-6** against hAChE showed a mixed-type non-competitive inhibition profile (Figure 5. 1A). However, the Lineweaver-Burk plot has also demonstrated increased K_m (Michaelis constant) at increased inhibitory

concentrations. The dissociation-constant K_i was also determined for compound **SD-6** using the Dixon plot (Figure 5. 1 B), which was constructed by plotting inhibitors concentration on the *x*-axis and the slope of the Lineweaver-Burk plot on the *y*-axis. The dissociation-constant K_i was calculated as the value of an intersecting point on the negative *x*-axis, which was found to be 0.26. The final experimental value was determined as an average of three individual experiments (n=3).

5.1.2.1.3 hBACE-1 inhibition assay

The increased Aβ aggregation or its reduced clearance result in senile plaque formation that leads to AD development and its progression [Verma et al. 2021]. Inhibition of BACE-1 controls the formation of APPβ subunits and reduces the Aβ aggregation through the amyloidogenic pathway [Cole and Vassar 2007, Rajmohan and Reddy 2017]. An hBACE-1 inhibition analysis was performed using a FRET-based assay to determine the multifunctional inhibition potential of the synthesized derivatives which have shown a good to moderate inhibition profile. Compounds **SD-1**, **SD-2**, **SD-4**, **SD-6**, **SD-7**, **SD-8,** and **SD-14** have shown (Table 5. 1) good hBACE-1 inhibitory activity (three-digit nanomolar range) amongst which compound **SD-4** (IC_{50} = 0.753 ± 0.018) has shown promising hBACE-1 inhibition which was better than the donepezil (IC_{50} = 1.413 ± 0.017 μM). The compounds **SD-3, SD-5, SD-9, SD-12, SD-13, SD-15, SD-16,** and **SD-17** have exhibited moderate hBACE-1 inhibition (Table 5. 1) while, the other compounds of the series **SD-10** and **SD-11** have exhibited diminished BACE-1 inhibitory profile (IC_{50} > 5 μM) (Table 5. 1). The overall structure-activity relationship (SAR) of the compounds **(SD1-17)** against hAChE, hBChE and hBACE-1 has been represented in (Figure 5. 2).

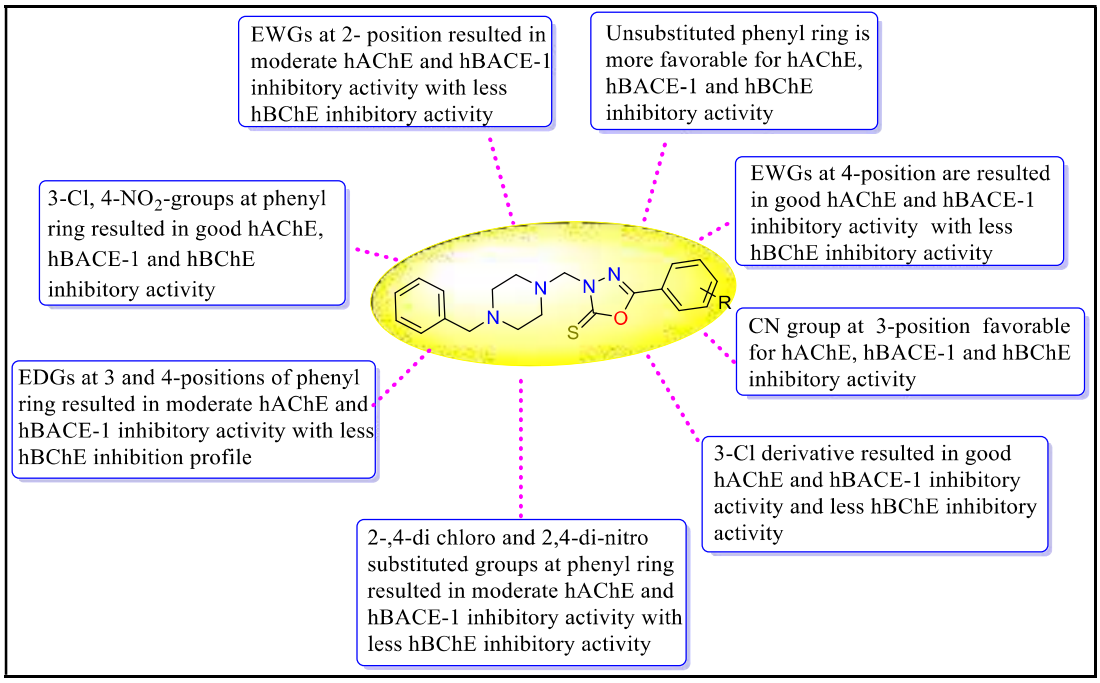

Figure 5. 2 SAR of the compounds **SD1-17**

5.1.2.1.4 Propidium iodide displacement assay

Propidium iodide (PI) assay is a well-established protocol to estimate the binding of a chemical scaffold to the AChE-PAS site. PI has a high affinity towards the AChE-PAS binding site, and it shows up to 10 fold increase in the fluorescence activity upon interaction with the active site [Silva et al. 2013a]. The enzyme kinetics study of the compound **SD-6** has shown a mixed-type non-competitive inhibitory profile which suggested that the compound was interacting with the CAS as well as with the PAS site of the enzyme. To affirm the binding of the compounds in the AChE-PAS region the PI displacement assay was performed. The four compounds (10 µM and 50 µM concentrations) were selected for the PI displacement assay owing to their good dual AChE and BChE inhibitory activity. The PI assay results demonstrated that both compounds **SD-4** (10 µM: 24.6 % and 50 µM: 55.1 %) and **SD-6** (10 µM: 27.3 % and 50 µM: 56.2 %) have significantly displaced the PI as compared to the standard donepezil (10 µM: 23 % and 50 µM: 37.1 %). While compounds **SD-08** (10 µM: 21.4

% and 50 μM: 41.7 %) and **SD-14** (10 μM: 19.7 % and 50 μM: 36.8 %) have comparable PI displacement properties to that of the donepezil (Table 5. 2).

Table 5. 2 PI displacement assay and PAMPA-BBB permeability assay results of the compounds.

Compound	(%) PAS-AChE Propidium Iodide displacement		Prediction of BBB permeability PAMPA-BBB assay results	
			$Pe_{(exp)}$	
	[I] = 10 μM	**[I] = 50 μM**	(4.8×10^{-6} cm s^{-1})	Prediction
SD-4	24.661 ± 1.421	55.157± 1.247	6.127 ± 0.019	CNS+[b]
SD-6	27.316 ± 1.208	56.238 ± 1.338	5.643 ± 0.021	CNS+[b]
SD-8	21.446 ± 1.147	41.709± 1.271	5.019 ± 0.033	CNS+[b]
SD-14	19.773 ± 1.216	36.841 ± 1.069	4.858 ± 0.016	CNS+[b]
donepezil	23.041 ± 1.019	37.193± 1.422	5.264 ± 0.022	CNS+[b]

[a]Displacement of PI from AChE-PAS region at 10 μM and 50 μM concentrations. [b]" CNS+ compounds with value Pe > 4.8×10^{-6} cm s^{-1} showing excellent BBB permeability". The results of three individual experiments (n = 3) are represented as mean ± SEM.

5.1.2.1.5 PAMPA-BBB assay

The blood-brain barrier (BBB) is a dynamic interface membrane that allows only selective biomolecules, chemicals, and ions meanwhile it also restricts the entry of toxic chemicals and pathogens into neuronal compartments [Pulicherla and Verma 2015]. The prime requisite for any of the drug molecules to treat brain disorders is to be able to be partitioned across the BBB. To examine the capability of the compounds under investigation to cross BBB, an *in vitro* PAMPA-BBB assay was performed as per the reported method [Di et al. 2003]. The experimental protocol was validated with 7 commercially available drugs with reported BBB permeability as a positive and negative control. A linear correlation graph was plotted between the BBB permeability values obtained for the 7 commercially available drugs, and the limit of permeability

was defined based on the linear correlation values. The $P_{e(exp)} > 4.8 \times 10^{-6}$ cm.s^{-1} was selected as the significant value to cross BBB while the $P_{e(exp)} < 4.8\text{-}1.5 \times 10^{-6}$ cm.s^{-1} was decided as uncertain BBB properties based on the experiments with the positive and negative controls. The PAMPA-BBB assay result demonstrated that all the compounds **SD-4** (6.127×10^{-6} cm.s^{-1}), **SD-6** (5.643×10^{-6} cm.s^{-1}), **SD-8** (5.019×10^{-6} cm.s^{-1}), and **SD-14** (4.848×10^{-6} cm.s^{-1}) were had excellent BBB permeability (Table 5. 2). Based on the results of PI displacement and PAMPA-BBB assay compounds, **SD-4** and **SD-06** can further be evaluated as potential leads for other pharmacological investigations.

5.1.2.1.6 Neurotoxicity estimation on RA/BDNF differentiated SH-SY5Y cell lines

To investigate the neurotoxic liabilities of the compounds **SD-4** and **SD-6** against the neuronal cells, an MTT-based neurotoxicity assay was performed on retinoic acid (RA) and brain-derived neurotrophic factor (BDNF)-induced differentiated SH-SY5Y cell lines. The SH-SY5Y cells upon treatment with RA, exhibited neuron-like properties, i.e., enlarged neurite structures and increased axon span as compared to the normal cells, and have also shown neurite connections with neighboring cells [Lingappa et al. 2021]. Both compounds **SD-4** and **SD-6** were tested in 10, 20, 40, and 80 μM concentrations and compared with the donepezil at the same concentrations (Figure 5. 3). The MTT assay results suggested that at a maximal concentration range of 80 μM; there was no noticeable decrease in the differentiated neuroblastoma cells population as compared to donepezil ($p < 0.01$). All the selected concentrations of both compounds have also shown neither a change in the shape (neuron-like properties) nor in the neuritic connections (Figure 5. 4) of the cells. Therefore, it can be stated that both of the compounds **SD-4** and **SD-6** under investigation are non-neurotoxic and can be used further for preclinical research.

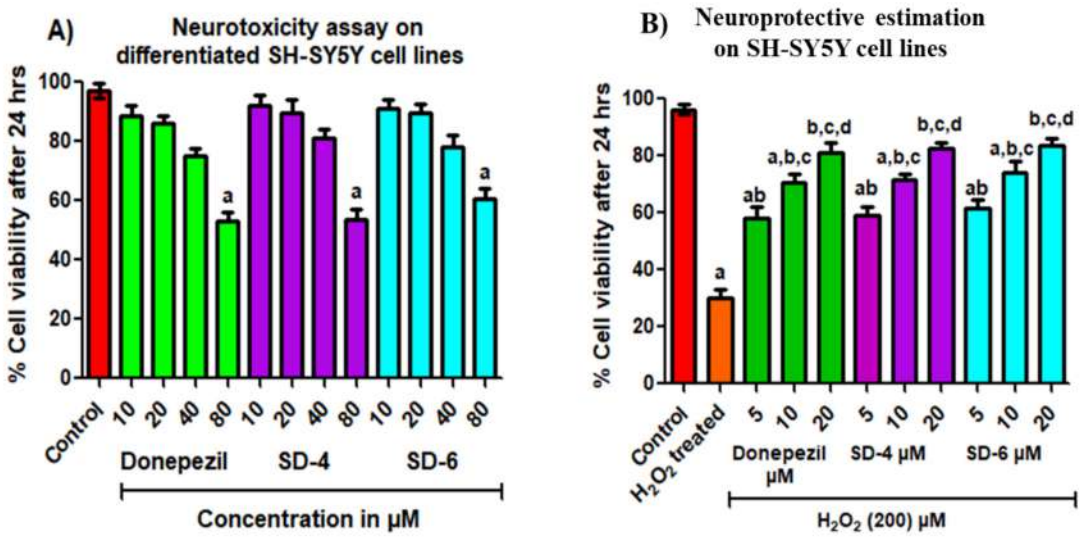

Figure 5. 3 Neurotoxicity and neuroprotective estimation of compounds **SD-4** and **SD-6;** A) Cytotoxicity estimation of compounds **SD-4** and **SD-6** along with donepezil on differentiated SH-SY5Y cell lines B) Neuroprotective estimation of **SD-4**, **SD-6,** and donepezil on non-differentiated SH-SY5Y cell lines in presence of H_2O_2 (200 µM). (^{a} $p < 0.01$) compared to the control. (^{a,b} $p < 0.05$) (^{a,b,c} $p < 0.01$) (^{b,c,d} $p < 0.001$) compared to H_2O_2 treated.

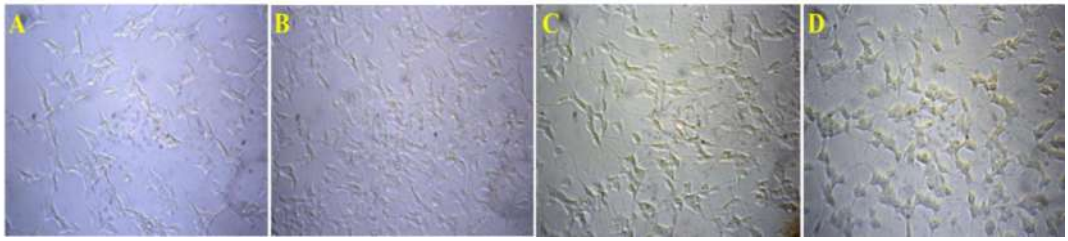

Figure 5. 4 Morphological estimation of neurotoxicity profile of the compounds **SD-4** and **SD-6** in RA/BDNF differentiated SH-SY5Y cells A) Differentiated SH-SY5Y cells alone; B) Cell morphology after incubation with compound **SD-4** (40 µM) for 24 h; C) Cell morphology after incubation with compound **SD-6** (40 µM) for 24 h; cell morphology after incubation with donepezil (40 µM) for 24 h. The images were captured through phase contrast microscopy.

5.1.2.1.7 Neuroprotective estimation on SH-SY5Y cell lines

The neuroprotective activity of the compounds **SD-4** and **SD-6** was estimated on the SH-SY5Y cell lines. Initially, the cells were treated with the different concentrations of both compounds (5, 10, and 20 µM) for 2 h and H_2O_2 (200 µM) was then added to the

cells and incubated further for 24 h. The results suggested that the cell viability was increased in a dose-dependent manner for both the compounds while the cell viability was significantly decreased to 30.02 % in untreated (H_2O_2 treated) cells. Compound **SD-4** has shown cell viability of 59.1 % ($p < 0.01$) at 5 µM, 71.62 % ($p < 0.001$) for 10 µM, and 82.47 % ($p < 0.001$) for 20 µM concentrations. Similarly, compound **SD-6** has also exhibited cell viability of 61.40 % ($p < 0.01$) at 5 µM, 73.95 % ($p < 0.001$) for 10 µM, and 83.57 % ($p < 0.001$) for 20 µM concentrations. The results of cell viability data of both compounds were compared with the standard donepezil 57.92% ($p < 0.01$) at 5 µM, 70.82% ($p < 0.001$) for 10 µM and 81.29 % ($p < 0.001$) for 20 µM concentrations, which suggested that both the compounds are equally neuroprotective as donepezil. The Cell morphology was also estimated with and without treatment which has shown that both compounds have inhibited cell death as compared to cells treated with H_2O_2 (Figure 5. 5).

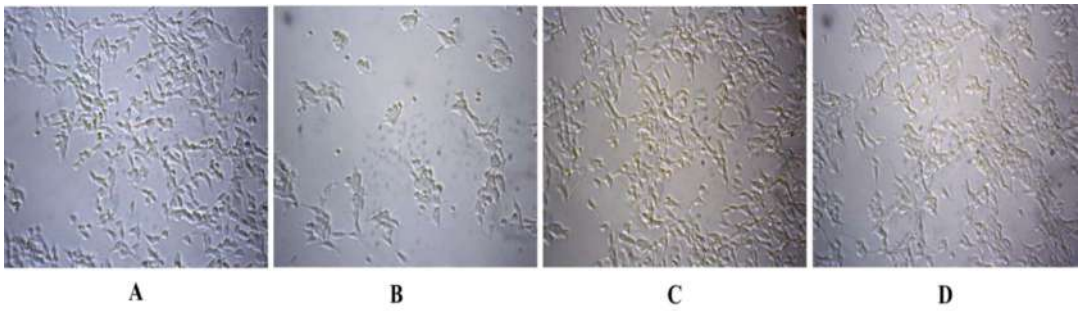

Figure 5. 5 Cell morphology estimation of neuroprotective activity of compounds **SD-4** and **SD-6** on non-differentiated SH-SY5Y cells upon co-treatment with H_2O_2 A) Cells without treatment; B) cells upon H_2O_2 treatment only; C) Cells treated with **SD-4** (20 µM) in the presence of H_2O_2 (200 µM); D) Cells treated with **SD-6** (20 µM) in the presence of H_2O_2 (200 µM). The images were captured through Phase contrast microscopy.

5.1.2.1.8 Aβ-aggregation inhibition (self and AChE-induced) Thioflavin T assay

The findings of *in vitro* hAChE inhibition and PI assay indicated that both these compounds could be promising candidates for reducing the Aβ overexpression through

an amyloidogenic pathway. A self and hAChE-induced Aβ experiments were performed using thioflavin-T and the anti-Aβ aggregation potential of compounds **SD-4** and **SD-6** were determined**.** Three different concentrations (5, 10, and 20 μM) of both compounds were tested against a fixed Aβ concentration (10 μM), and the results are expressed as % Aβ aggregation inhibition and as normalized fluorescence intensity (NFI). ThT experiment has shown that upon incubation of compounds **SD-4** and **SD-6** at a 20 μM:10 μM ratio (compound: Aβ) has resulted in reduced fluorescence intensity indicating anti-Aβ aggregation potential of the compounds.

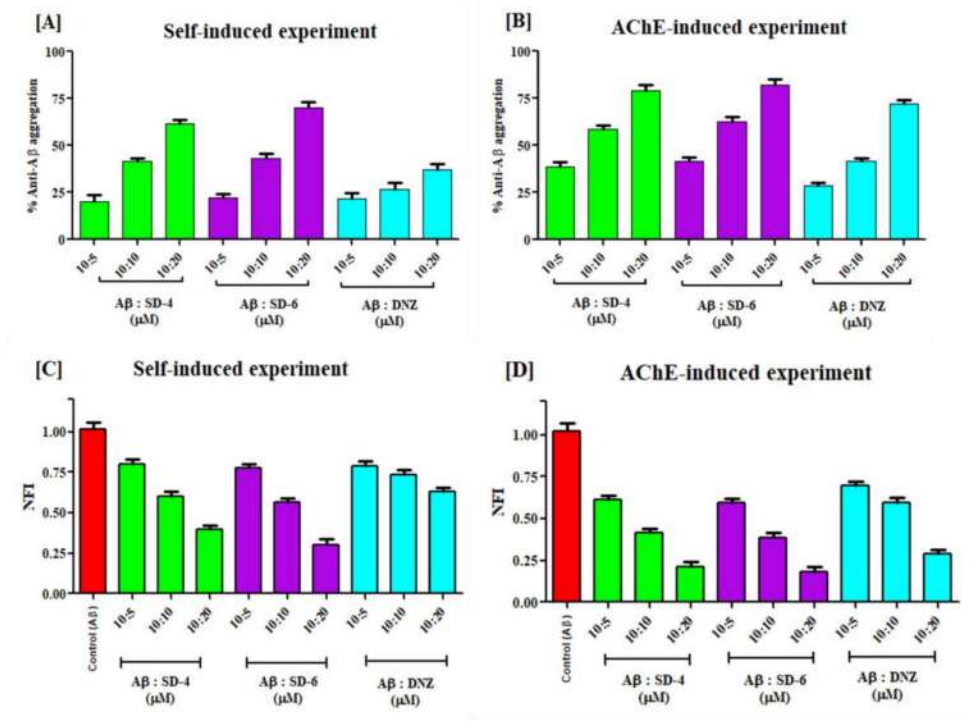

Figure 5. 6 Anti-Aβ aggregation experiments of compounds **SD-4** and **SD-6**: A) Self-induced % anti-Aβ aggregation: B) AChE-induced % anti-Aβ aggregation: C) Self-induced anti-Aβ aggregation reduced NFI: D) AChE-induced anti-Aβ aggregation reduced NFI.

The self and AChE-induced experiments have shown that the anti-Aβ aggregation potential of both the compounds **SD-4** and **SD-6** was increased at increasing compound concentrations. Compound **SD-4** (self-induced: 20-61 %, hAChE-induced 38-79 %) and **SD-6** (self-induced: 22-69 %, hAChE-induced 41-81 %) have shown slightly higher

anti-Aβ aggregation potential as compared to donepezil (self-induced: 21-37 %, hAChE-induced 28-72 %) Figure 5. 6 A & B). The normalized fluorescence intensity was also calculated for both self and AChE-induced anti-Aβ aggregation experiments and has shown decreased NFI at increasing compound concentrations (Figure 5. 6 C & D) which was better than donepezil at similar concentrations as compared to control (Aβ). Based on our *in vitro* findings compound **SD-6** was chosen further for *in vivo* investigation.

5.1.2.2 In vivo behavioral studies and ex vivo studies

5.1.2.2.1 Acute toxicity studies

Compound **SD-6** was given to healthy non-pregnant female Wistar rats (220-280 gm) aged 10-11 weeks to examine the safety profile of the compound. The compound was administered orally following OECD guidelines 423 to the overnight fasted animals in the graduated dose of 100-500 mg/kg, p.o., and was observed for up to 14 days for any abnormal or toxic reactions [Sharma et al. 2019a, Wang et al. 2015]. The results of the acute toxicity study suggested a slight weight loss (12-25 %) initially in some animals but regained in 10-12 days in a total 14-day period. Subsequently, the blood samples of the experimental animals were collected and subjected to hepatic and renal function tests which indicated all the associated parameters were within the range (Table 5. 3). After 14 days, the animals were sacrificed and their internal organs such as the kidney, liver, lungs, and heart were examined for any tissue or organ toxicity after H & E staining. The kidney slices have shown normal Distal Convoluted tubules (DCT) Proximal convoluted Tubules (PCT) and Glomerulus, the liver tissue slices have shown normal Kuepfer cells and central vein while the lung and heart slices have shown normal tissue appearance (Figure 5. 7 A-D). The acute toxicity study exhibited that the compound **SD-6** was safe and well tolerated by the animals at given doses.

Table 5. 3 Liver and Kidney function tests of the experimental animals under acute toxicity studies

Parameters	Control (±SD)	100mg//kg (±SD)	300mg/kg (±SD)	500mg/kg (±SD)
AST (U/L)	126±13.4	123±13.4	120±13.4	124±13.4
ALT (U/L)	45±3.4	40±4.4	43±3.2	41±3.3
ALP (KA/dL)	12±1.2	11±1.02	12.6±1.07	13±1.02
Creatinine (mg/dL)	0.62±0.03	0.60±0.04	0.63±0.05	0.62±0.07

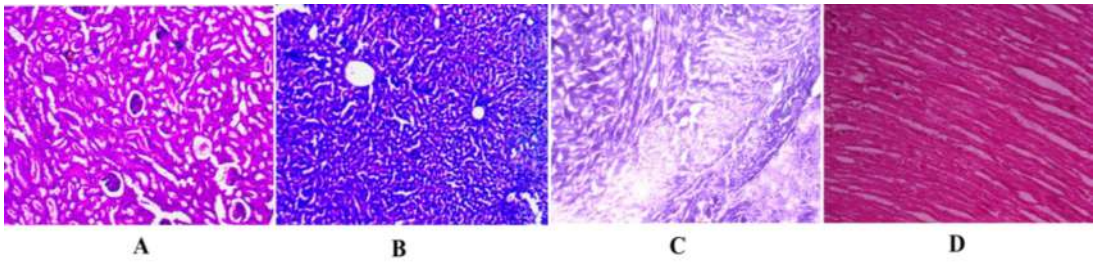

Figure 5. 7 Histopathology of the animal organs after acute toxicity investigation through H & E staining; A) Kidney tissue showing normal DCT, PCT, and Glomerulus; B) Liver tissue showing the presence of normal Kuepfer cells; C) Normal lung tissue; D) Heart image showing normal cardiac muscles.

5.1.2.2.2 Scopolamine induced Y-maze test

The scopolamine-induced rat model was used to study the *in vivo* behavioral improvement efficacy of the compound **SD-6**. The healthy male Wistar rats (10-11 weeks old and 220-280 gm weight) were used in the experiments following i.p. administration of scopolamine (1mg/kg) to induce cognition and memory deficit functions in animals [Klinkenberg and Blokland 2010]. Compound **SD-6** was given in

three divided doses of 2.5, 5, and 10 mg/kg, p.o., while the standard drug donepezil was given at 5 mg/kg, p.o for seven days in divided doses.

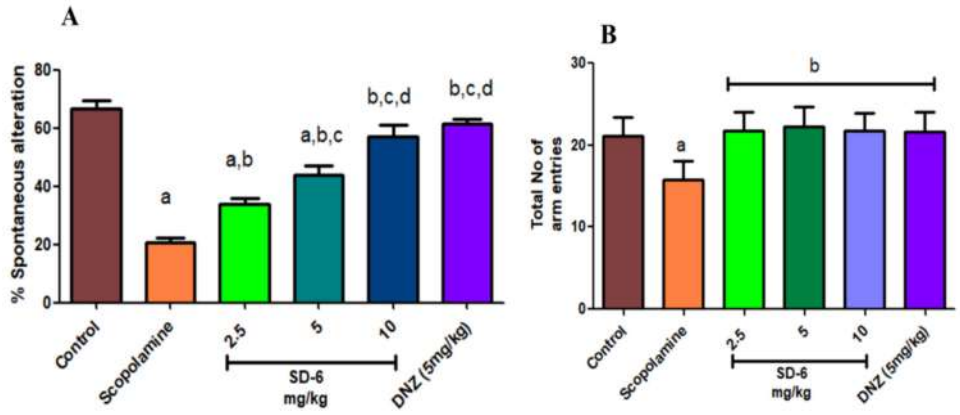

Figure 5. 8 Estimation of **SD-6** and donepezil effects in cognition and memory improvement in scopolamine-induced behavioral models by Y-maze test; A) % spontaneous alterations; B) a total number of arm entries, All results are expressed in mean ± SEM (n=6). ($^{a}p < 0.001$) vs control. ($^{a,b}p < 0.05$), ($^{a,b,c}p < 0.01$) and ($^{b,c,d}p < 0.001$) vs scopolamine, ($^{b}p < 0.001$) vs scopolamine.

A Y-maze test was performed to determine total arm entries and spontaneous alterations. The animal group treated with scopolamine has shown a significant reduction in % spontaneous alterations ($^{a}p < 0.001$) owing to memory and cognition impairment caused by scopolamine as compared to the control group. The donepezil (5 mg/kg) treated group has shown a significant ($^{b,c,d}p < 0.001$) increase in % spontaneous alteration as compared to the scopolamine-treated group. However, the animals treated with compound **SD-6** (2.5, 5, and 10 mg/kg) have also shown a significant increase in % spontaneous alterations in a dose-dependent manner (Figure 5. 8 A) as compared to the scopolamine-treated group in which 10 mg/kg dose has shown the maximum significant ($^{b,c,d}p < 0.001$) increase in % spontaneous alteration. The results of the Y-maze test have also suggested that the total number of arm entries remained unchanged and were almost equal in each group showing scopolamine did not alter the locomotor activity in the experimental animals (Figure 5. 8 B).

5.1.2.2.3 Aβ-induced Morris water maze test

The BACE-1 enzyme directly affects the formation and deposition of Aβ via an amyloidogenic pathway. BACE-1 propagates Aβ formation through APP cleavage and results in $A\beta_{1-42}$ formation which affects neuronal cell survival. The effect of compound **SD-6** in a reversal of learning and memory functions in intracerebrovascular (ICV) $A\beta_{1-42}$ induced male Wistar rat model was evaluated through the Morris water maze test using donepezil as a positive control. The ICV infusion (4 μM, 5 μL) of $A\beta_{1-42}$ in rat hippocampal region through stereotaxic surgery produces AD-like properties due to microglial activation and neuroinflammation, which leads to memory and cognition deficit and mimics the AD-like behavior [Gutti et al. 2019a]. After ICV infusion of $A\beta_{1-42}$ to each group (except the sham group) both donepezil and compound **SD-6,** 5 mg/kg and 10 mg/kg respectively were administered orally for up to 9 days consecutively to each corresponding group and the only vehicle was administered to the control group (Aβ). The test was performed post-treatment in the animals of each group and the time to find the hidden submerged platform i.e escape latency time (EL), the total number of entries to the platform zone, and time spent in the platform quadrant were predicted for 90 s as a test of retention of memory. The results of the test exhibited an initial extension in escape latency time in all groups of animals on day 1, while it declined significantly in other groups as compared to the Aβ group. The donepezil treatment group has shown a maximum decline in ELT over the five days as compared to the Aβ group. The treatment group with compound **SD-6** has also demonstrated a non-significant change in ELT as compared to the donepezil-treated group, while it has demonstrated a significant change as compared to the Aβ group (Figure 5. 9 A). The retention of memory was estimated by time spent in the platform zone which was significantly (^{b} $p < 0.001$) higher for the donepezil (5 mg/kg) and **SD-6** treated group as

compared to the Aβ treated group (Figure 5. 9 B). The effect on the search accuracy of the compound **SD-6** was estimated through the total entries to the platform zone. The animals treated with donepezil and **SD-6** showed non-significant (^{a} $p < 0.001$) results in the total number of entries to the platform zone as compared to the control group while the results were significantly (^{b} $p < 0.001$) different from the Aβ treated animal group (Figure 5. 9 C).

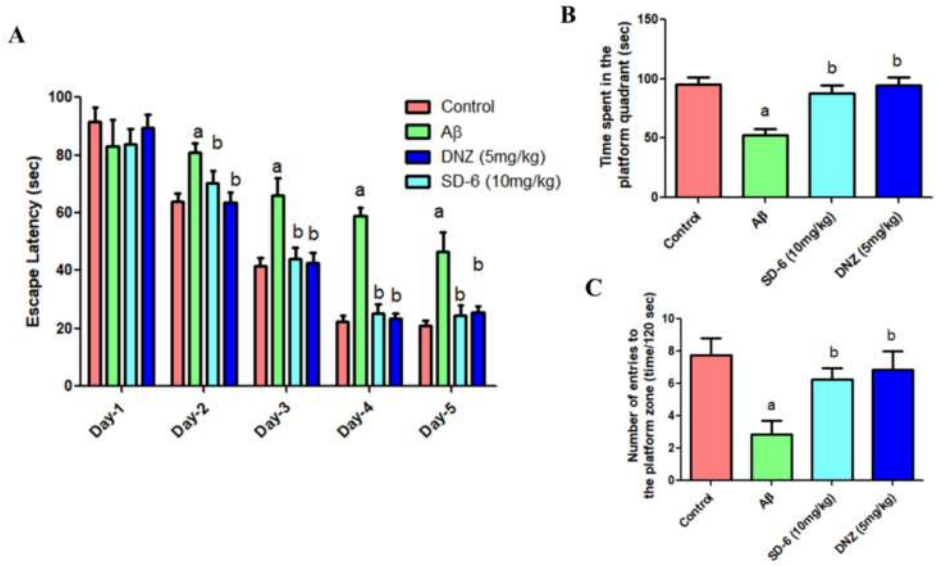

Figure 5. 9 Estimation of **SD-6** and donepezil effects in ICV $A\beta_{1\text{-}42}$ induced Morris water maze test; A) escape latency; B) Time spent in the platform quadrant in the probe trial; C) a number of entries to the platform zone during probe trial, All results are expressed in mean ± SEM (n=6). ($^{a}p < 0.001$ vs. control, and ^{b} $p < 0.001$ vs. an Aβ)

5.1.2.2.4 Ex vivo biochemical estimation

The neurochemical effects of compound **SD-6** were studied by *ex vivo* biochemical estimation in scopolamine-treated rat brains (hippocampal). The *ex vivo* AChE estimation was performed using a modified Ellman's method [Ellman et al. 1961]. The results exhibited that the AChE level was significantly (^{a} $p < 0.001$) higher in scopolamine treated group as compared to the control group and showed a dose-dependent decrease in AChE levels in the **SD-6** treated (2.5, 5, and 10 mg/kg) groups (Figure 5. 10 A). The animals treated with **SD-6** (10 mg/kg) showed a statistically non-

significant difference to that of the donepezil (5 mg/kg) treated group as compared with the control group while it has shown significant (^{b,c,d} $p < 0.001$) difference from the scopolamine treated group.

The Acetylcholine (ACh) level in the brain was also analyzed as per the manufacturer's protocol (Rat Acetylcholine ACh GENLISA ELISA kit, KRISHGEN Biosystems, USA), and suggested a dose-dependent increase in the ACh brain level in **SD-6** treated rat group. The results of the 10 mg /kg treatment group of **SD-6** were found statistically non-significant with the donepezil 5mg/ kg treated group as compared to the control group, while the results were significantly different (^{b,c,d} $p < 0.001$) from the scopolamine-treated group (Figure 5. 10 B).

The estimation of biomarkers like malonaldehyde (MDA) and superoxide dismutase (SOD) (oxidative stress biomarkers) in the brain hippocampal homogenates was performed to evaluate the MDA, a byproduct of lipid peroxidation reaction and dismutation of the superoxide radicals into free oxygen as the measure of SOD. Our *ex vivo* findings suggested that scopolamine administration induces oxidative stress and elevates MDA levels meanwhile it declines the superoxide dismutation and so the SOD levels. In the **SD-6** treated group declines in MDA and elevation of SOD levels were observed in a dose-dependent (2.5, 5, and 10 mg/kg) manner, and were found that the results of **SD-6** (10 mg/kg) and donepezil (5 mg/kg) were significantly different (^{b,c,d} $p < 0.001$) than scopolamine treated groups and were also non-significant to control group (Figure 5. 10 C & D). The estimation of GSH (ROS neutralization capabilities) and catalase activity (conversion of H_2O_2 into the water and free oxygen) was also determined in brain hippocampal homogenate, which resulted in the dose-dependent (2.5, 5, and 10 mg/kg of **SD-6**) elevation of both the biomarkers. The **SD-6** (10 mg/kg) and donepezil (5 mg/kg) treated group showed statistically significant (^{b,c,d} $p < 0.001$)

differences in GSH and catalase levels as compared with the scopolamine-treated group (Figure 5. 10 E & F).

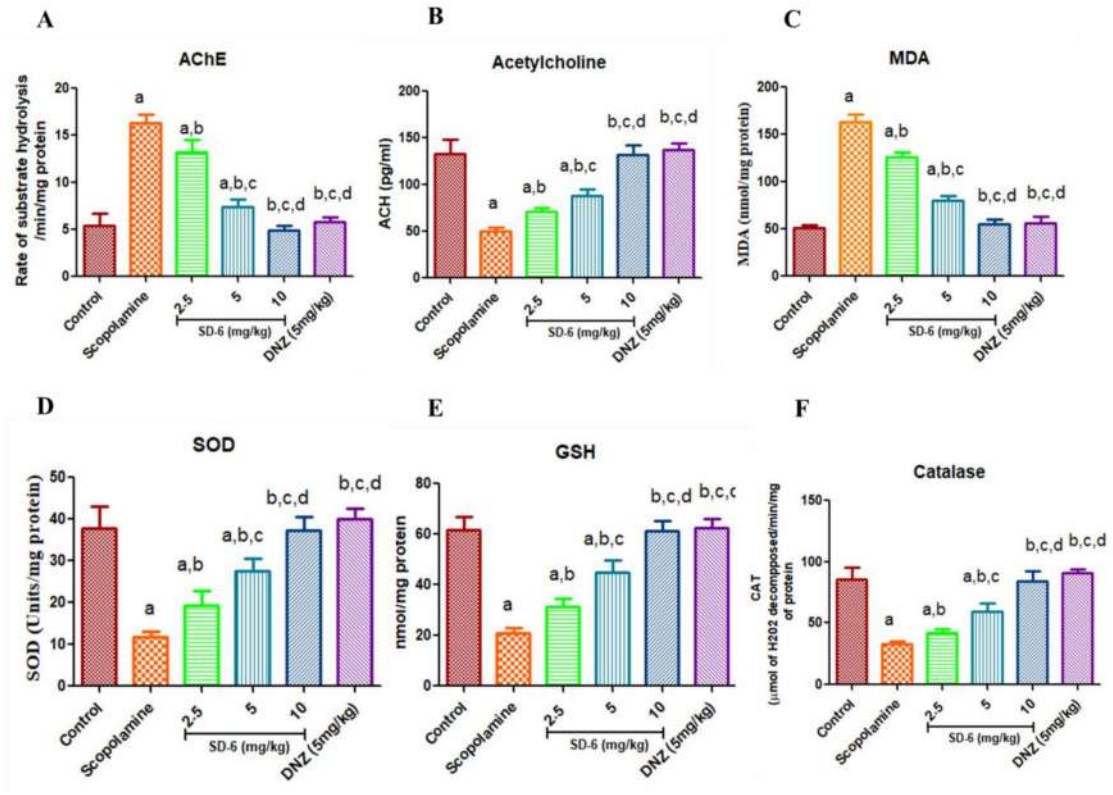

Figure 5. 10 *Ex vivo* studies of the compound **SD-6** to estimate the levels of A) AChE: B) Acetylcholine (ACh): C) MDA: D) SOD: E) GSH: and F) Catalase. The results are expressed as mean ± SEM (n=6), (^{a} $p < 0.001$) vs control. (^{a,b} $p < 0.05$), (^{a,b,c} $p < 0.01$) and (^{b,c,d} $p < 0.001$) vs scopolamine.

5.1.2.2.5 Animal brain tissue histopathology

The rat brain tissue histopathology was performed in control, $A\beta_{1\text{-}42,}$ **SD-6**, and donepezil-treated groups, and neuronal morphology and density were examined after the Nissl staining protocol. The histopathological examination of the group infused with $A\beta_{1\text{-}42}$ has resulted in a disordered arrangement of neurons and the formation of vacuolar fibers (Figure 5. 11 A & B) along with the decline in neuronal density as compared with the control group. However, the histopathological examination of the hippocampal brain (dentate gyrus) treated with **SD-6** (10 mg/kg) and donepezil (5

mg/kg) has resulted in less disordered neuronal arrangement and vacuolar fibrosis (Figure 5. 11 C & D) while the neuronal density (Figure 5. 11 E) was also higher in these groups as compared to the $A\beta_{1-42}$ treated group.

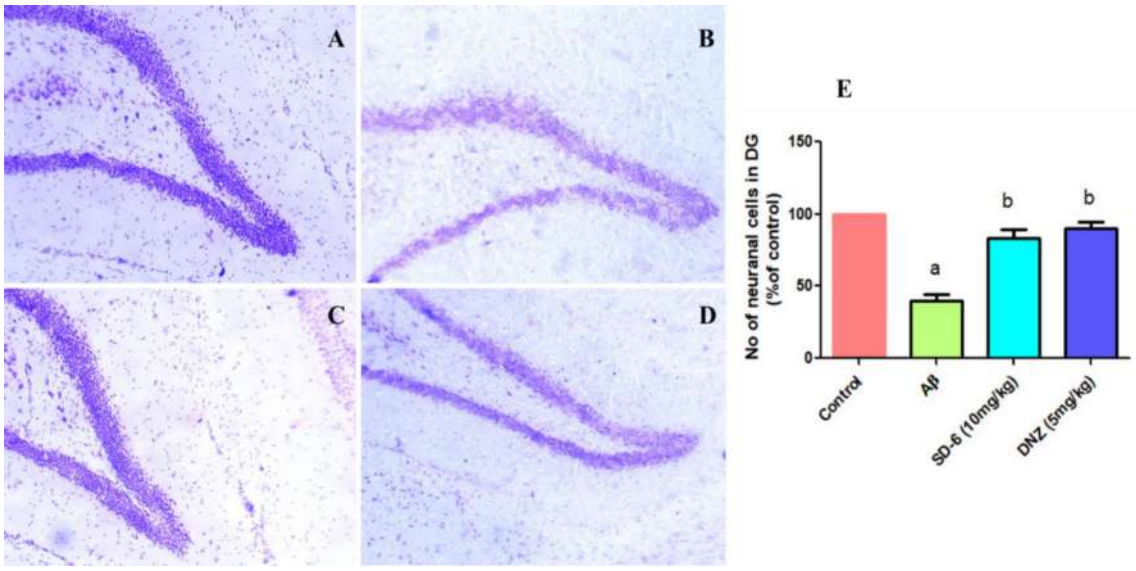

Figure 5. 11 Histomorphological representation dentate gyrus (DG) region of brain hippocampal of the control (A); $A\beta_{1-42}$ treated group (B); **SD-6** treated (10 mg/kg) group (C); donepezil (DNZ) treated (5mg/kg) group (D); and density graph of total neuronal cells (% of control) present in DG (E).

5.1.3 In silico studies

5.1.3.1 Molecular Dockings

The rigid molecular docking studies of the compounds **SD-4** and **SD-6** were performed using the Glide XP module of the Schrödinger Maestro 2018.1 on Linux based workstation. In the rigid molecular docking studies, the protein was considered rigid whereas all degrees of the freedom of the ligands (flexible) were explored to achieve optimum interaction with the protein. Initially, the docking protocols were validated by extracting and redocking the co-crystallized bound ligand (donepezil for hAChE and F1M for hBACE-1) in the active site of both the enzymes and calculated the RMSD value, which was found to be 1.50 and 1.20 Å (acceptable range ≤ 2 Å) for hAChE and hBACE-1 respectively. The superimposition and XP visualizer tools were used to study

the binding modes of the co-crystallized and re-docked ligands to ascertain validation of the prepared grid and docking protocols. The docking studies affirmed the consensual binding pattern of both the compounds in the active site of the enzymes hAChE (PDB: 4EY7) and hBACE-1 (PDB: 2ZJM).

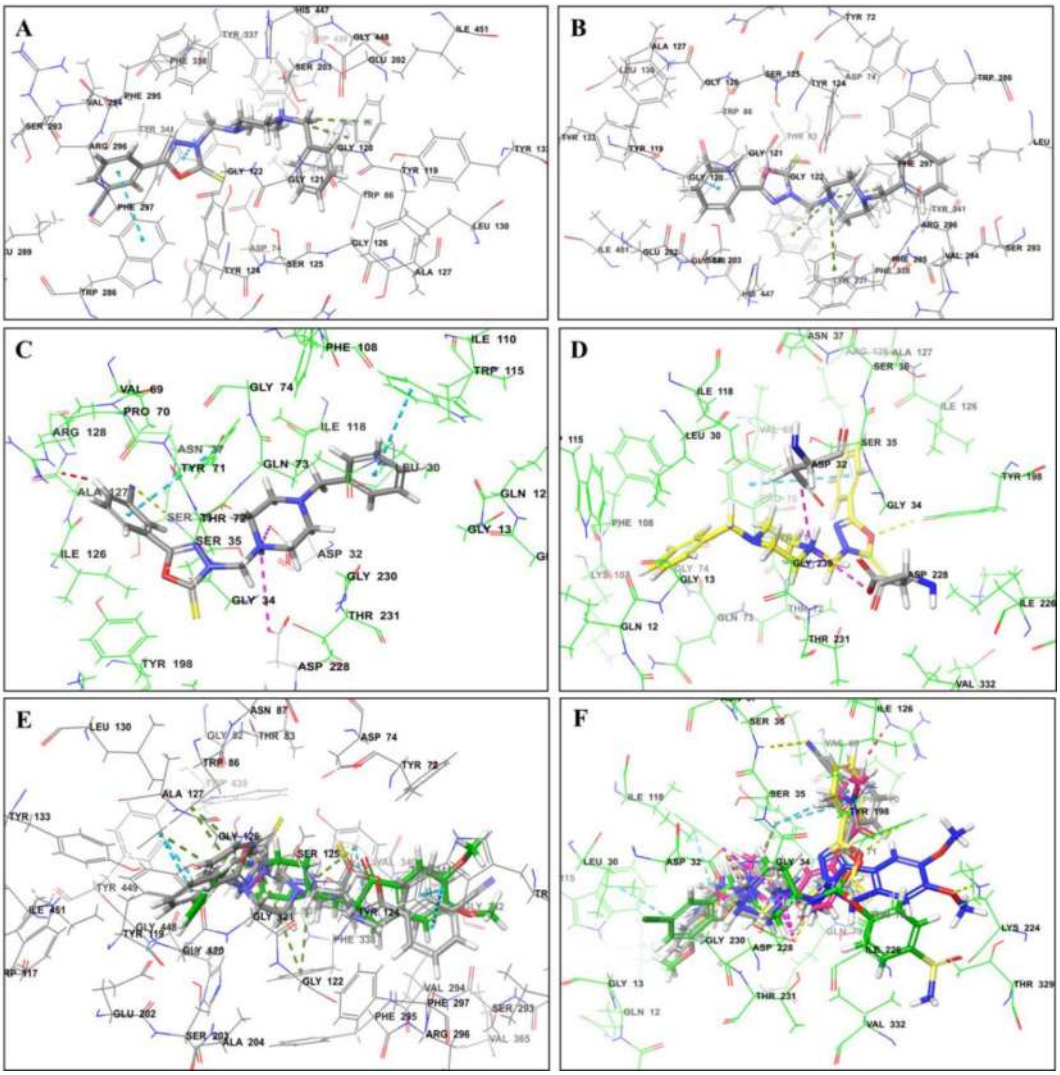

Figure 5. 12 Molecular docking 3D interaction representation of the compounds **SD-4** and **SD-6** with hAChE (PDB: 4EV7) and hBACE-1 (PDB: 2ZJM): A) 3D docked pose of compound **SD-4** with hAChE; B) 3D docked pose of compound **SD-6** with hAChE; C) 3D docked pose of compound **SD-4** with hBACE-1; D) 3D docked pose of compound **SD-6** with hBACE-1; E) 3D docked superimposition of compound **SD-4**, **SD-6** (bold gray sticks) and donepezil (green sticks) with hAChE; F) 3D docked

superimposition of compound **SD-4**, **SD-6** (gray and bold yellow sticks) and F1M (bold blue sticks) with hBACE-1.

The docking result of the compound **SD-4** (Figure 5. 12 A) and **SD-6** (Figure 5. 12 B) against hAChE suggested that the phenyl and 1,3,4-oxadiazole-2-thione rings of the compounds were interacting with the Trp286 and Tyr341 residues of the AChE-PAS region via strong hydrophobic π-π stacking interaction while compound **SD-6** showed an additional π-π stacking interaction with Tyr124 residue of AChE-PAS region. One of the protonated nitrogen atoms of the BP ring present in both compounds was interacting with the Trp86 residue of anionic subsite by π-cationic interactions (Figure 5. 12 B). The benzyl ring of both the compounds was also interacting with the acyl-binding pocket residues Gly120, Gly121, and Gly122 via glycine-rich interactions and AChE-CAS residues His447 and Ser203 via polar interactions (Figure 5. 12 A-B). However, the benzyl ring of **SD-6** was interacting with His447 via an additional π-π stacking interaction (Figure 5. 12 A-B) corroborating it's *in vitro* hAChE inhibitory activity. The docked pose superimposition of compounds **SD-4, SD-6,** and donepezil in the hAChE active site suggested that all three compounds are almost aligned in the same plan and share common amino acid residue interactions (Figure 5. 12 E).

The molecular docking results of compounds **SD-4** (Figure 5. 12 C) and **SD-6** (Figure 5. 12 D) against hBACE-1 suggested that the protonated nitrogen of the BP ring present in both the compounds was interacting with the catalytic dyad residues Asp32 and Asp228 via salt bridge interaction which in necessary for inhibition of the enzymatic activity. However, the phenyl ring of both the compounds was interacting with the Tyr71 residue via π-π stacking interaction. The 3–C≡N group present in the phenyl ring of **SD-4** also exhibited water-mediated H-bond interaction with the Ser36, the benzyl ring showed π-π stacking interaction with Trp115 residue while, an oxygen atom of 1,3,4-oxadiazole-2-thione of **SD-6** showed H-bond interaction with Tyr198 residue

(Figure 5. 12, C-D). The presence of H-bond and π-π stacking interaction other than catalytic dyad residue interactions are believed to be accountable for better BACE-1 inhibitory potential of the compounds **SD-4** and **SD-6**. The docked pose superimposition of compounds **SD-4**, **SD-6,** and F1M in the active site of the BACE-1 suggested that all compounds were interacting with the catalytic dyad residues (Asp32 and Asp228) and sharing almost the same plane (Figure 5. 12 F). The overall molecular docking studies of the compounds **SD-4** and **SD-6** against hAChE and hBACE-1 enzymes confirmed their binding with the hAChE-CAS, PAS residues, and the catalytic dyad residues of the hBACE-1enzymes respectively which are in complete agreement of the *in vitro* (**SD-4** and **SD-6**) and *in vivo* (**SD-6**) studies of the compounds.

The molecular docking studies of the compounds **SD-4** and **SD-6** were also performed against the hBChE enzyme (PDB: 4TPK) to see the interaction of both the compounds in the active site of the enzyme suggesting that both the molecules are interacting with the CAS and PAS residues of the enzymes and sharing the same plan to that of the rivastigmine (BChE inhibitor) in the hBChE active site**.** The glide scores (kcal/mol) of the compounds **SD-4** and **SD-6** against hAChE, hBChE, and hBACE-1 were also determined using the Glide XP visualizer module of the Schrödinger 2018-1 and the results suggested that the Glide scores of both the compounds were comparable to standard molecules donepezil, rivastigmine, and F1M for hAChE, hBChE, and hBACE-1 respectively (Table 5. 5).

5.1.3.2 Molecular Dynamics

To understand the stability of the docked complex a molecular dynamic (MD) simulation run of 100 ns was performed for both the ligand-protein complex (**SD-4, SD-6** with hAChE, hBChE, and BACE-1). The Desmond module of the Schrödinger suite was utilized to run the MD studies of the complexes on the graphical processing unit

(GPU). The MD results of both the docked complex have shown that the root means square deviation (RMSD) value was within the acceptable range of 1-3 Å with stable trajectories during the entire run of 100 ns. The protein-ligand root mean square fluctuations (RMSF) were also found within the range under 3 Å. The "Simulation interaction diagram" tool of Desmond was used to understand the protein-ligand interaction through PL-histogram, PL-RMSD, PL-timeline, and PL-2D interaction diagrams.

The MD simulation results of the compounds **SD-4** and **SD-6** against hAChE suggested that the phenyl ring of both the compounds was interacting with the Trp86 (100%) and Trp286 (70%) respectively via face-to-face π-π stacking interaction. The protonated nitrogen atom of the BP ring of **SD-4** and **SD-6** was interacting with the anionic subsite residue Glu202 (87%) and AChE-PAS residue Asp74 (99%), respectively via H-bond interaction. Compound **SD-4** demonstrated a strong hydrophobic π-π stacking interaction with AChE-CAS residue His447 (74%) while, the sulfur atom of the 1,3,4-oxadiazole-2-thione ring of **SD-6** showed water bridge interaction with Phe295 (64%) and Arg296 (49%) of acyl binding pocket. Compound **SD-6** showed an additional hydrophobic π-π stacking interaction with AChE-PAS residue Tyr72 (50%) and Tyr341(95%) imparting its strong hAChE inhibition potential (Figure 5. 13 & Figure 5. 16).

The MD simulation studies of compound **SD-4** and **SD-6** complexed with hBACE-1 also suggested that the protonated nitrogen atom of the BP ring was interacting with the catalytic dyad residues Asp32 (100% & 87%) via H-bond interaction and Asp228 (90% &100%) via ionic bond interaction. The phenyl ring of the compounds **SD-4** and **SD-6** showed π-π stacking interaction with Tyr71 (38% & 58%) while the BP ring of compound **SD-4** showed an additional π-π stacking interaction with Tyr71 (36%). The

3-C≡N group present on the phenyl ring of the **SD-4** showed H-bond interaction with the Asn37 (37%) while the sulfur atom of the 1,3,4-oxadiazole-2-thione ring of **SD-6** showed water bridge interaction with the Arg235 (33%) residue (Figure 5. 14 & Figure 5. 15) suggesting more stable confirmation of **SD-6** over **SD-4** with BACE-1.

The MD simulation studies of the compounds **SD-4** and **SD-6** complexed with hBChE have also been performed to see the stability of both the docked complexes. The results of the MD studies suggested that the protonated nitrogen atom of the BP ring present in both compounds was interacting with the BChE-PAS residue Asp70 (100%) via strong H-bond interaction. Compound **SD-4** showed hydrophobic π-π stacking interaction with anionic subsite residue Trp82 (90%) while compound **SD-6** showed strong hydrophobic π-π stacking interactions with anionic subsite residue Trp82 (100%), and the acyl binding pocket residues Trp231 (80%) and Phe329 (100%) (Figure 5. 17 & Figure 5. 18).

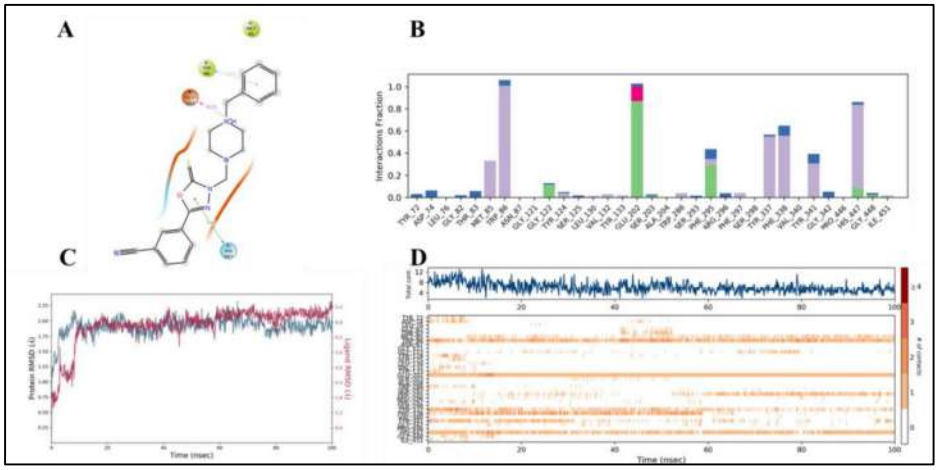

Figure 5. 13 Results of 100 ns MD simulation run of the compound **SD-4** complexed with hAChE (PDB: 4EY7); A) 2D interaction diagram representing the interaction of the molecule with amino acid residues; B) ligand-protein interaction histogram showing interaction fractions (e.g. for a value of 0.6 indicates 60% of interaction in total simulation run); C) ligand-protein RMSD relative to protein backbone structure; D) time-line graphical representation showing interaction with individual residues in each trajectory frame.

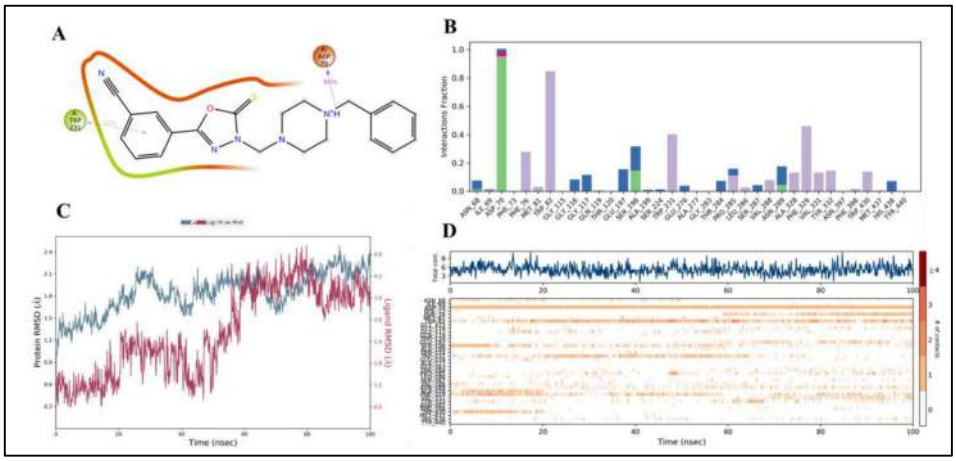

Figure 5. 14 Results of 100 ns MD simulation run of the compound **SD-4** complexed with hBChE (PDB: 4TPK); A) 2D interaction diagram representing the interaction of the molecule with amino acid residues; B) ligand-protein interaction histogram showing interaction fraction (e.g. for a value of 0.8 indicates 80% of interaction in total simulation run); C) ligand-protein RMSD relative to protein backbone structure; D) time-line graphical representation showing interaction with individual residues in each trajectory frame.

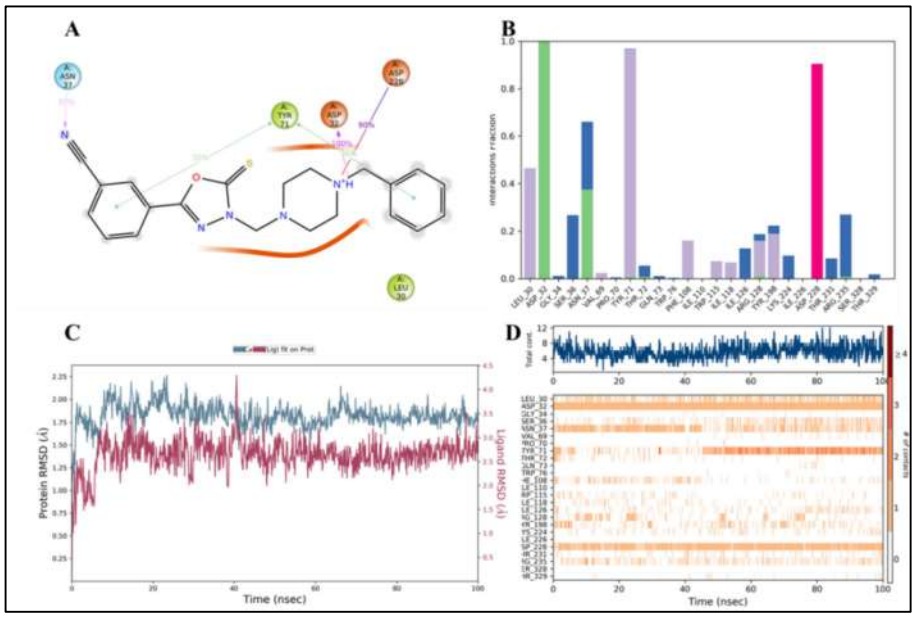

Figure 5. 15 Results of 100 ns MD simulation run of the compound **SD-4** complexed with hBACE-1 (PDB: 2ZJM); A) 2D interaction diagram representing the interaction of the molecule with amino acid residues; B) ligand-protein interaction histogram showing interaction fractions (e.g. for a value of 0.6 indicates 60% of interaction in total simulation run); C) ligand-protein RMSD relative to protein backbone structure; D)

time-line graphical representation showing interaction with individual residues in each trajectory frame.

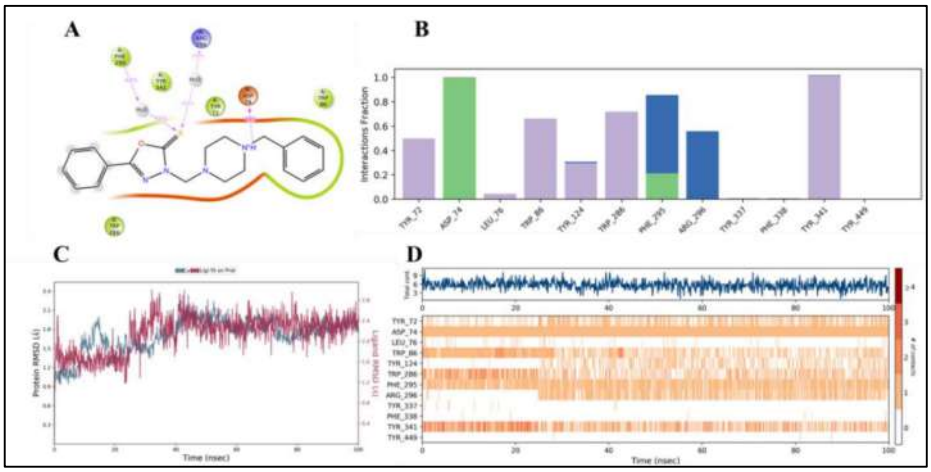

Figure 5. 16 Results of 100 ns MD simulation run of the compound **SD-6** complexed with hAChE (PDB: 4EY7); A) 2D interaction diagram representing the interaction of the molecule with amino acid residues; B) ligand-protein interaction histogram showing interaction fractions (e.g. for a value of 0.6 indicates 60% of interaction in total simulation run); C) ligand-protein RMSD relative to protein backbone structure; D) time-line graphical representation showing interaction with individual residues in each trajectory frame.

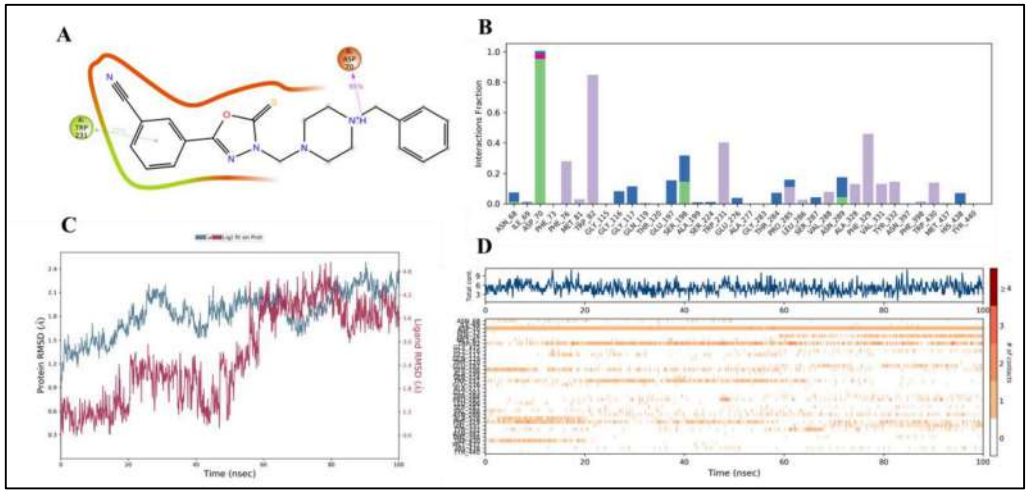

Figure 5. 17 Results of 100 ns MD simulation run of the compound **SD-4** complexed with hBChE (PDB: 4TPK); A) 2D interaction diagram representing the interaction of the molecule with amino acid residues; B) ligand-protein interaction histogram showing interaction fraction (e.g. for a value of 0.8 indicates 80% of interaction in total simulation run); C) ligand-protein RMSD relative to protein backbone structure; D)

time-line graphical representation showing interaction with individual residues in each trajectory frame.

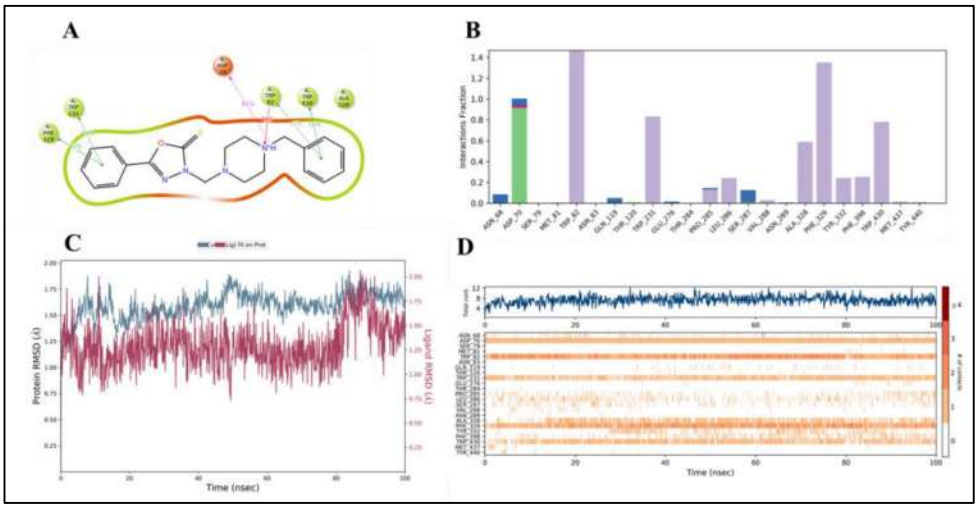

Figure 5. 18 Results of 100 ns MD simulation run of the compound **SD-6** complexed with hBChE (PDB: 4TPK); A) 2D interaction diagram representing the interaction of the molecule with amino acid residues; B) ligand-protein interaction histogram showing interaction fraction (e.g. for a value of 0.8 indicates 80% of interaction in total simulation run); C) ligand-protein RMSD relative to protein backbone structure; D) time-line graphical representation showing interaction with individual residues in each trajectory frame.

The molecular dockings and dynamics results of both the compounds **SD-4** and **SD-6** also corroborate our *in vitro* and *in vivo* findings that both of these compounds are representative molecules of the series and **SD-6** was the most suitable compound for the *in vivo* experiments.

5.1.3.3 In-silico determination of drug-like properties

To target any molecule in the central nervous system (CNS) the estimation of its physicochemical parameters are crucial in developing a drug-like molecule. The various parameters of the molecules **SD-4** and **SD-6** were predicted using the Quikprop module of the Schrodinger such as total solvent accessible surface area (SASA), donor-HB, accept-HB, octanol/water partition coefficient (QPlogPo/w), Caco-2 cell permeability

(QPPCaco), brain/blood partition coefficient (QPlogBB), % human oral absorption (%HOA), Lipinski's rule of five and predicted apparent MDCK cell permeability (QPPMDCK). The predicted properties of both the molecules were compared with the standard drugs donepezil and rivastigmine which suggested that compounds **SD-4** and **SD-6** retain drug-like properties in the acceptable limits with high BBB permeation capability (Table 5. 4)**.** The drug-likeness properties of the compound **SD-6** have also revealed that it was the most promising molecule of the series and so did the *in vitro* and *in vivo* activities.

5.1.3.4 Binding free energy (MM/GB-SA) calculation

The molecular mechanics/generalized born surface area (MM/GBSA) was used to predict the binding free energy (ΔG_{bind} in Kcal/mol) between protein and ligand. The binding free energy was calculated based on the combination of gas-phase energy (MM), electrostatic solvation energy (GB), and non-electrostatic contribution to solvation energy (SA). The ΔG_{bind} energy of both the compounds **SD-4** and **SD-6** was calculated and compared with the standard donepezil, rivastigmine, and F1M molecules using the prime MM/GBSA module of Schrödinger 2018-1. The detailed results are expressed in Table 5. 5 and suggested that the ΔG_{bind} energy of the compounds **SD-4** and **SD-6** was comparable to donepezil, rivastigmine, and F1M molecules against hAChE and hBACE-1 enzymes while ΔG_{bind} energy of both the compounds was better than the standard donepezil, rivastigmine and F1M against hBChE enzyme.

Table 5. 4 ADME predicted properties of the compounds and standard drugs

Compound Code	SASA	Donor HB	Accept HB	QPlog Po/w	QPP Caco	Qplog BB	% HOA	Rule of five	Qpp MDCK
SD-4	722.8	0	9	2.18	82.84	0.22	74.07	0	94.90
SD-6	684.9	0	7.5	3.02	398.88	1.075	89.95	0	534.34
Donepezil	720.2	0	5.5	4.47	893.17	0.11	100	0	484.39
Rivastigmine	565.2	0	5	2.48	1086.04	0.38	95.83	0	617.56

SASA total solvent accessible surface area in square angstroms (range 300-1000 Å), *donor* HB H-bond donors (range 0-6), *accept* H-bond acceptor (range 2-20), *QPlogPo/w* predicted log of octanol/water partition coefficient (range 2-6), *QPPCaco* predicted apparent Caco-2 cell permeability in nm/s (range <25 poor, >500 great), *QPlog BB* predicted brain/blood partition coefficients (range −3 to 1.2), *%HOA* predicted human oral absorption (>80% is high, <25% is poor), *QppMDCK* cells are considered to be a good mimic for the BBB (< 25—poor; > 500—great).

Table 5. 5 Results of docking (Glide score) and MM/GBSA.

Enzyme	Compound	Glide score*	ΔG binding energy*
hAChE			
	Donepezil	-14.150	-65.258
	Rivastigmine	-13.150	-55.196
	F1M	-15.005	-58.482
	SD-4	-15.120	-61.425
	SD-6	-13.746	-62.166
hBChE			
	Rivastigmine	-4.969	-35.037
	Donepezil	-7.212	-48.086
	F1M	-6.590	-36.773
	SD-4	-6.961	-54.993
	SD-6	-7.759	-63.777
hBACE-1			
	F1M	-7.641	-63.257
	Donepezil	-5.782	-58.023
	Rivastigmine	-5.158	-39.593
	SD-4	-6.312	-51.650
	SD-6	-6.191	-51.709

5.2 PART-II: SERIES II-III

5.2.1 Computational studies

5.2.1.1 Pharmacophore modelling

An e-pharmacophore hypothesis of structure-based drug design was generated using two co-crystal structures utilized to screen an in-house database. Two e-pharmacophore models (hAChE, PDB code: 4EY7, and hBACE-1, PDB code: 2ZJM) were generated using co-crystal structures. The e-pharmacophore model of hAChE incorporated one hydrogen bond acceptor, two aromatic rings, and two hydrophobic residues, while the

hBACE-1 e-pharmacophore model suggested the presence of two hydrogen bond donors, a single positive ionic group, and two aromatic rings as necessary features (Figure 5. 19). The in-house database was screened utilizing the Phase module of Schrödinger Maestro suite 2018 resulting in 379 hits which were further subjected to virtual screening workflow (vsw).

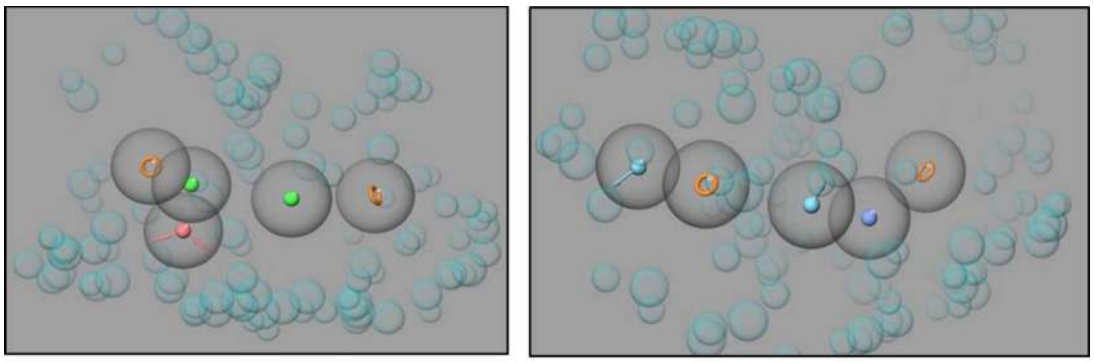

Figure 5. 19 e-Pharmacophore models A) AChE (PDB: 4EY7) B) BACE-1 (PDB: 2ZJM)

5.2.1.2 Virtual screening

The vsw comprised high throughput virtual screening (HTVS), standard precision (SP), and extra precision (XP) docking and was set at 30% filtration criteria in every step. The screening resulted in 10 compounds, from which 5 hits were selected based on their docking scores and interactions with the catalytic active site (CAS) region (His447, Glu334, and Ser 203) and the peripheral active site (PAS) region (Tyr124, Tyr72, Tyr341, Trp286, and Asp74) of the AChE and catalytic dyad (Asp32 and Asp228) region of BACE-1.

5.2.1.3 Molecular Docking

Molecular docking studies of the compounds **5d** and **5f** were performed to gain insights into the respective intermolecular interactions in the active site of the hAChE (PDB: 4EY7), hBChE (PDB: 4TPK), and hBACE-1 (PDB: 2ZJM) enzymes. The docking model predicts key features for both compounds suggesting that the N-benzylpiperidine

moiety of both compounds was well accommodated in the catalytic active site (CAS) while the 5-phenyl-1,3,4-oxadiazole was oriented towards the peripheral active site (PAS) residues of the hChEs. Furthermore, interactions were apparent with the catalytic dyad residues (Asp32 and Asp228) of the hBACE-1 necessary for their inhibitory function. The binding of both compounds in the hAChE active site was also compared with the binding of donepezil which showed all the molecules were aligned in one plan and shared almost equal amino acid interactions.

The molecular docking of **5d** and **5f** in the hAChE enzyme implicates the oxadiazole ring interactions with the Trp286 amino acid residues through π-π interaction (Figure 5. 20 A-B and Figure 5. 21 A-B). The benzylpiperidine ring of both compounds extended into the AChE-CAS region with polar interactions with side chains of His447 and Ser203 residues. The benzyl moiety shows potential π-π stacking and π-cationic interactions with the Trp86, Tyr337, and Phe338 residues of the AChE-anionic subsite Also, the oxygen atom of the amide spacer group of compound **5d** has potential H-bond interaction with the Tyr124 of the AChE-PAS region.

A similar docking study of both the compounds **5d** and **5f** in hBChE (PDB: 4TPK) and the docking poses suggest a common that the 5-phenyl ring interaction with the Trp82 at the anionic subsite, along with Trp231and Phe329 at acyl binding pocket via hydrophobic and π-π stacking interactions, respectively. However, the nitrogen of N-benzylpiperidine ring of compound **5d** and –NH of the amide spacer group present in **5f** were differentially interacting with the Pro285 putatively via a backbone H-bond interaction (Figure 5. 20 C-D and Figure 5. 21 C-D).

The docking studies of the compounds **5d** and **5f** against the hBACE-1 enzyme were also performed to predict their potential molecular interactions with the enzyme active site necessary to achieve the multi-targeting effects. The docking results suggested that

both these compounds were interacting with the catalytic dyad residues (Asp32 and Asp228) through hydrogen bonding and electrostatic interactions. The protonated nitrogen atom present on N-benzylpiperidine ring in both compounds implicates salt bridge interactions with Asp32 residue. The -NH of the amide spacer group of both the compounds **5d** and **5f** have shown H-bond interactions with the Asp228 and Gly34 residue respectively which could contribute to an increase in BACE-1 inhibitory activity of both the molecules (Figure 5. 20 E-F and Figure 5. 21 E-F).

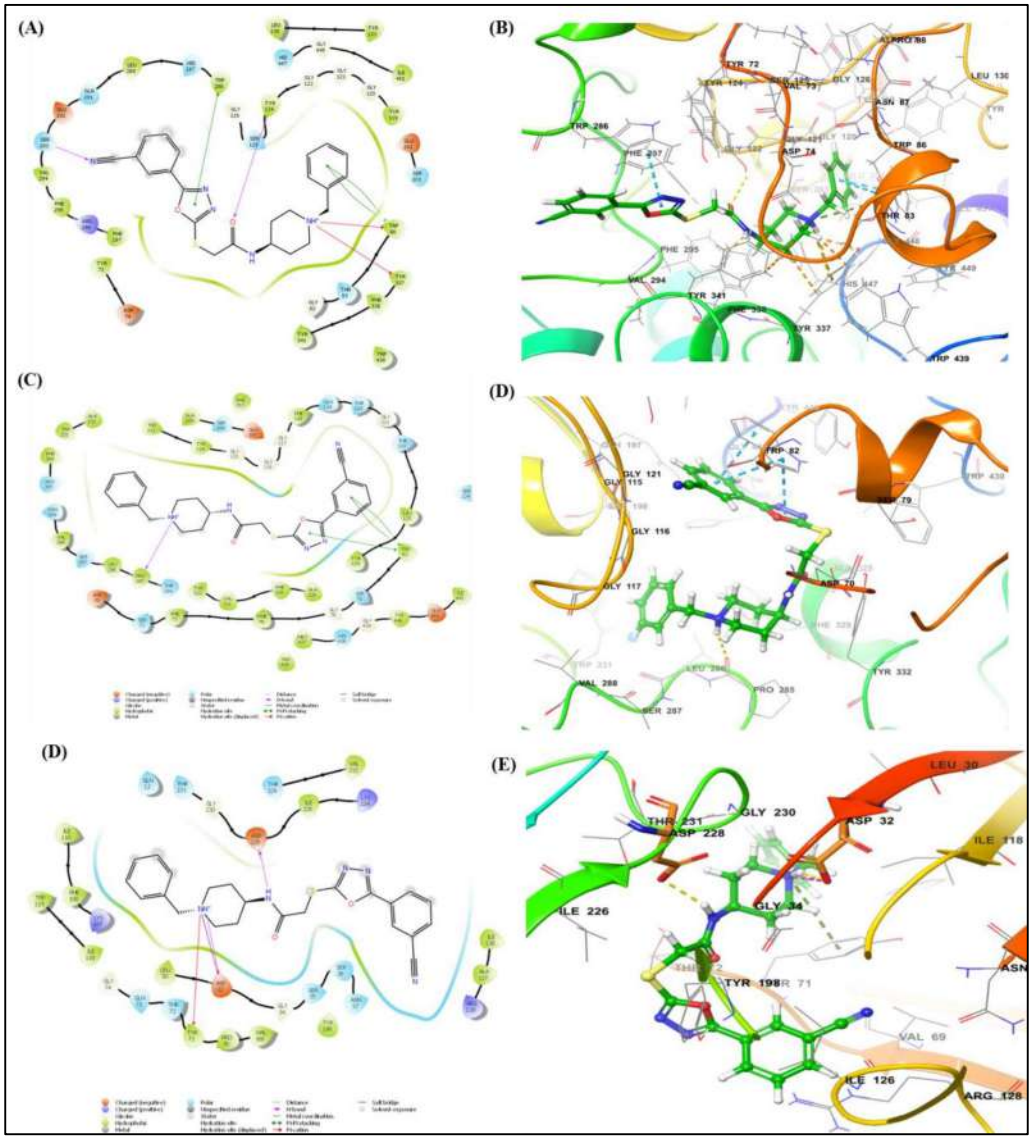

Figure 5. 20 Molecular Docking studies of the compound **5d** in active site of the enzymes. A & B) 2D and 3D representation of compound **5d** in hAChE active site

(PDB : 4EY7); C & D) 2D and 3D representation of compound **5d** in hBChE active site(PBD: 4TPK) E & F) 2D and 3D representation of compound **5d** in hBACE-1 active site (PDB: 2ZJM).

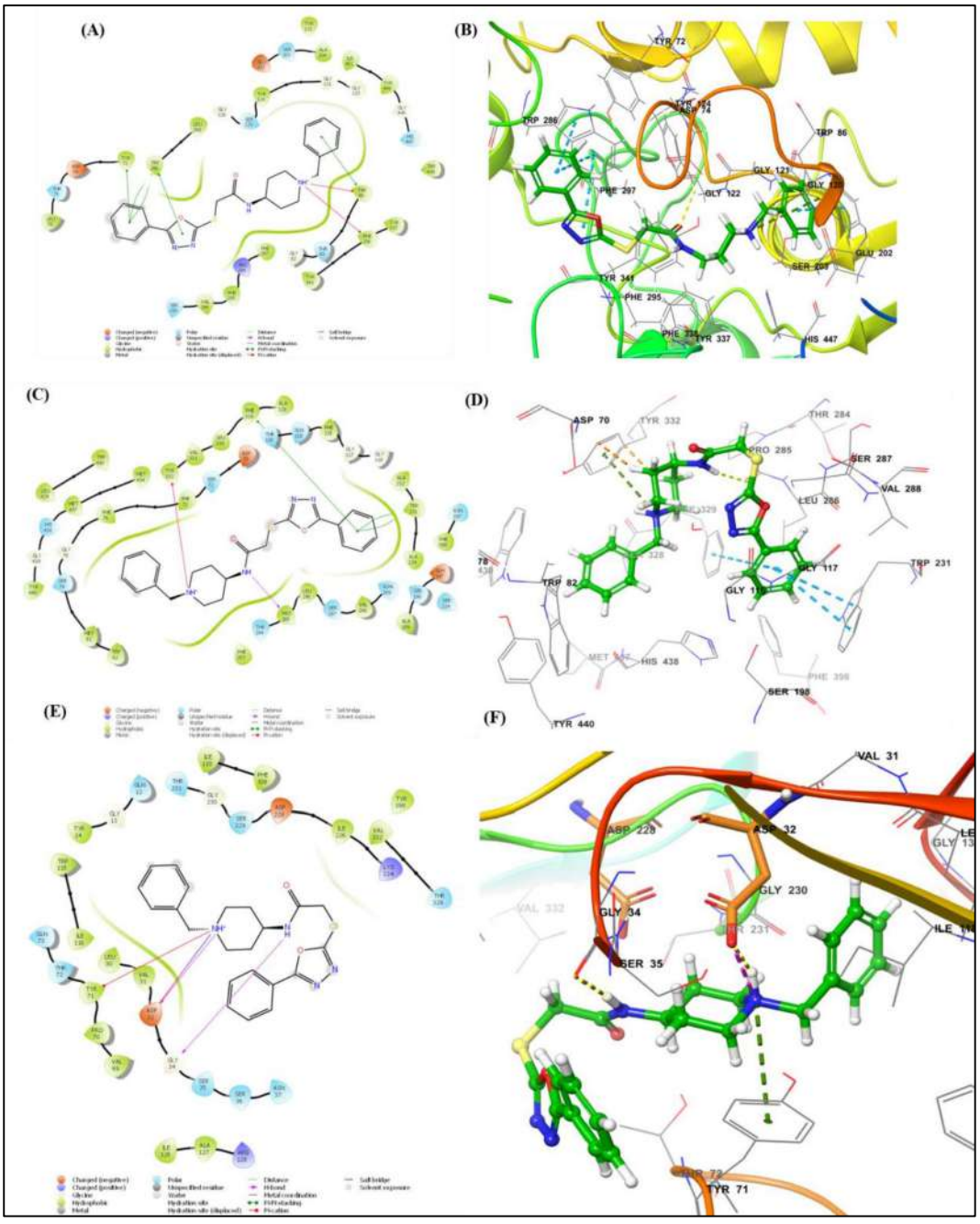

Figure 5. 21 Molecular Docking studies of the compound **5f** in the active site of the enzymes. A & B) 2D and 3D representation of compound **5f** in hAChE active site (PDB: 4EY7); C & D) 2D and 3D representation of compound **5f** in hBChE active site (PBD: 4TPK) E & F) 2D and 3D representation of compound **5f** in hBACE-1 active site (PDB: 2ZJM).

The overall docking results suggested that an alkyl acetamide linkage introduced between 5-Phenyl-1,3,4-oxadiazole-2-thione and N-benzylpiperidine ring is judicious to extend the molecule in CAS and PAS region of the ChE (hAChE and hBChE) enzymes. The oxygen and nitrogen atom of the sulfur-allied alkylacetamide linkage itself interacts with the backbone residues through H-bond interactions and positioned 5-Phenyl-1,3,4-oxadiazole-2-thione into the PAS region and angled the N-benzylpiperidine ring into CAS region of the ChE enzymes. However, this alkylacetamide linkage also looks necessary for interaction with one of the catalytic dyad residues Asp228 of hBACE-1 enzyme via H-bond interaction and aligns the N-benzylpiperidine ring towards the second dyad residue Asp32 to establish another H-bond bond interaction with protonated nitrogen of the piperidine ring.

5.2.1.4 MMGB-SA

The MMGB-SA module of the Schrodinger suite 2018 was used to determine the binding energies of the docked ligand-protein complex. The MMGB-SA of the representative compounds of the series was calculated against hAChE, hBChE, and hBACE-1 enzymes and suggested that the compounds **5a** (hAChE ΔG = -69.50, hBChE ΔG = -53.20 and hBACE-1 ΔG = -62.85), **5d** (hAChE ΔG = -71.44, hBChE ΔG = -42.89 and hBACE-1 ΔG = -52.54), **5f** (hAChE ΔG = -68.10, hBChE ΔG = -63.63 and hBACE-1 ΔG = -60.67) and **5h** (hAChE ΔG = -75.25, hBChE ΔG = -58.43 and hBACE-1 ΔG = -56.29) were having the minimum ΔG binding score which was comparable to standard donepezil (hAChE ΔG = -59.06 and hBACE-1 ΔG = -57.31) and rivastigmine (hBChE ΔG = -39.32).

5.2.1.5 Molecular Dynamics Simulations

To gain more detailed insights and assess the stability of the docking poses, molecular dynamics (MD) simulations of the compounds **5d** and **5f** complexed with hAChE, hBChE, and hBACE-1 were also performed (Figure 5. 28 A-D).

MD simulation runs of 100 ns were performed for each docked complex using Desmond (Schrodinger). The results of the MD simulation studies suggested that all the docked complexes were stable throughout the entire run of 100 ns, and the protein – ligand RMSD of each docked complex was in the acceptable range of 1-3 Å. The results of the MD simulations of the **5d -**hAChE complexes (Figure 5. 22) suggested that the phenyl and oxadiazole rings of the compound were interacting with the AChE-PAS residues Try341 (32 & 42%) and Phe297 (33 & 32%) while, the phenyl and oxadiazole rings of **5f** (Figure 5. 23) were interacting with the Tyr124 (14%), Tyr77 (24%)of AChE-PAS residues via π-π stacking interaction. The –NH of the amide linkage present in **5d** and **5f** interacting with the Gly342 (91%) and Tyr337 (64%) residues via H-bond interactions respectively. However, the oxygen atom of the amide linkage present in compound **5d** showed water-mediated H-bond interactions with the Ser293 (23%), Phe295 (32%), and Arg296 (37%) while in compound **5f** it has shown H-bond interaction with the Tyr341 (96%). The N-benzylpiperidine ring of compound **5d** was interacting with the anionic subsite residues Trp 86 (38%), Phe297 (67%), and PAS residue Tyr341(100%) via hydrophobic interactions while in compound **5f** the protonated nitrogen of N-benzylpiperidine ring was interacting with the anionic subsite residues Tpr86 (100%) and Glu202 (81%).

The MD simulations studies of docked poses of **5d** and **5f** with hBChE (Figure 5. 24 and Figure 5. 25) also revealed that both compounds were interacting with the hBChE-CAS, PAS, and anionic subsite residues and the respective docked complex of both the

compounds were also stable throughout the 100 ns simulation run (RMSD < 3 Å) which substantiates our in vitro findings.

The MD simulation run of the **5d** and **5f** complexed with hBACE-1 (Figure 5. 26 and Figure 5. 27) suggested that the protonated nitrogen atom of the N-benzylpiperidine ring and the –NH group of amide linkage was interacting with the Asp32 (99 & 85 %) and the Asp228 (99 & 40%) residues of catalytic dyad respectively via electrostatic charged interactions of catalytic dyad residue. In the compound **5d**, the 3–C≡N group was interacting with the Asn37 (43%) and Ser36 (90%) via water-mediated H-bond interaction, the oxadiazole moiety was interacting with Tyr198 (47%) via π-π stacking interaction and the amide oxygen was interacting with the Thr72 (44%) via water-mediated H-bond interaction. However, in compound **5f,** the amide oxygen was interacting with the Arg235 (45%) via water-mediated H-bond interaction, and the benzyl ring was interacting with the Phe108 (38%) via π-π stacking interaction. The amide –NH of the compound **5f** also showed water-mediated H-bond interaction with the catalytic dyad residue Asp32 (28%).

The overall MD simulations studies of **5d** and **5f** predict that both compounds occupy hChE-CAS and PAS pockets with a common set of molecular interactions and a significant residence time. At the same time, they also interact with the anionic subsite and glycine-rich loop of the enzymes, which leverage the ChE inhibitory potencies. Both compounds also exhibit backbone H-bond and ionic-charged interactions with the catalytic dyad residues of the BACE-1. It is also observed that the acetamide spacer group present in the compounds provides enough flexibility to both the ring systems to adopt different conformations to achieve the inhibitory activity. The molecular dockings and MD results corroborated our *in vitro* and *in vivo* findings; suggesting both these

compounds have the potential that needs to be explored further to get a promising candidate as MTDL for AD therapy.

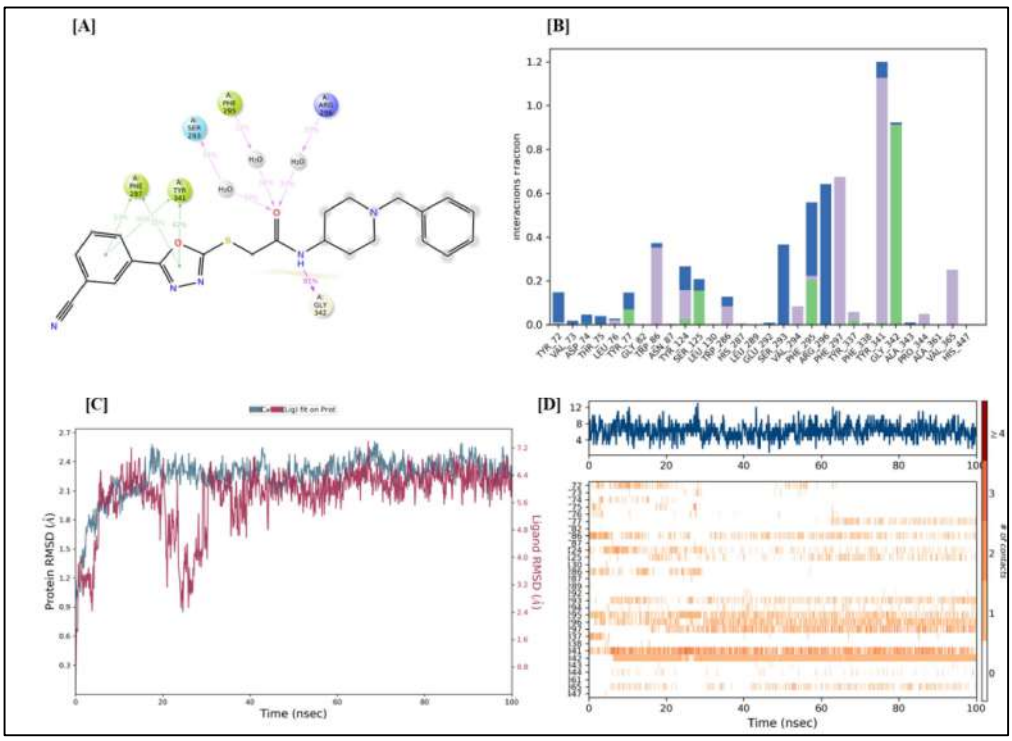

Figure 5. 22 Molecular dynamics (MD) studies of compound **5d** -AChE (4EY7) docked complex. (A) 2D representation showing % interaction with amino acid residues in the active site; B) Histogram presentation of interaction fraction with amino acid residues; C) RMSD graph of ligand-protein (**5d-**AChE) interaction of 100 ns MD; D) Timeline graph indicating all amino acid interactions with the ligand on each time frame.

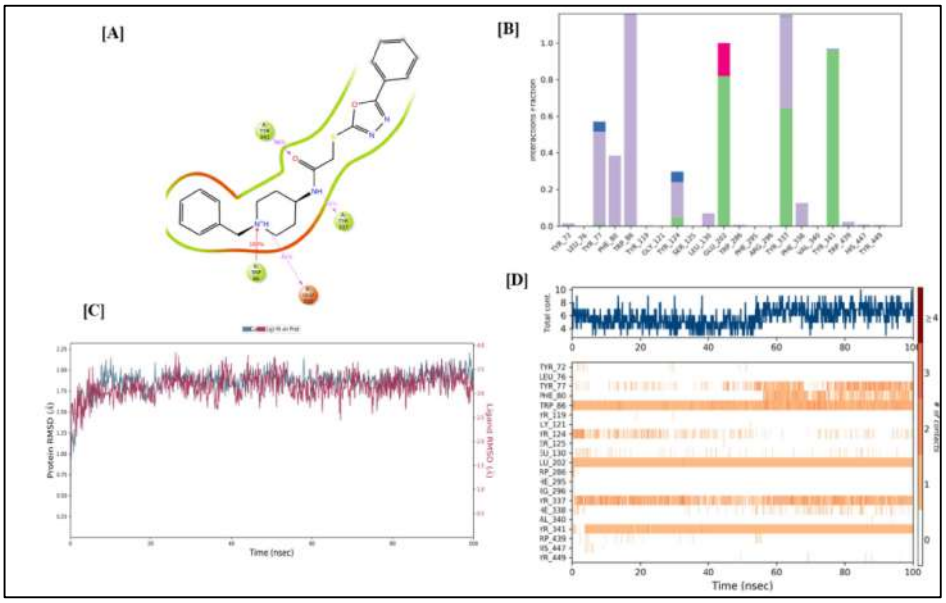

Figure 5. 23 Molecular dynamics (MD) studies of compound **5f–**hAChE (4EY7) docked complex. (A) 2D representation showing % interaction with amino acid residues in active site; B) Histogram presentation of interaction fraction with amino acid residues; C) RMSD graph of ligand-protein (**5f-**AChE) interaction of 100 ns MD; D) Timeline graph indicating all amino acid interactions with the ligand on each time frame.

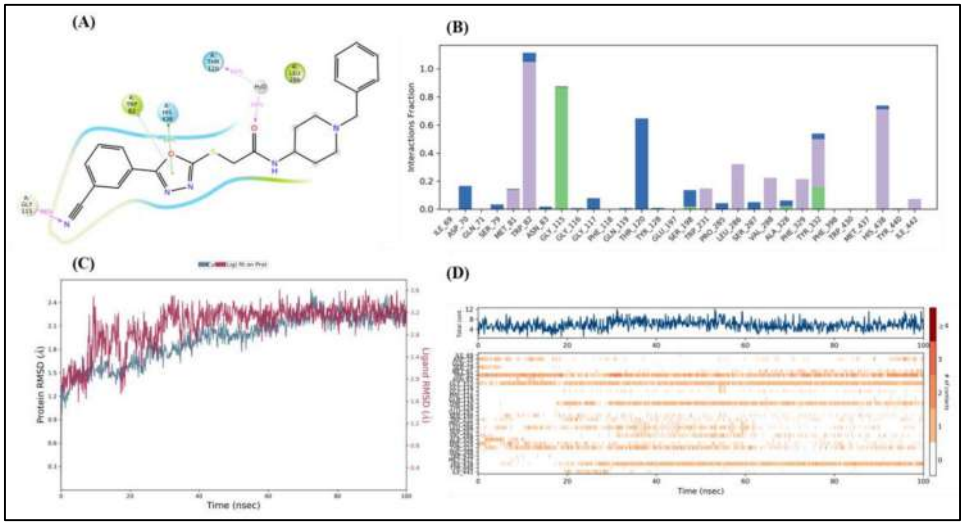

Figure 5. 24 Molecular dynamics (MD) studies of compound **5d -**BChE (4TPK) docked complex. (A) 2D representation showing % interaction with amino acid residues in active site; B) Histogram presentation of interaction fraction with amino acid residues; C) RMSD graph of ligand-protein (**5d-**BChE) interaction of 100 ns MD; D) Timeline graph indicating all amino acid.

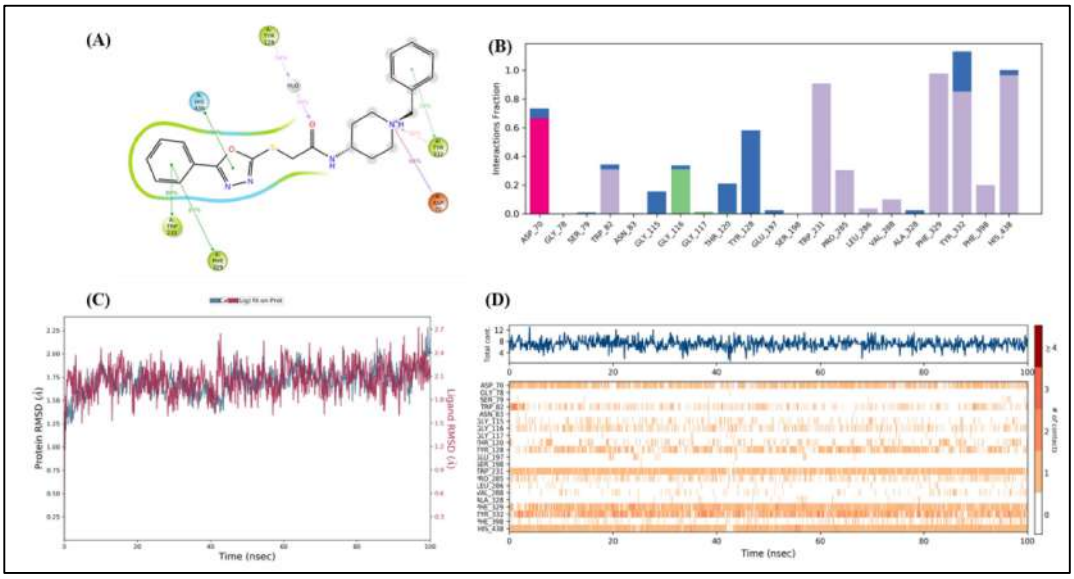

Figure 5. 25 Molecular dynamics (MD) studies of compound **5f** -BChE (4TPK) docked complex. (A) 2D representation showing % interaction with amino acid residues in active site; B) Histogram presentation of interaction fraction with amino acid residues; C) RMSD graph of ligand-protein (**5f**-BChE) interaction of 100 ns MD; D) Timeline graph indicating all amino acid interactions with the ligand on each time frame.

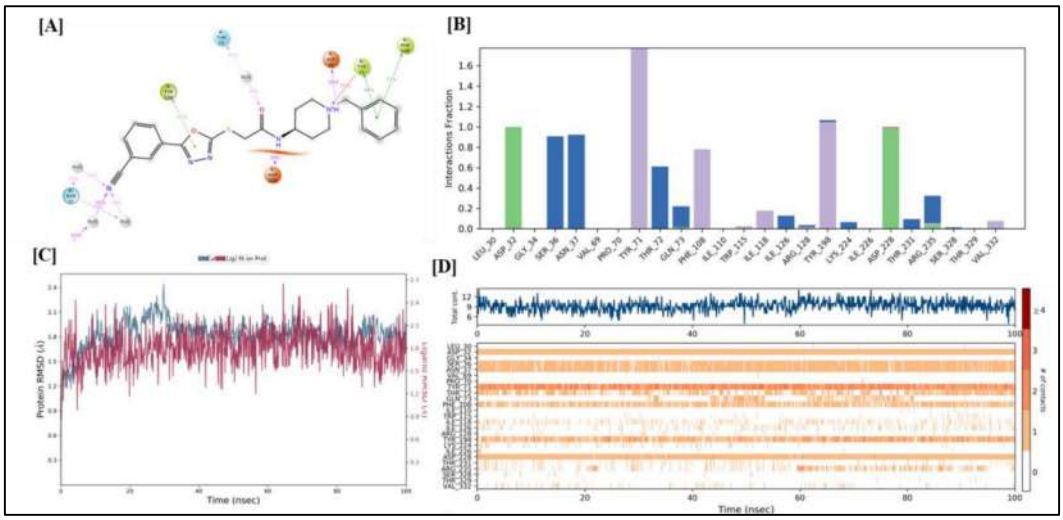

Figure 5. 26 Molecular dynamics (MD) studies of compound **5d**–BACE-1 (2ZJ7) docked complex. (A) 2D representation showing % interaction with amino acid residues in active site; B) Histogram presentation of interaction fraction with amino acid residues; C) RMSD graph of ligand-protein (**5d-**BACE-1) interaction of 100 ns MD; D) Timeline graph indicating all amino acid interactions with the ligand on each time frame.

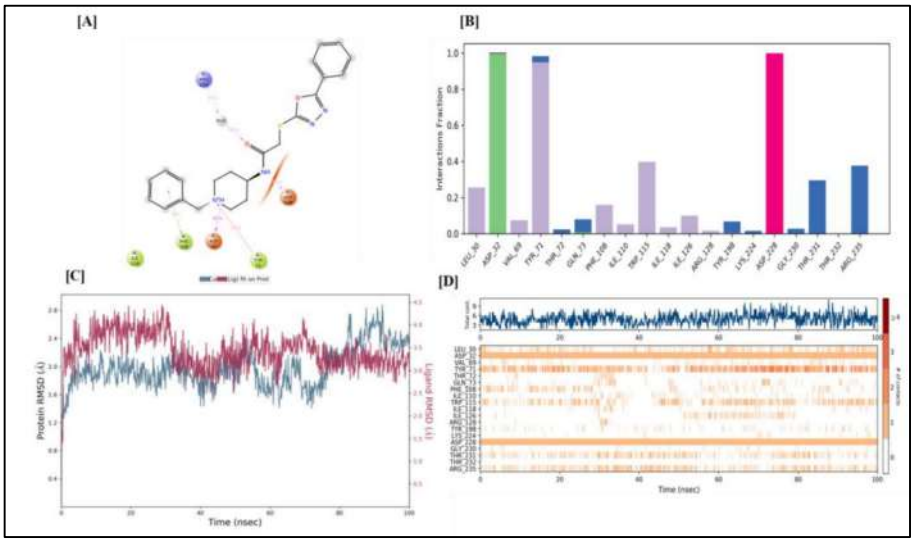

Figure 5. 27 Molecular dynamics (MD) studies of compound **5f**–BACE-1 (2ZJ7) docked complex. (A) 2D representation showing % interaction with amino acid residues in active site; B) Histogram presentation of interaction fraction with amino acid residues; C) RMSD graph of ligand-protein (**5f**-BACE-1) interaction of 100 ns MD; D) Timeline graph indicating all amino acid interactions with the ligand on each time frame.

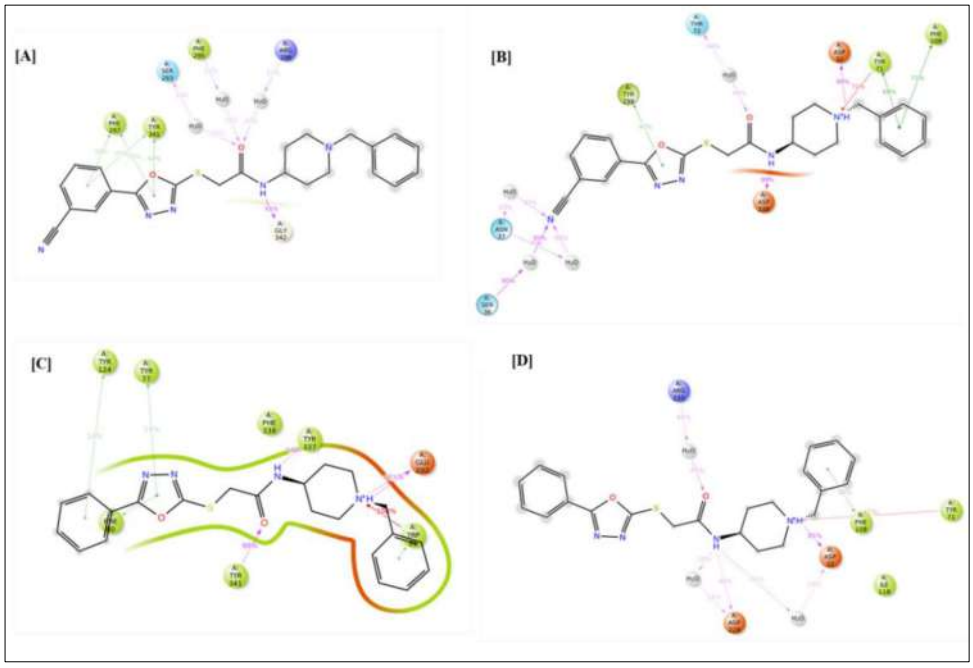

Figure 5. 28 Molecular dynamics (MD) studies of 100 ns for the compound **5d** and **5f** against AChE and BACE-1 enzyme complex showing active site molecular interactions; (A) **5d** –AChE complex B) **5d** –BACE-1 complex; C) **5f** –AChE complex; D) **5f** –BACE-1 complex.

5.2.1.6 Density function (DFT) calculation

Further, the Jaguar module of the Schrodinger 2018-1 was used for DFT analysis of the compounds **5d** and **5f** to assess their electrostatic properties**.** The frontier molecular orbitals i.e. highest occupied molecular orbitals (HOMO) and the lowest unoccupied molecular orbitals (LUMO), predict the chemical reactivity and kinetic stability of the molecules. E_{LUMO} and E_{HOMO} termed are used to designate the energies of the LUMO and HOMO states respectively.

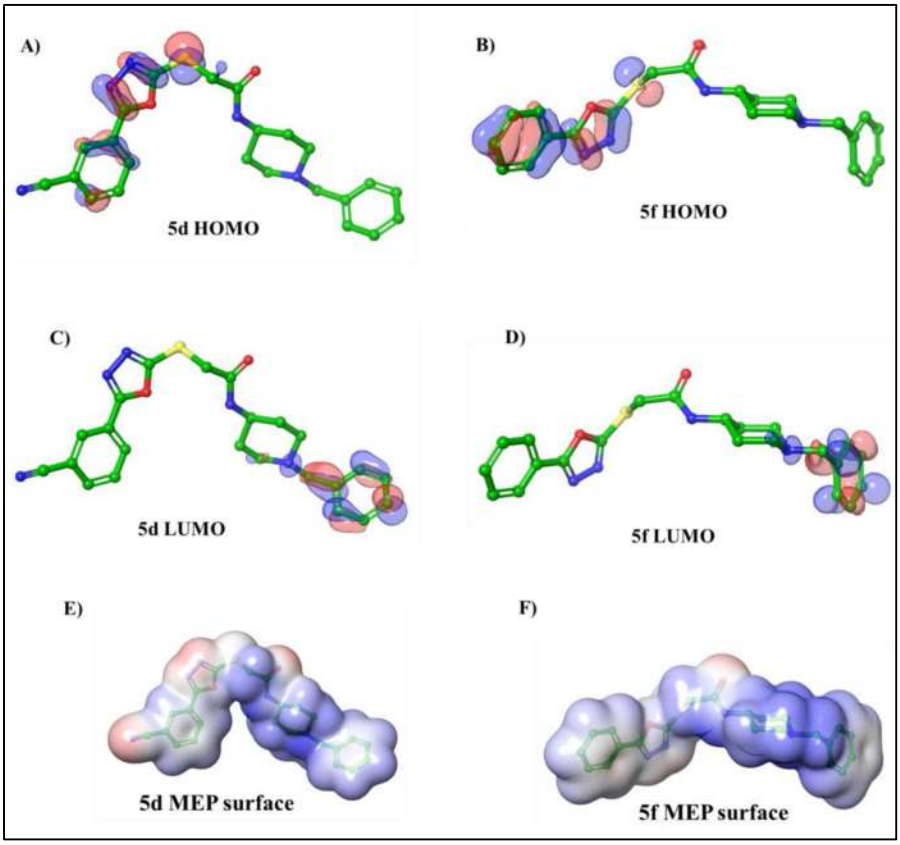

Figure 5. 29 HOMO-LUMO orbital density and molecular electrostatic potential (MEP) surface of the compound **5d** and **5f;** A & C) HOMO and LUMO orbital density of compound **5d**, B & D) HOMO and LUMO orbital density of compound **5f**; E & F) molecular electrostatic potential (MEP) surface of the compound **5d** and **5f**.

The difference between these two states is termed as HOMO-LUMO gap energy and is employed in predicting drug interaction, stability, and reactivity of the molecule. High gap energy represents increased stability and lower reactivity while low gap energy

shows decreased stability and high reactivity. Based on the HOMO and LUMO orbital density (Figure 5. 29 A-D) and energy calculated for both compounds (Table 5. 6) suggested that both possess negative energy differences between HOMO and LUMO orbital which attributes its stability and reactivity towards ChE and BACE-1 enzymes [Tripathi et al. 2023].

Table 5. 6 The energy values of HOMO and LUMO orbital and energy gap of the identified hits.

S.No.	Compound	HOMO (eV)	LUMO (eV)	Energy gap (eV)	Electrostatic potential (Kcal/mol)
1	**5d**	-0.319810	-0.152527	-0.167283	-14.77
2	**5f**	-0.296687	-0.147402	-0.149285	-13.27

The molecular electrostatic potential (MEP) surface is also calculated for compounds **5d** and **5f** to envisage more of the electrophilic and nucleophilic properties of the compounds. As depicted in Figure 5. 29 E-F, the red color represents the negative region which is around the amide C=O group, both the -N of the oxadiazole ring and the C≡N group of phenyl ring showing the favorable site prone to electrophilic attack. The blue color represents the positive region which was around the BP, S atom, and phenyl rings showcasing the site favorable for nucleophilic attack.

Further to examine the tendency of a molecule to lose or gain electrons and predict which atom is more favorable for nucleophilic or electrophilic attack a Fukui function analysis was performed. The – ve f (r) values of the atoms represented the sites prone to electrophilic attack while the + ve f (r) values indicated the atoms prone to nucleophilic attack. The Fukui function analysis of compounds **5d** and **5f** suggested that the -N atom of N-benzylpiperidine ring in both molecules is a probable site for an electrophilic attack, while the 5-phenyl oxadiazole-2-thione ring in both compounds is

more favorable for nucleophilic attack (Figure 5. 30). The overall DFT calculations suggested that both compounds are stable and have proven their binding affinity within the CAS, PAS region of the AChE, and the catalytic dyad of BACE-1 enzymes.

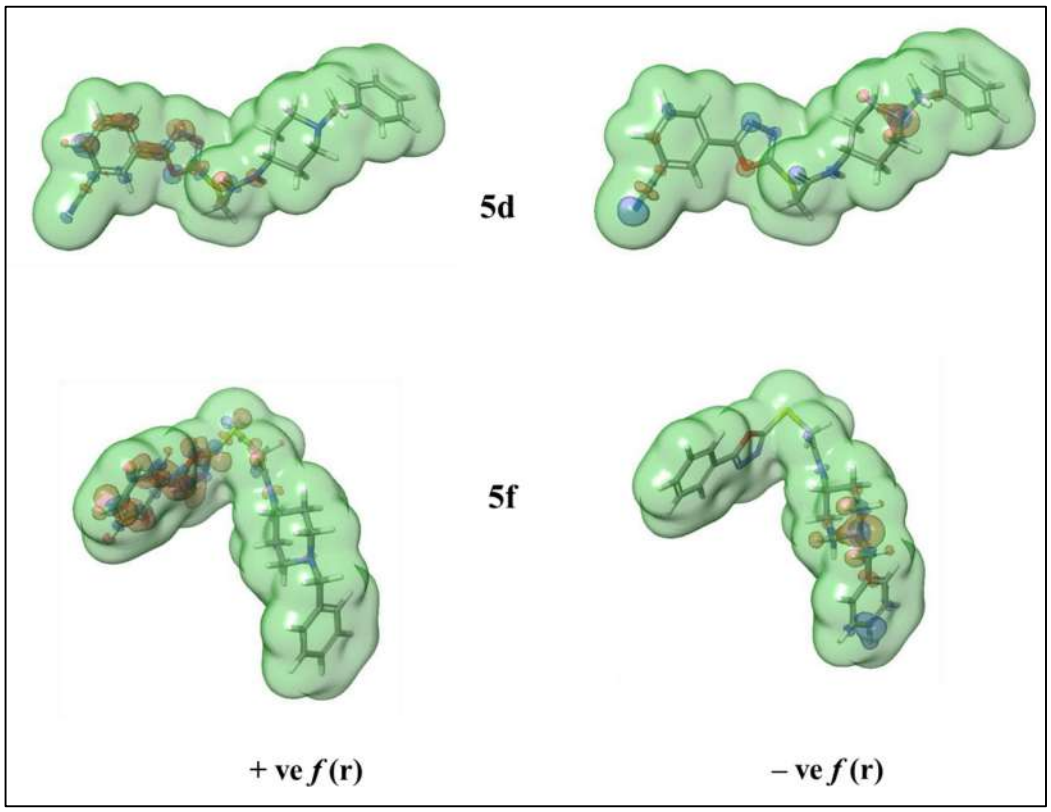

Figure 5. 30 Graphical representation of electrophilic fukui function + ve *f* (r) left column and nucleophilic fukui function– ve *f* (r) right column of the compounds **5d** and **5f**.

5.2.1.7 In-silico prediction of Drug likeness

The prediction of drug-likeness characteristics of the lead compounds was estimated using the QikProp module of the Schrodinger suite 2018-1. Some of the important physicochemical properties such as molecular weight, hydrogen bond donor (HBD), hydrogen bond acceptor (Haccep), total solvent accessible surface area (SASA) log rhythm of octanol/water partition coefficient (QPlogPo/w), brain/blood partition coefficient (QPlogBB), and the Lipinski's rule of five were predicted. The most active compounds amongst the designed series have shown no violation of the predicted

physicochemical properties and the results are mentioned in Table 5. 7. The results suggested that the representative compounds of the series have shown partition coefficient by QPlogPo/w value (**5a** = 3.99, **5d** = 2.82, **5f** = 3.50, and **5h** = 4.51) which were similar to those of the standards donepezil (4.25) and rivastigmine (2.47). The designed series of compounds were also evaluated for Lipinski's rule of five (Mol. wt.≤500, QPlogPo/w<5, acceptHB 2-20 and donorHB 0-6) and found that they were obeying the rule of five (Table 5. 7).

Table 5. 7 Predicted ADME properties of the designed series of compounds**.**

S.No.	Compound	Mol.wt.	Accept HB	Donor HB	SASA	QPlog BB	QPlog o/w	Rule of Five[a]
1	**5a**	442.96	7	1	763.93	-0.36	3.994	Yes
2	**5d**	433.52	8	1	807.98	-1.26	2.821	Yes
3	**5f**	408.51	7	1	770.17	-0.51	3.501	Yes
4	**5h**	476.51	7	1	819.08	-0.20	4.518	Yes
5	**Donepezil**	393.61	7	1	759.67	0.14	4.25	Yes
6	**Rivastigmine**	25034	5	0	553.58	0.47	2.47	Yes

AcceptHB H-bond acceptors (range 2 to 20), donorHB H-bond donors (range 0 to 6), SASA total solvent accessible surface area in square angstroms using a probe with a 1.4 Å radius (range 300 to 1000 Å), QPlog BB predicted brain/blood partition coefficient (range − 3 to 1.2), QPlog Po/w predicted log of octanol/water partition coefficient (range 2 to 6), [a] following Lipinski's rule of five.

5.2.2 Chemistry

5.2.2.1 Synthesis of Series II (4a-j) and III (5a-q) compounds: 1.3.4-oxadiazole-2-thiol linked with substituted piperazines and N-(1-benzylpiperidin-4-yl)-2-chloroacetamide (NBPC)

The targeted compounds **4a-j** and **5a-q** were synthesized in a 3-4 step synthetic protocol as depicted in schemes 2-3**.** The first step in both schemes involves the reaction of

respective benzoic acid in the presence of HOBt and EDC.HCl followed by *in situ* reaction with hydrazine hydrate provided the respective benzohydrazides **2** and **2a-q.** The structures of the compounds **2a-q** were confirmed by the FT-IR spectra where a broad signal of –OH at 3615-3540 cm^{-1} was replaced by the two stretching bands of –NH at 3426-33 cm^{-1} and a stretching band of $–NH_2$ at 3260-3135 cm^{-1} while, the ^1H NMR spectra of the compound **2** and **2a-q** have shown the presence of amide -NH- proton between 10.11-9.03 ppm, presence of $–NH_2$ proton between 5.31-4.79 ppm and the presence of aromatic protons between 7.97-7.34 ppm. Subsequently, refluxing of the benzohydrazides with carbon disulfide (CS_2) under basic conditions (potassium hydroxide in ethanol) yielded 5-phenyl-1,3,4-oxadiazole-2-thiol compounds **3** and **3a-q**. The structures of compounds **3a-q** were confirmed by ^1H NMR spectra which showed the presence of an –SH proton at 11.21- 10.34 ppm and aromatic protons at 7.98-7.26 ppm. Compounds **4a-j** were prepared by reacting ethanolic solutions of **3** with the respective substituted piperazines in the presence of formaldehyde (HCHO) to afford the N-substituted 1,3,4-oxadiazole-2(*3H*)thiones Scheme 2. All product structures were confirmed ^1H NMR and ^{13}C NMR spectra which indicated the presence of two methylene protons from 5.5-5.0 ppm, and presence of 8 aliphatic protons of the piperazine ring from 3.5-2.5 ppm while the ^{13}C NMR spectra of the compound (4a-j) showed the presence of singlet peaks of oxadiazole and aromatic ring C between 180-120 ppm, presence of aliphatic piperazinyl C between 70-40 ppm confirms the formation of the compounds. In Scheme 3, 1-benzylpiperidine-4-amine in dichloromethane (DCM) was reacted with chloroacetylchloride at cold conditions (0°C) to obtain compound N-(1-benzylpiperidin-4-yl)-2-chloroacetamid which was characterized by FT-IR and showed the presence of –NH and C=O of amide at 3354 cm^{-1} and 1685 $cm^{-}1$ while the ^1H NMR spectrum has shown the presence of 5 Ar-H

7.34-7.28 ppm, presence of –NH proton at 6.47 ppm, presence of 8-CH_2 protons of piperidine ring at 2.85-1.51 ppm and 1-CH proton at 3.85 ppm, and presence of two pairs of aliphatic –CH_2 protons at 4.05 and 3.50 ppm respectively. The final step for scheme 3 involved the refluxing of ethanolic solution of intermediate (**3 a-q**) with N-(1-benzylpiperidin-4-yl)-2-chloroacetamid in the presence of triethylamine (TEA) which leads to the formation of final compounds **(5 a-q).** Compounds **(5a-q)** were further characterized via ^{1}H NMR and showed the presence of amide –NH proton between 9.5-8 ppm, aromatic protons between 8-7 ppm, presence of two methylene proton between 4.5-3.5 ppm presence of aliphatic protons of piperidine ring between 3.5-1.25 ppm. The ^{13}C NMR spectra of the compound **(5a-q)** also showed the presence of singlet peaks of oxadiazole and aromatic ring C between 170-120 ppm, presence of aliphatic C between 65-30 ppm confirms the formation of the final compounds. The final compounds (**4a-j** and **5a-q**) were also characterized by High-resolution mass spectrometry (HRMS) for exact mass determination, and melting point for physicochemical determination.

5.2.2.2 Characterization of the synthesized compounds (Series II and III)

5.2.2.2.1 N-(1-benzylpiperidin-4-yl)-2-chloroacetamide (NBPC)

^{1}H NMR (500 MHz, $CDCl_3$) δ 7.32 (dd, *J* = 15.8, 12.6 Hz, 5H), 6.47 (d, *J* = 5.4 Hz, 1H), 4.05 (s, 2H), 3.90 – 3.79 (m, 1H), 3.52 (s, 2H), 2.84 (d, *J* = 11.5 Hz, 2H), 2.17 (dd, *J* = 17.9, 6.9 Hz, 2H), 2.02 – 1.89 (m, 2H), 1.55 (ddd, *J* = 23.6, 11.2, 3.7 Hz, 2H). ^{13}C NMR (126 MHz, $CDCl_3$) δ 165.12, 138.31, 129.08, 128.26, 127.10, 63.01, 52.07, 47.03, 42.69, 31.94, 0.01.

5.2.2.2.2 3-((4-(4-methoxyphenyl)piperazin-1-yl)methyl)-5-phenyl-1,3,4-oxadiazole-2(3H)-thione (4a)

Compound 4a was synthesized as per the described procedure D**,** an off-white solid (0.320 gm, 0.837 mmol, 74%); mp-201-203 ^{0}C, TLC (DCM: MeOH 90:10 v/v); Rf =

0.28. FT-IR (Alpha, ATR, υ cm^{-1}) 2923 (CH_2 methylene), 1512 (C=N), 1249 (C=S),; ^{1}H NMR (500 MHz, $CDCl_3$) δ 7.99 – 7.95 (m, 2H), 7.61 – 7.56 (m, 1H), 7.56 – 7.50 (m, 2H), 6.93 – 6.87 (m, 2H), 6.87 – 6.83 (m, 2H), 5.17 (s, 2H), 3.78 (d, *J* = 1.6 Hz, 3H), 3.12 (d, *J* = 4.3 Hz, 4H), 3.09 – 3.04 (m, 4H). ^{13}C NMR (126 MHz, $CDCl_3$) δ 178.31, 159.05, 154.10, 145.62, 132.42, 129.18, 126.55, 122.41, 118.64, 114.47, 70.29, 55.56, 50.86, 50.39. HRMS (m/z): Calculated 382.1463, found 382.1455 $[M+H]^+$. HPLC purity: 96.80% retention time: 3.54 min.

5.2.2.2.3 3-((4-(2-methylbenzyl)piperazin-1-yl)methyl)-5-phenyl-1,3,4-oxadiazole-2(3H)-thione (4b)

Compound 4b was synthesized as per the described procedure D, a white solid (0.387 gm, 0.863 mmol, 72%); mp 202-204 ^{0}C, TLC (DCM : MeOH 90:10 v/v); Rf = 0.31. FT-IR (Alpha, ATR, υ cm^{-1}) 2923 (CH_2 methylene), 1550 (C=N), 1231 (C=S),; ^{1}H NMR (500 MHz, $CDCl_3$) δ 7.94 (dd, *J* = 7.1, 1.4 Hz, 6H), 7.58 – 7.53 (m, 5H), 7.50 (dd, *J* = 11.5, 4.4 Hz, 7H), 7.22 (d, *J* = 7.3 Hz, 4H), 7.15 – 7.09 (m, 10H), 5.09 (s, 7H), 3.45 (s, 7H), 2.87 (s, 16H), 2.49 (s, 15H), 2.32 (s, 12H). ^{13}C NMR (126 MHz, $CDCl_3$) δ 178.30, 158.93, 137.46, 136.22, 132.35, 130.25, 129.79, 129.15, 127.06, 126.54, 125.47, 122.50, 70.46, 60.72, 53.01, 50.41, 19.22. HRMS (m/z): Calculated 380.1671, found 380.1561 $[M+H]^+$. HPLC purity: 97.50% retention time: 3.76 min.

5.2.2.2.4 3-((4-benzhydrylpiperazin-1-yl)methyl)-5-phenyl-1,3,4-oxadiazole-2(3H)-thione (4c)

Compound 4c was synthesized as per the described procedure D, an off-white solid (0.371 gm, 0.839 mmol, 70%); mp 209-211 ^{0}C, TLC (DCM : MeOH 90:10 v/v); Rf = 0.38. FT-IR (Alpha, ATR, υ cm^{-1}) 2925 (CH_2 methylene), 1497 (C=N), 1242 (C=S), ^{1}H NMR (500 MHz, $CDCl_3$) δ 7.99 (d, *J* = 7.9 Hz, 2H), 7.60 (dd, *J* = 8.0, 5.3 Hz, 1H), 7.55 (t, *J* = 6.8 Hz, 2H), 7.40 (d, *J* = 7.5 Hz, 4H), 7.27 (t, *J* = 7.5 Hz, 4H), 7.18 (dd, *J* = 7.9,

6.4 Hz, 2H), 5.11 (d, *J* = 1.7 Hz, 2H), 4.24 (s, 1H), 2.92 (s, 4H), 2.46 (s, 4H). ^{13}C NMR (126 MHz, $CDCl_3$) δ 178.38, 158.97, 142.57, 132.38, 129.19, 128.50, 127.89, 126.97, 126.58, 122.55, 76.15, 70.35, 51.77, 50.50. HRMS (m/z): Calculated 442.1827, found 442.1815 $[M+H]^+$. HPLC purity: 95.90% retention time: 3.47 min.

5.2.2.2.5 5-phenyl-3-((4-(pyridin-2-yl)piperazin-1-yl)methyl)-1,3,4-oxadiazole-2(3H)-thione (4d)

Compound 4d was synthesized as per the described procedure D, an off-white solid (0.302 gm, 0.855 mmol, 73%); mp 199-201 ^{0}C, TLC (DCM : MeOH 90:10 v/v); Rf = 0.30. FT-IR (Alpha, ATR, υ cm^{-1}) 2924 (CH_2 methylene), 1568 (C=N), 1245 (C=S), ^{1}H NMR (500 MHz, $CDCl_3$) δ 8.17 – 8.14 (m, 1H), 7.92 (dd, *J* = 7.4, 0.9 Hz, 2H), 7.58 – 7.52 (m, 1H), 7.51 – 7.42 (m, 3H), 6.64 – 6.57 (m, 2H), 5.14 (d, *J* = 0.5 Hz, 2H), 3.64 – 3.50 (m, 4H), 3.06 – 2.94 (m, 4H). ^{13}C NMR (126 MHz, $CDCl_3$) δ 178.27, 159.25, 159.05, 147.95, 137.50, 132.42, 129.16, 126.54, 122.36, 113.43, 107.17, 70.42, 50.12, 45.18. HRMS (m/z): Calculated 353.1310, found 353.2674 $[M+H]^+$. HPLC purity: 98.10% retention time: 3.04 min.

5.2.2.2.6 3-((4-(4-nitrophenyl)piperazin-1-yl)methyl)-5-phenyl-1,3,4-oxadiazole-2(3H)-thione (4e)

Compound 4e was synthesized as per the described procedure D, a yellow solid (0.340 gm, 0.856 mmol, 71%); mp 203-205 ^{0}C, TLC (DCM : MeOH 90:10 v/v); Rf = 0.32 FT-IR (Alpha, ATR, υ cm^{-1}) 2946 (CH_2 methylene), 1594 (C=N), 1249 (C=S),^{1}H NMR (500 MHz, $CDCl_3$) δ 8.14 – 8.09 (m, 2H), 7.95 (dd, *J* = 5.3, 3.3 Hz, 2H), 7.61 – 7.57 (m, 1H), 7.56 – 7.50 (m, 2H), 6.84 – 6.79 (m, 2H), 5.17 (s, 2H), 3.52 – 3.45 (m, 4H), 3.11 – 3.01 (m, 4H). ^{13}C NMR (126 MHz, $CDCl_3$) δ 178.33, 159.19, 154.64, 138.68, 132.57, 129.22, 126.54, 125.95, 122.26, 112.90, 70.08, 49.81, 47.16. HRMS (m/z):

Calculated 397.1209, found 397.1979 $[M+H]^+$. HPLC purity: 97.80% retention time: 3.17 min.

5.2.2.2.7 3-((4-(4-methylbenzyl)piperazin-1-yl)methyl)-5-phenyl-1,3,4-oxadiazole-2(3H)-thione (4f)

Compound 4f was synthesized as per the described procedure D, an off-white solid (0.338 gm, 0.889 mmol, 71%); mp 204-206 ^{0}C, TLC (DCM : MeOH 90:10 v/v); Rf = 0.29. FT-IR (Alpha, ATR, υ cm^{-1}) 2930 (CH_2 methylene), 1569 (C=N), 1229 (C=S),[1]) ^{1}H NMR (500 MHz, $CDCl_3$) δ 7.96 – 7.90 (m, 2H), 7.59 – 7.54 (m, 1H), 7.51 (dd, *J* = 10.3, 4.6 Hz, 2H), 7.17 (d, *J* = 7.9 Hz, 2H), 7.10 (d, *J* = 7.8 Hz, 2H), 5.10 (s, 2H), 3.47 (s, 2H), 2.90 (t, *J* = 4.7 Hz, 4H), 2.49 (s, 4H), 2.33 (s, 3H). ^{13}C NMR (126 MHz, $CDCl_3$) δ 178.27, 158.91, 136.70, 134.77, 132.35, 129.16, 129.15, 128.91, 126.52, 122.46, 70.35, 62.74, 52.87, 50.23, 21.08. HRMS (m/z): Calculated 380.1671, found 381.1737 $[M+H]^+$. HPLC purity: 96.60% retention time: 4.12 min.

5.2.2.2.8 3-((4-(4-fluorobenzyl)piperazin-1-yl)methyl)-5-phenyl-1,3,4-oxadiazole-2(3H)-thione (4g)

Compound 4g was synthesized as per the described procedure D, a white solid (0.347 gm, 0.903 mmol, 74%); mp 205-207 ^{0}C, TLC (DCM : MeOH 90:10 v/v); Rf = 0.31. FT-IR (Alpha, ATR, υ cm^{-1}) 2926(CH_2 methylene), 1507 (C=N), 1216(C=S), ^{1}H NMR (500 MHz, $CDCl_3$) δ 7.96 (s, 4H), 7.58 (dd, *J* = 8.3, 6.5 Hz, 4H), 7.52 (t, *J* = 7.6 Hz, 6H), 7.29 – 7.23 (m, 7H), 6.99 (dd, *J* = 12.1, 5.1 Hz, 6H), 5.11 (s, 6H), 3.47 (s, 6H), 2.91 (t, *J* = 4.6 Hz, 12H), 2.48 (s, 11H). ^{13}C NMR (126 MHz, $CDCl_3$) δ 178.28, 162.99, 161.05, 158.93, 133.68, 133.66, 132.38, 130.61, 130.55, 129.16, 126.52, 122.44, 115.10, 114.93, 70.33, 62.15, 52.83, 50.21. HRMS (m/z): Calculated 384.2420, found 385.1920 $[M+H]^+$. HPLC purity: 98.30% retention time: 3.62 min.

5.2.2.2.9 5-phenyl-3-((4-phenylpiperazin-1-yl)methyl)-1,3,4-oxadiazole-2(3H)-thione (4h)

Compound 4h was synthesized as per the described procedure D, a white solid (0.297 gm, 0.843 mmol, 70%); mp 197-199 ^{0}C, TLC (DCM : MeOH 90:10 v/v); Rf = 0.32. FT-IR (Alpha, ATR, υ cm^{-1}) 2932 (CH_2 methylene), 1597 (C=N), 1239 (C=S),^{1}H NMR (500 MHz, $CDCl_3$) δ 7.99 – 7.95 (m, 2H), 7.61 – 7.57 (m, 1H), 7.56 – 7.50 (m, 2H), 7.30 – 7.26 (m, 2H), 6.93 (dd, *J* = 8.7, 0.9 Hz, 2H), 6.90 – 6.86 (m, 1H), 5.17 (s, 2H), 3.23 (dd, *J* = 6.0, 4.0 Hz, 4H), 3.06 (dd, *J* = 6.0, 4.0 Hz, 4H). ^{13}C NMR (126 MHz, $CDCl_3$) δ 178.32, 159.07, 151.25, 132.44, 129.18, 129.14, 126.56, 122.40, 120.10, 116.48, 70.30, 50.30, 49.40. HRMS (m/z): Calculated 352.1358, found 353.1408 $[M+H]^{+}$. HPLC purity: 97.40% retention time: 3.66 min.

5.2.2.2.10 5-phenyl-3-((4-(p-tolyl)piperazin-1-yl)methyl)-1,3,4-oxadiazole-2(3H)-thione (4i)

Compound 4i was synthesized as per the described procedure D, a white solid (0.324gm, 0.885 mmol, 75%); mp 204-206 ^{0}C, TLC (DCM : MeOH 90:10 v/v); Rf = 0.33. FT-IR (Alpha, ATR, υ cm^{-1}) 2923 (CH_2 methylene), 1570 (C=N), 1256 (C=S), ^{1}H NMR (500 MHz, $CDCl_3$) δ 7.97 – 7.93 (m, 2H), 7.59 – 7.55 (m, 1H), 7.51 (t, *J* = 7.5 Hz, 2H), 7.06 (d, *J* = 8.5 Hz, 2H), 6.83 (d, *J* = 8.5 Hz, 2H), 5.15 (s, 2H), 3.21 – 3.12 (m, 4H), 3.10 – 3.00 (m, 4H), 2.26 (s, 3H). ^{13}C NMR (126 MHz, $CDCl_3$) δ 178.31, 159.05, 149.16, 132.42, 129.66, 129.18, 126.55, 122.41, 116.83, 70.31, 50.32, 49.96, 20.42. HRMS (m/z): Calculated 366.1514, found 366.1584 $[M+H]^{+}$. HPLC purity: 97.30% retention time: 3.78 min.

5.2.2.2.11 3-((4-(4-fluorophenyl)piperazin-1-yl)methyl)-5-phenyl-1,3,4-oxadiazole-2(3H)-thione (4j)

Compound 4j was synthesized as per the described procedure D, a white solid (0.327 gm, 0.884 mmol, 76%); mp 210-212 ^{0}C, TLC (DCM : MeOH 90:10 v/v); Rf = 0.38. FT-IR (Alpha, ATR, υ cm^{-1}) 2954 (CH_2 methylene), 1507 (C=N), 1235 (C=S), ^{1}H NMR (500 MHz, $CDCl_3$) δ 7.97 (d, *J* = 7.4 Hz, 2H), 7.59 (t, *J* = 7.3 Hz, 1H), 7.53 (t, *J* = 7.5 Hz, 2H), 6.97 (t, *J* = 8.7 Hz, 2H), 6.92 – 6.83 (m, 2H), 5.17 (s, 2H), 3.18 – 3.11 (m, 4H), 3.11 – 2.99 (m, 4H). ^{13}C NMR (126 MHz, $CDCl_3$) δ 178.31, 159.07, 158.33, 156.43, 147.90, 132.45, 129.19, 126.55, 122.38, 118.30, 118.24, 115.64, 115.47, 70.24, 50.39, 50.29. HRMS (m/z): Calculated 370.1264, found 370.1381 $[M+H]^+$. HPLC purity: 97.40% retention time: 3.57 min.

5.2.2.2.12 N-(1-benzylpiperidin-4-yl)-2-((5-(4-chlorophenyl)-1,3,4-oxadiazol-2-yl)thio)acetamide(5a).

Compound 5a was synthesized as per the described procedure E, an off-white solid (0.374 gm, 0.846 mmol, 65%); mp 264-266 ^{0}C, TLC (EtOAc: Hexane, 30:70 v/v); R_f= 0.47, FT-IR (Alpha, ATR, υ cm^{-1}) 3305 (N-H amide), 2935 (CH_2 methylene), 1634 (C=O) 1537 (C=N). ^{1}H NMR (500 MHz, DMSO-d_6): δ 8.30 (d, *J* = 7.5 Hz, 1H), 7.98 (d, *J* = 8.6 Hz, 2H), 7.70 – 7.59 (m, 2H), 7.36 – 7.18 (m, 5H), 4.09 (s, 2H), 3.60 – 3.51 (m, 1H), 3.43 (s, 2H), 2.71 (d, *J* = 11.4 Hz, 2H), 2.00 (t, *J* = 10.7 Hz, 2H), 1.71 (d, *J* = 10.1 Hz, 2H), 1.40 (td, *J* = 14.3, 3.5 Hz, 2H). ^{13}C NMR (126 MHz, DMSO- d_6): δ 165.62, 164.78, 164.21, 137.22, 130.07, 129.18, 128.65, 128.62, 127.33, 122.36, 62.54, 52.12, 36.39, 31.81. HRMS (m/z): Calculated 442.1230, found 443.1266 $[M+H]^+$. HPLC purity: 97.30% retention time: 6.35 min.

5.2.2.2.13 N-(1-benzylpiperidin-4-yl)-2-((5-(4-nitrophenyl)-1,3,4-oxadiazol-2-yl)thio)acetamide (5b)

Compound 5b was prepared following procedure E, a yellow solid, (0.381 gm, 0.841 mmol, 68%); mp 259-261 ^{0}C, TLC (EtOAc: Hexane, 30:70 v/v); R_f= 0.51, FT-IR (Alpha, ATR, υ cm^{-1}) 3303 (N-H amide), 2965 (CH_2 methylene), 1637 (C=O) 1517 (C=N). ^{1}H NMR (500 MHz, DMSO-d_6): δ 8.45 – 8.38 (m, 2H), 8.34 (d, *J* = 8.4 Hz, 1H), 8.26 – 8.19 (m, 2H), 7.39 – 7.20 (m, 5H), 4.14 (s, 2H), 3.57 (s, 1H), 3.49 (s, 1H), 2.76 (s, 2H), 2.08 (s, 2H), 1.74 (d, *J* = 10.7 Hz, 2H), 1.43 (d, *J* = 10.5 Hz, 2H). ^{13}C NMR (126 MHz, DMSO- d_6): δ 166.26, 164.88, 164.13, 147.9, 130.72, 129.82, 128.57, 128.27, 127.36, 122.64, 62.44, 52.22, 36.94, 31.21. HRMS (m/z): Calculated 453.1471, found 454.1514 $[M+H]^+$. HPLC purity: 95.80% retention time: 3.79 min.

5.2.2.2.14 N-(1-benzylpiperidin-4-yl)-2-((5-(4-(trifluoromethoxy)phenyl)-1,3,4-oxadiazol-2yl)thio)acetamide (5c)

Compound 5c was prepared following procedure E, a light green solid, (0.416 gm, 0.845 mmol, 72%); mp 267-269 ^{0}C, TLC (EtOAc: Hexane, 30:70 v/v); R_f= 0.57, FT-IR (Alpha, ATR, υ cm^{-1}) 3296 (N-H amide), 2923 (CH_2 methylene), 1632 (C=O) 1544 (C=N) 1210 (C=S). ^{1}H NMR (500 MHz, DMSO-d_6): δ 8.30 (d, *J* = 7.5 Hz, 1H), 8.15 – 8.06 (m, 2H), 7.59 (s, 2H), 7.31 – 7.22 (m, 5H), 4.10 (s, 2H), 3.57 – 3.51 (m, 1H), 3.43 (s, 2H), 2.71 (d, *J* = 11.5 Hz, 2H), 2.00 (t, *J* = 10.7 Hz, 2H), 1.78 – 1.64 (m, 2H), 1.40 (td, *J* = 14.6, 3.7 Hz, 2H). ^{13}C NMR (126 MHz, DMSO- d_6): δ 165.60, 129.24, 129.17, 128.61, 127.32, 122.28, 62.55, 52.13, 36.42, 31.84. HRMS (m/z): Calculated 492.1443, found 493.1473 $[M+H]^+$. HPLC purity: 96.80% retention time: 7.43 min.

5.2.2.2.15 N-(1-benzylpiperidin-4-yl)-2-((5-(3-cyanophenyl)-1,3,4-oxadiazol-2-yl)thio)acetamide (5d)

Compound **5d** was prepared following procedure E, an off-white solid, (0.377 gm, 0.870 mmol, 76%); mp 263-265 ^{0}C, TLC (EtOAc: Hexane, 30:70 v/v); R_f= 0.61, FT-IR (Alpha, ATR, υ cm^{-1}) 3297 (N-H amide), 2926 (CH_2 methylene), 1651 (C=O) 1532 (C=N) 1259 (C=S). ^{1}H NMR (500 MHz, DMSO- d_6): δ 8.41 (d, *J* = 1.5 Hz, 1H), 8.30 (ddd, *J* = 8.0, 6.8, 4.4 Hz, 2H), 8.11 (dd, *J* = 7.8, 1.4 Hz, 1H), 7.82 (t, *J* = 7.9 Hz, 1H), 7.37 – 7.19 (m, 5H), 4.12 (s, 2H), 3.60 – 3.52 (m, 1H), 3.43 (s, 2H), 2.71 (d, *J* = 10.2 Hz, 2H), 2.01 (s, 2H), 1.71 (d, *J* = 10.2 Hz, 2H), 1.40 (td, *J* = 14.3, 3.4 Hz, 2H). ^{13}C NMR (126 MHz, DMSO- d_6): δ 165.61, 164.77, 164.05, 135.83, 131.26, 130.36, 129.17, 128.63, 113.15, 52.11, 36.32, 31.83. HRMS (m/z): Calculated 433.1572, found 434.1603 $[M+H]^+$. HPLC purity: 98.90% retention time: 2.95 min.

5.2.2.2.16 N-(1-benzylpiperidin-4-yl)-2-((5-(2-nitrophenyl)-1,3,4-oxadiazol-2-yl)thio)acetamide (5e)

Compound 5e was prepared following procedure E, a yellow solid, (0.372 gm, 0.821 mmol, 77%); mp 262-264 ^{0}C, TLC (EtOAc: Hexane, 30:70 v/v); R_f= 0.54, FT-IR (Alpha, ATR, υ cm^{-1}) 3310 (N-H amide), 2911 (CH_2 methylene), 1654 (C=O) 1538 (C=N) 1244 (C=S). H NMR (500 MHz, DMSO- d_6): δ 8.37 – 8.33 (m, 2H), 8.31 (d, *J* = 7.3 Hz, 1H), 8.23 – 8.16 (m, 2H), 7.35 – 7.17 (m, 5H), 4.11 (s, 2H), 3.51 (s, 1H), 3.42 (s, 1H), 2.71 (s, 2H), 2.03 (s, 2H), 1.69 (d, *J* = 9.6 Hz, 2H), 1.38 (d, *J* = 9.4 Hz, 2H). ^{13}C NMR (126 MHz, DMSO- d_6): δ 164.34, 163.19, 163.08, 144.82, 128.69, 128.48, 128.24, 127.96, 127.54, 121.25, 60.82, 51.33, 34.73, 29.46. HRMS (m/z): Calculated 453.1471, found 454.1173 $[M+H]^+$. HPLC purity: 96.40% retention time: 3.54 min.

5.2.2.2.17 N-(1-benzylpiperidin-4-yl)-2-((5-phenyl-1,3,4-oxadiazol-2-yl)thio)acetamide (5f)

Compound **5f** was prepared following procedure E, a white solid, (0.327 gm, 0.801 mmol, 80%); mp 261-263 ^{0}C, TLC (EtOAc: Hexane, 30:70 v/v); R_f= 0.59, FT-IR (Alpha, ATR, υ cm^{-1}) 3316 (N-H amide), 2924(CH_2 methylene), 1641 (C=O) 1541 (C=N) 1180 (C=S). ^{1}H NMR (500 MHz, DMSO- d_6): δ 8.32 (d, *J* = 7.5 Hz, 1H), 8.02 – 7.92 (m, 2H), 7.65 – 7.57 (m, 3H), 7.34 – 7.22 (m, 5H), 4.09 (s, 2H), 3.58 – 3.52 (m, 1H), 3.44 (s, 2H), 2.71 (d, *J* = 11.0 Hz, 2H), 2.00 (t, *J* = 10.5 Hz, 2H), 1.71 (d, *J* = 9.9 Hz, 2H), 1.40 (td, *J* = 14.4, 3.5 Hz, 2H). ^{13}C NMR (126 MHz, DMSO) δ 165.67, 165.52, 163.91, 132.52, 129.90, 129.21, 128.63, 127.35, 126.84, 123.45, 62.52, 52.12, 47.10, 36.36, 31.80. HRMS (m/z): Calculated 408.1620, found 409.1667 $[M+H]^{+}$. HPLC purity: 97.90% retention time: 3.73 min.

5.2.2.2.18 N-(1-benzylpiperidin-4-yl)-2-((5-(3-chlorophenyl)-1,3,4-oxadiazol-2-yl)thio)acetamide (5g)

Compound 5g was prepared following procedure E, a yellow solid, (0.373 gm, 0.843 mmol, 72%); mp 262-264 ^{0}C, TLC (EtOAc: Hexane, 30:70 v/v); R_f= 0.57, FT-IR (Alpha, ATR, υ cm^{-1}) 3287 (N-H amide), 2929 (CH_2 methylene), 1631 (C=O) 1522 (C=N) 1214 (C=S).^{1}H NMR (500 MHz, DMSO-d_6): δ 8.32 (d, *J* = 7.1 Hz, 1H), 8.02 (d, *J* = 8.3 Hz, 2H), 7.73 – 7.62 (m, 2H), 7.39 – 7.22 (m, 5H), 4.12 (s, 2H), 3.63 – 3.54 (m, 1H), 3.46 (s, 2H), 2.78 (d, *J* = 10.2 Hz, 2H), 2.09 (t, *J* = 9.4 Hz, 2H), 1.75 (d, *J* = 9.3 Hz, 2H), 1.44 (td, *J* = 13.4, 3.2 Hz, 2H). ^{13}C NMR (126 MHz, DMSO- d_6): δ 165.57, 164.88, 164.39, 137.48, 130.13, 129.53, 128.48, 128.23, 127.13, 122.55, 62.98, 52.26, 36.41, 31.38. HRMS (m/z): Calculated 442.1230, found 443.1107 $[M+H]^{+}$. HPLC purity: 97.20% retention time: 3.29 min.

5.2.2.2.19 N-(1-benzylpiperidin-4-yl)-2-((5-(4-(trifluoromethyl)phenyl)-1,3,4-oxadiazol-2yl)thio)acetamide (5h)

Compound 5h was prepared following procedure E, a yellow solid, (0.412 gm, 0.865 mmol, 79%); mp 268-270 ^{0}C, TLC (EtOAc: Hexane, 30:70 v/v); R_f= 0.62, FT-IR (Alpha, ATR, υ cm^{-1}) 3293 (N-H amide), 2924 (CH_2 methylene), 1631 (C=O) 1548 (C=N) 1186 (C=S).^{1}H NMR (500 MHz, DMSO- d_6): δ 8.32 (d, *J* = 7.5 Hz, 1H), 8.19 (d, *J* = 8.2 Hz, 2H), 7.98 (d, *J* = 8.3 Hz, 2H), 7.38 – 7.18 (m, 5H), 4.13 (s, 2H), 3.58 – 3.50 (m, 1H), 3.43 (s, 2H), 2.71 (d, *J* = 11.4 Hz, 2H), 2.00 (t, *J* = 10.6 Hz, 2H), 1.71 (d, *J* = 10.0 Hz, 2H), 1.46 – 1.31 (m, 2H). ^{13}C NMR (126 MHz, DMSO) δ 165.54, 164.92, 164.49, 139.06, 129.16, 128.61, 127.71, 127.31, 126.87, 62.57, 52.15, 36.44, 31.86. HRMS (m/z): Calculated 476.1494, found 477.1231 $[M+H]^+$. HPLC purity: 98.40% retention time: 3.54 min.

5.2.2.2.20 N-(1-benzylpiperidin-4-yl)-2-((5-(2,4-dichlorophenyl)-1,3,4-oxadiazol-2-yl)thio)acetamide (5i)

Compound 5i was prepared following procedure E, a white solid, (0.398 gm, 0.834 mmol, 72%); mp 262-264 ^{0}C, TLC (EtOAc: Hexane, 30:70 v/v); R_f= 0.55, FT-IR (Alpha, ATR, υ cm^{-1}) 3248 (N-H amide), 2925 (CH_2 methylene), 1645 (C=O) 1556 (C=N) 1196 (C=S). ^{1}H NMR (500 MHz, DMSO- d_6): δ 8.32 (d, *J* = 7.5 Hz, 1H), 7.99 (d, *J* = 8.5 Hz, 1H), 7.93 (d, *J* = 2.0 Hz, 1H), 7.66 (dd, *J* = 8.5, 2.1 Hz, 1H), 7.39 – 7.19 (m, 5H), 4.11 (s, 2H), 3.55 (d, *J* = 6.5 Hz, 1H), 3.45 (s, 2H), 2.73 (s, 2H), 2.03 (s, 2H), 1.72 (d, *J* = 11.0 Hz, 2H), 1.40 (dd, *J* = 20.5, 10.4 Hz, 2H). ^{13}C NMR (126 MHz, DMSO) δ 165.50, 164.78, 162.91, 137.64, 133.20, 132.72, 131.24, 129.29, 128.66, 121.60, 52.09, 46.69, 36.40, 31.67. HRMS (m/z): Calculated 476.0841, found 477.1004 $[M+H]^+$. HPLC purity: 96.30% retention time: 3.78 min.

5.2.2.2.21 N-(1-benzylpiperidin-4-yl)-2-((5-(4-hydroxyphenyl)-1,3,4-oxadiazol-2-yl)thio)acetamide (5j)

Compound 5j was prepared following procedure E, a yellowish-brown solid, (0.361 gm, 0.851 mmol, 67%); mp 259-261 ^{0}C, TLC (EtOAc: Hexane, 30:70 v/v); R_f= 0.47, FT-IR (Alpha, ATR, υ cm^{-1}) 3295 (N-H amide), 2921 (CH_2 methylene), 1631 (C=O) 1519 (C=N) 1201 (C=S). 1H NMR (500 MHz, DMSO- d_6): δ 9.67 (s, 1H), 8.35 (d, J = 7.3 Hz, 2H), 8.08 (dd, J = 43.2, 8.9 Hz, 3H), 7.89 (t, J = 9.4 Hz, 3H), 7.66 – 7.47 (m, 6H), 7.09 – 6.83 (m, 3H), 6.48 (dddd, J = 34.9, 22.1, 11.8, 7.3 Hz, 7H), 4.41 – 4.29 (m, 2H), 4.17 – 4.01 (m, 6H), 3.14 (dd, J = 15.4, 7.8 Hz, 5H), 2.88 (s, 6H), 2.34 – 2.17 (m, 5H), 2.14 (s, 4H). HRMS (m/z): Calculated 424.1569, found 425.1236 $[M+H]^+$. HPLC purity: 96.80% retention time: 3.44 min.

5.2.2.2.22 2-((5-(4-aminophenyl)-1,3,4-oxadiazol-2-yl)thio)-N-(1-benzylpiperidin-4-yl)acetamide (5k)

Compound 5k was prepared following procedure E, a white solid, (0.316 gm, 0.747 mmol, 61%); mp 257-259 ^{0}C, TLC (EtOAc: Hexane, 30:70 v/v); R_f= 0.49, FT-IR (Alpha, ATR, υ cm^{-1}) 3291 (N-H amide), 2931 (CH_2 methylene), 1644 (C=O) 1529 (C=N) 1224 (C=S). 1H NMR (500 MHz, DMSO- d_6): δ 8.29 (d, J = 7.5 Hz, 2H), 8.13 (dd, J = 44.1, 7.8 Hz, 3H), 7.97 (t, J = 9.5 Hz, 3H), 7.64 – 7.44 (m, 6H), 7.01 – 6.77 (m, 3H), 6.42 (dddd, J = 34.3, 22.7, 11.2, 7.8 Hz, 7H), 5.24 (s, 2H), 4.36 – 4.25 (m, 2H), 4.13 – 4.04 (m, 6H), 3.10 (dd, J = 15.1, 7.3 Hz, 5H), 2.82 (s, 6H), 2.30 – 2.13 (m, 5H), 2.09 (s, 4H). HRMS (m/z): Calculated 423.1729, found 423.1729 $[M+H]^+$. HPLC purity: 96.10% retention time: 3.18 min.

5.2.2.2.23 N-(1-benzylpiperidin-4-yl)-2-((5-(3-methoxyphenyl)-1,3,4-oxadiazol-2-yl)thio)acetamide (5l)

Compound 5l was prepared following procedure E, a white solid, (0.351 gm, 0.801 mmol, 78%); mp 269-271 ^{0}C, TLC (EtOAc: Hexane, 30:70 v/v); R_f= 0.61, FT-IR (Alpha, ATR, υ cm^{-1}) 3290 (N-H amide), 2925 (CH_2 methylene), 1655 (C=O) 1549 (C=N) 1241 (C=S). ^{1}H NMR (500 MHz, DMSO- d_6): δ 8.29 (d, *J* = 7.5 Hz, 1H), 7.91 (d, *J* = 8.9 Hz, 2H), 7.36 – 7.20 (m, 5H), 7.14 (d, *J* = 9.0 Hz, 2H), 4.07 (s, 2H), 3.85 (d, *J* = 5.9 Hz, 3H), 3.58 – 3.49 (m, 1H), 3.42 (s, 2H), 2.71 (d, *J* = 11.4 Hz, 2H), 2.00 (t, *J* = 10.7 Hz, 2H), 1.71 (d, *J* = 10.3 Hz, 2H), 1.40 (td, *J* = 14.4, 3.6 Hz, 2H). ^{13}C NMR (126 MHz, DMSO) δ 165.68, 165.49, 163.06, 162.52, 139.06, 129.16, 128.73, 128.62, 127.31, 115.83, 115.33, 62.56, 56.01, 52.15, 47.10, 36.39, 31.86. HRMS (m/z): Calculated 438.1725, found 439.1421 $[M+H]^+$. HPLC purity: 97.80% retention time: 3.79 min.

5.2.2.2.24 N-(1-benzylpiperidin-4-yl)-2-((5-(4-methoxyphenyl)-1,3,4-oxadiazol-2-yl)thio)acetamide (5m)

Compound 5m was prepared following procedure E, a white solid, (0.347 gm, 0.792 mmol, 77%); mp 268-270 ^{0}C, TLC (EtOAc: Hexane, 30:70 v/v); R_f= 0.59, FT-IR (Alpha, ATR, υ cm^{-1}) 3288 (N-H amide), 2927 (CH_2 methylene), 1644 (C=O) 1553 (C=N) 1255 (C=S). ^{1}H NMR (500 MHz, DMSO) δ 8.28 (d, *J* = 7.5 Hz, 1H), 7.91 (d, *J* = 8.9 Hz, 2H), 7.36 – 7.21 (m, 5H), 7.13 (d, *J* = 9.0 Hz, 2H), 4.07 (s, 2H), 3.84 (d, *J* = 5.9 Hz, 3H), 3.59 – 3.50 (m, 1H), 3.42 (s, 2H), 2.70 (d, *J* = 11.4 Hz, 2H), 1.99 (t, *J* = 10.7 Hz, 2H), 1.70 (d, *J* = 10.3 Hz, 2H), 1.39 (td, *J* = 14.4, 3.6 Hz, 2H). ^{13}C NMR (126 MHz, DMSO) δ 165.68, 165.49, 163.06, 162.52, 139.06, 129.16, 128.73, 128.62, 127.31, 115.83, 115.33, 62.56, 56.01, 52.15, 47.10, 36.39, 31.86. HRMS (m/z):

Calculated 438.1726, found 439.1527 $[M+H]^+$. HPLC purity: 98.03% retention time: 3.02 min.

5.2.2.2.25 N-(1-benzylpiperidin-4-yl)-2-((5-(4-chloro-3-nitrophenyl)-1,3,4-oxadiazol-2-yl)thio)acetamide (5n)

Compound 5n was prepared following procedure E, a yellowish brown solid, (0.375 gm, 0.770 mmol, 66%); mp 267-269 ^{0}C, TLC (EtOAc: Hexane, 30:70 v/v); R_f= 0.62, FT-IR (Alpha, ATR, υ cm^{-1}) 3316 (N-H amide), 2928 (CH_2 methylene), 1629 (C=O) 1546 (C=N) 1231 (C=S).^{1}H NMR (500 MHz, DMSO-d_6): δ 8.54 (s,1H), 8.41 (d, J = 7.2 Hz, 1H), 8.14 (s, 1H), 8.10 (d, J = 6.8 Hz, 1H), 7.45 – 7.26 (m, 5H), 4.14 (s, 2H), 3.63 – 3.55 (m, 1H), 3.47 (s, 2H), 2.77 (d, J = 9.8 Hz, 2H), 2.23 (t, J = 9.2 Hz, 2H), 1.76 (d, J = 9.4 Hz, 2H), 1.48 (td, J = 13.6, 3.1 Hz, 2H). ^{13}C NMR (126 MHz, DMSO- d_6): δ 168.56, 167.24, 165.62, 164.78, 164.21, 137.22, 130.07, 129.18, 128.65, 128.62, 127.33, 122.36, 62.54, 52.12, 36.39, 31.81 HRMS (m/z): Calculated 487.1081, found 488.1011 $[M+H]^+$. HPLC purity: 97.70% retention time: 3.21 min.

5.2.2.2.26 N-(1-benzylpiperidin-4-yl)-2-((5-(2,4-dinitrophenyl)-1,3,4-oxadiazol-2-yl)thio)acetamide (5o)

Compound 5o was prepared following procedure E, a yellow solid, (0.386 gm, 0.775 mmol, 69%); mp 270-272 ^{0}C, TLC (EtOAc: Hexane, 30:70 v/v); R_f= 0.64, FT-IR (Alpha, ATR, υ cm^{-1}) 3304 (N-H amide), 2921 (CH_2 methylene), 1648 (C=O) 1511 (C=N) 1220 (C=S). ^{1}H NMR (500 MHz, DMSO-d_6): δ 8.54 (s, 1H), 8.49 (d, J = 8.5 Hz, 1H), 8.42 (s, 1H), 8.16 (d, J = 8.7 Hz, 1H), 7.40 – 7.29 (m, 5H), 4.16 (s, 2H), 3.66 – 3.58 (m, 1H), 3.51 (s, 2H), 2.81 (d, J = 8.8 Hz, 2H), 2.27 (t, J = 9.5 Hz, 2H), 1.79 (d, J = 9.1 Hz, 2H), 1.53 (td, J = 13.9, 3.7 Hz, 2H). ^{13}C NMR (126 MHz, DMSO- d_6): δ 170.53, 170.22, 167.64, 165.89, 165.13, 138.39, 131.72, 130.47, 129.67, 129.43,

128.42, 123.66, 63.49, 53.54, 37.45, 32.81. HRMS (m/z): Calculated 498.1322, found 499.1132 $[M+H]^+$. HPLC purity: 98.10% retention time: 3.22 min.

5.2.2.2.27 N-(1-benzylpiperidin-4-yl)-2-((5-(2-bromophenyl)-1,3,4-oxadiazol-2-yl)thio)acetamide (5p)

Compound 5p was prepared following procedure E, an off white solid, (0.347 gm, 0.712 mmol, 82%); mp 268-270 ^{0}C, TLC (EtOAc: Hexane, 30:70 v/v); R_f= 0.59, FT-IR (Alpha, ATR, υ cm^{-1}) 3298 (N-H amide), 2934 (CH_2 methylene), 1654 (C=O) 1541 (C=N) 1237 (C=S).^{1}H NMR (500 MHz, DMSO- d_6): δ 8.33 (d, *J* = 7.4 Hz, 2H), 8.04 (dd, *J* = 44.6, 8.6 Hz, 3H), 7.86 (t, *J* = 9.1 Hz, 3H), 7.61 – 7.43 (m, 6H), 7.00 – 6.80 (m, 3H), 6.40 (dddd, *J* = 35.7, 21.3, 11.1, 7.8 Hz, 7H), 4.38 – 4.24 (m, 2H), 4.15 – 3.97 (m, 6H), 3.09 (dd, *J* = 14.5, 7.2 Hz, 5H), 2.81 (s, 6H), 2.30 – 2.16 (m, 5H), 2.09 (s, 4H). HRMS (m/z): Calculated 486.0725, found 487.0025 $[M+H]^+$. HPLC purity: 96.80% retention time: 3.31 min.

5.2.2.2.28 N-(1-benzylpiperidin-4-yl)-2-((5-(2,4-dihydroxyphenyl)-1,3,4-oxadiazol-2-yl)thio)acetamide (5q)

Compound 5q was prepared following procedure E, an off-white solid, (0.331 gm, 0.752 mmol, 78%); mp 262-264 ^{0}C, TLC (EtOAc: Hexane, 30:70 v/v); R_f= 0.49, FT-IR (Alpha, ATR, υ cm^{-1}) 3315 (N-H amide), 2932 (CH_2 methylene), 1638 (C=O) 1544 (C=N) 1216 (C=S). ^{1}H NMR (500 MHz, DMSO-d_6): δ 8.54 (s,1H), 8.41 (d, *J* = 7.2 Hz, 1H), 8.14 (s, 1H), 8.10 (d, *J* = 6.8 Hz, 1H), 7.45 – 7.26 (m, 5H), 4.14 (s, 2H), 3.63 – 3.55 (m, 1H), 3.47 (s, 2H), 2.77 (d, *J* = 9.8 Hz, 2H), 2.23 (t, *J* = 9.2 Hz, 2H), 1.76 (d, *J* = 9.4 Hz, 2H), 1.48 (td, *J* = 13.6, 3.1 Hz, 2H). ^{13}C NMR (126 MHz, DMSO- d_6): δ 168.56, 167.24, 165.62, 164.78, 164.21, 137.22, 130.07, 129.18, 128.65, 128.62, 127.33, 122.36, 62.54, 52.12, 36.39, 31.81. HRMS (m/z): Calculated 440.1518, found 441.1401 $[M+H]^+$. HPLC purity: 97.80% retention time: 3.14 min.

5.2.1.2.29 Single crystal X-ray crystallography

Compound **5f** was successfully converted into needle shape crystals in ethanol on slow evaporation method. Single crystal X-ray diffraction data of **5f** collected at 100 K displays that it crystallizes in the triclinic *P*-1 space group Figure 5. 31. The asymmetric unit of **5f** comprises two identical ligand units where the amide oxygen atoms (O2 and O4) form a strong hydrogen bonding interaction (N7-H7…O2, N7….O2 = 2.842 Å and N3-H3…O4, N3….O4 = 2.862 Å) with the neighboring ligand unit (Table S1)[Barbour 2020, Blessing 1995, Sheldrick 2008].

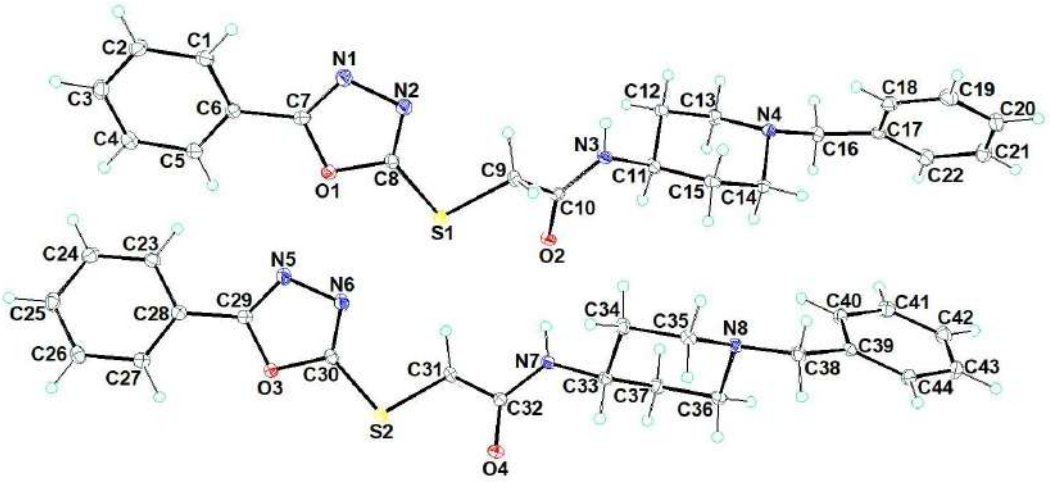

Figure 5. 31 ORTEP diagram of compound **5f** obtained at 100 K

Table 5. 8 Crystallographic data for compound **5f**

Crystal data and structure refinement for 5f	
Identification code	**5f**
Empirical formula	$C_{22}H_{24}N_4O_2S$
Formula weight	408.51
Temperature/K	100(2)
Crystal system	triclinic
Space group	P-1
a/Å	9.2875(3)
b/Å	9.9964(3)
c/Å	22.3023(7)

α/°	81.5170(10)
β/°	82.6330(10)
γ/°	89.5110(10)
Volume/Å^3	2030.91(11)
Z	4
ρ_{calc}g/cm^3	1.336
μ/mm^{-1}	0.186
F(000)	864.0
Crystal size/mm^3	0.3 × 0.28 × 0.23
Radiation	MoKα (λ = 0.71073)
2Θ range for data collection/°	4.264 to 50.7
Index ranges	-11 ≤ h ≤ 11, -11 ≤ k ≤ 12, -26 ≤ l ≤ 26
Reflections collected	27966
Independent reflections	7430 [R_{int} = 0.0307, R_{sigma} = 0.0289]
Data/restraints/parameters	7430/0/523
Goodness-of-fit on F^2	1.031
Final R indexes [I>=2σ (I)]	R_1 = 0.0327, wR_2 = 0.0751
Final R indexes [all data]	R_1 = 0.0407, wR_2 = 0.0794
Largest diff. peak/hole / e Å^{-3}	0.23/-0.29
CCDC number	2236383

5.2.3 Biological Evaluation

5.2.3.1 Pharmacology (In-vitro studies)

In considering the multifaceted pathophysiology involved in the early and late progression of the disease, the multi-targeting inhibitory effects are by design less selective while maintaining adequate potency for each target. Donepezil is a widely used FDA-approved drug that has inhibitory properties toward three enzymes but provides only symptomatic relief to the patient. The present series of molecules were designed to inhibit multiple targets. The ChE and BACE-1 inhibition is mainly considered to stop the progression of the disease. The desired inhibitory concentrations

against multiple targets to translate require submicromolar potency to minimize dose and avoid unwanted side effects. For the restoration of the behavioral alterations, the dose of standard donepezil was considered a gold standard for ChE inhibition. However, the BACE-1 inhibition potency needed to achieve effective anti-A*β* aggregation and anti-neuroinflammatory is considered a key differentiating feature for new drug design. Based on these assumptions, the present series of molecules were tested *in vitro* against hAChE, hBChE, and hBACE-1 enzymes to establish selectivity followed by cellular and *in vivo* testing to establish additional effects.

5.2.3.1.1 Human Cholinesterase (hAChE and hBChE) inhibition assay

The AChE and BChE inhibition profiles of the compounds **4a-j** and **5a-q** were determined using the colorimetry assay method reported by Ellman et al. with certain modifications in the assay protocol [Ellman et al. 1961]. Using donepezil and rivastigmine as reference standards, the IC_{50} values of the test compounds were evaluated and their inhibitory potential against hAChE and hBChE are represented in Table 5. 9. The IC_{50} values of most of the compounds have shown hAChE and hBChE inhibition in the micromolar to the nanomolar range. As stated, the primary design features are phenyl and benzyl piperazine moieties attached to 3-NH of 1,3,4-oxadiazole-2-thione ring, and the inhibitory profiles of these derivatives were investigated here. Among them, compounds **4a, 4e, 4i,** and **4j** contain the substituted phenyl piperazine while compounds **4b, 4c, 4f,** and **4g** have substituted benzyl piperazine derivatives with different electronic properties. All the compounds show moderate hAChE inhibition relative to donepezil. Only two compounds from this series compound **4d** containing 2-pyridine ring on piperazine and **4h** containing an unsubstituted phenyl ring exhibit hBChE inhibition in the micromolar range.

The second compound series contain the N-benzylpiperidine fragment linked through sulfur via an acetamide spacer to the substituted phenyl-1,3,4-oxadiazole-thiols. A number of these compounds exhibit significant hAChE and BChE inhibition with at least two (**5d** and **5f)** showing equivalent potency to donepezil and rivastigmine. Other compounds with these dual action inhibitory properties include **5a**, **5h**, **5i**, **5m**, and **5q** all with reduced potencies. A contrasting group of compounds includes **5b, 5g,** and **5n** bearing 4-NO_2 3-Cl, 4-Cl, and 3-NO_2 groups on phenyl rings respectively which show potent hAChE inhibitory effects while lacking significant hBChE inhibition IC_{50} > 10 μM.

Table 5. 9 IC_{50} values of the compounds (**4a-j** and **5a-5q**) against hAChE, hBChE and BACE-1

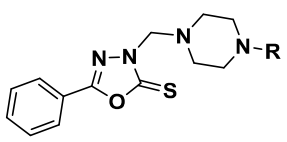

4a-j

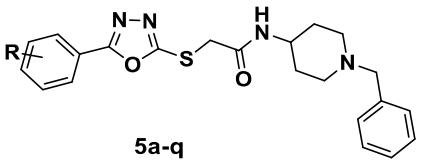

5a-q

Compound	R	hAChE IC_{50} ± SEM (μM)	hBChE IC_{50} ± SEM (μM)	*h*BACE-1 IC_{50} ± SEM (μM)	Selectivity for hAChE
4a	4-OCH_3 Phenyl	0.901 ± 0.026	>10	3.741 ± 0.046	--
4b	2-CH_3 benzyl	1.336 ± 0.019	>10	1.458 ± 0.037	--
4c	benzhydryl	0.862 ± 0.037	>10	2.365 ± 0.032	--
4d	2-Pyridine	1.072 ± 0.044	6.638 ± 0.058	2.732 ± 0.019	6.19
4e	4-NO_2 Phenyl	0.913 ± 0.020	>10	3.163 ± 0.025	--
4f	4-CH_3 benzyl	1.589 ± 0.036	>10	1.853 ± 0.023	--
4g	4-F benzyl	1.292 ± 0.041	>10	1.289 ± 0.013	--
4h	Phenyl	1.065 ± 0.029	2.746 ± 0.043	2.568 ± 0.016	2.57
4i	4-tolyl	1.574 ± 0.034	>10	3.441 ± 0.018	--
4j	4-F Phenyl	0.815 ± 0.017	>10	2.612 ± 0.046	--

5a	4-Cl	0.095 ± 0.008	1.503 ± 0.011	1.592 ± 0.014	15.63
5b	4-NO_2	0.086 ± 0.006	>10	0.410 ± 0.034	--
5c	4-OCF_3	0.287 ± 0.047	>10	0.560 ± 0.031	--
5d	3-CN	0.076 ± 0.007	1.204 ± 0.027	0.230 ± 0.011	12.53
5e	2-NO_2	0.122 ± 0.011	>10	2.741 ± 0.012	--
5f	-H	0.113 ± 0.009	1.480 ± 0.032	0.318 ± 0.009	12.28
5g	3-Cl	0.068 ± 0.008	>10	0.360 ± 0.015	--
5h	4-CF_3	0.271 ± 0.021	2.147 ± 0.044	3.323 ± 0.017	7.50
5i	2,4-di Cl	0.129 ± 0.024	5.85 ± 0.038	1.66 ± 0.028	41.34
5j	4-OH	0.188 ± 0.011	>10	2.141 ± 0.021	--
5k	4-NH_2	1.852 ± 0.039	>10	3.723 ± 0.037	--
5l	3-MeO	0.262 ± 0.017	>10	2.174 ± 0.026	--
5m	4-MeO	0.132 ± 0.019	5.741 ± 0.027	3.24 ± 0.016	44.64
5n	4-Cl, 3-NO_2	0.263 ± 0.041	>10	0.360 ± 0.008	--
5o	2, 4-di NO_2	1.113 ± 0.012	>10	1.879 ± 0.016	--
5p	2-Br	0.340 ± 0.041	>10	2.771 ± 0.011	--
5q	2,4-di OH	0.221± 0.011	1.151 ± 0.013	1.59 ± 0.021	7.61
Donepezil		0.044 ± 0.007	1.874 ± 0.024	1.241 ± 0.011	42.59
Rivastigmine		nd	1.009 ± 0.011	nd	

[a] *In-vitro* *h*AChE, *h*BChE, and *h*BACE-1 experimental data represented as the mean IC_{50} ± SEM of all the compnounds; all experiments were performed in triplicate (n = 3).

[b] *h*AChE selectivity has represented as selectivity index ratio = IC_{50} *h*BChE/ IC_{50} *h*AChE.

[c] nd = values not determined

The overall SAR of the compounds of both the series (**4a-j** and **5a-q**) against ChEs are represented in (Figure 5. 33). Generally, the unsubstituted and substituted phenyl rings of the 1,3,4-oxadiazole thiones or thiols with electron-withdrawing groups (4-Cl, 3-Cl, 4-NO_2, 3-CN) exhibit good to moderate hAChE inhibition. This property may be due to strong hydrophobic and π-π or π–cationic interaction of the phenyl ring with AChE-

PAS and CAS regions. Compounds **5d** and **5f** were selected as the best representative molecules of the present series based on their potencies in the hAChE and hBChE inhibition profiles.

5.2.3.1.2 Enzyme Kinetics study

To examine the binding mechanism for compounds **5d** and **5f** with hAChE and hBChE enzyme kinetics study was performed.

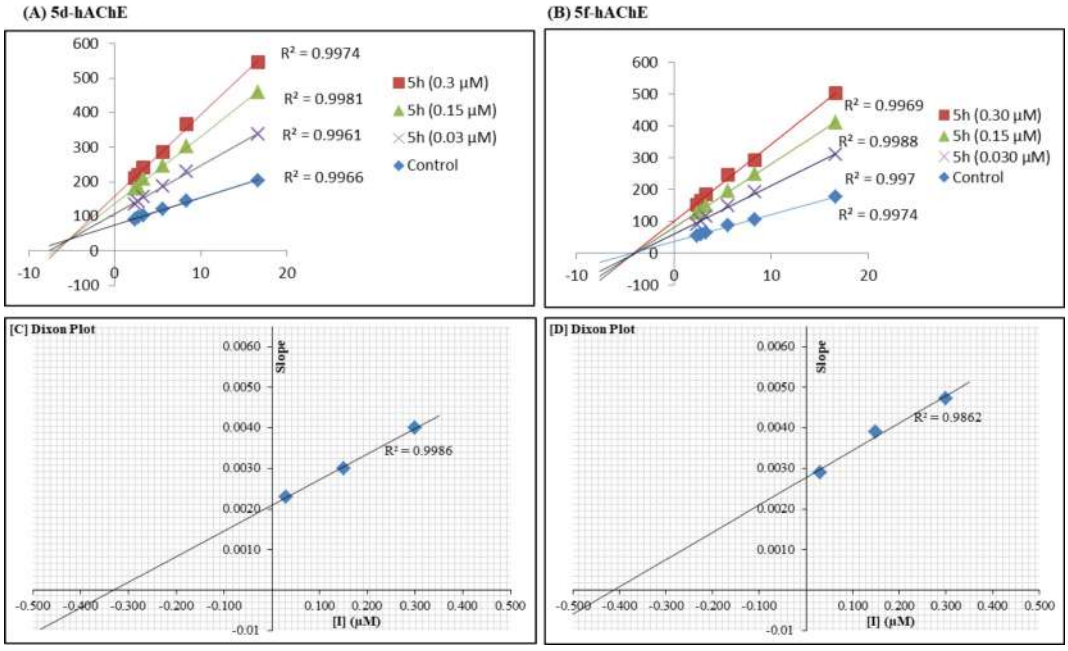

Figure 5. 32 The enzyme kinetics study of **5d** and **5f** compounds determined using Lineweaver-Burk double reciprocal plots, showing inhibition patterns A) hAChE inhibition by compound **5d** using ATCI as substrate; B) hAChE inhibition by compound **5f** using ATCI as substrate; C) Dixon plot showing dissociation constant Ki of the compound **5d**: D) Dixon plot showing dissociation constant Ki of the compound **5f**.

The Lineweaver-Burk double reciprocal plot was used to elucidate the type of inhibition by plotting initial velocity against the increasing concentration of substrate ATCI (acetylthiocholine iodide) for hAChE or BTCI (butyrylthiocholine iodide) for hBChE. The inhibition patterns are consistent with a decrease of K_m and V_{max} with the increasing concentration of **5d** and **5f** determined through the Michaelis Menten plot, consistent

with mixed type/non-competitive inhibition against hAChE (Figure 5. 32 A-B) and hBChE enzymes. Dixon plots were also constructed to determine the dissociation constant (K_i) value of the compounds **5d** and **5f** which was estimated as 0.32 μM and 0.41 μM against hAChE (Figure 5. 32 C-D).

5.2.3.1.3 Human BACE-1 (hBACE-1) Inhibition

In Table 1, the cholinesterase inhibitory properties are also compared with the BACE-1 to assess potency against a second target class (Aβ hypothesis). To investigate the multitargeting inhibitory potential of the test compounds, a FRET-based fluorometric hBACE-1 assay of the synthesized compounds was performed using donepezil (IC_{50} =1.241 ± 0.011 μM) as a reference drug. The present series of compounds were designed in such a way that they will interact with the catalytic dyad residue Asp32 and Asp228 of hBACE-1 to achieve maximum enzymatic inhibition. The *in vitro* hBACE-1 inhibition potential of the synthesized compounds **4a-j** and **5a-q** are summarized in Table 5. 9.

The 5-phenyl-1,3,4 oxadiazole-2-thione containing compounds **4a-j** all exhibit moderate inhibition of hBACE-1 within a narrow range of IC_{50} = 1.29 μM to 3.74 μM. These data suggest that the interactions with hBACE-1 are least dependent upon the aryl-piperazine substitutions. In contrast, several 5-phenyl-1,3,4 oxadiazole-2-thiol compounds exhibited promising hBACE-1 inhibition. Among them, compounds **5b, 5c, 5d, 5f, 5g,** and **5n** have shown significantly better *h*BACE-1 inhibition than that of donepezil. These *in vitro* hBACE-1 inhibition results suggest that compounds bearing electron-withdrawing groups in the 5-phenyl ring of 1,3,4-oxadiazole-2-thiol impart meaning inhibitory properties.

Compounds **5d** and **5f** hBACE-1 and cholinesterase inhibition potencies offer a chemical scaffold with properties rivaling donepezil. Based on our *in vitro* findings,

compounds **5d** and **5f** were chosen as MTDLs to be further investigated. The structure-activity relationship (SAR) of the compounds of both series against hAChE, hBChE, and hBACE-1 was established (Figure 5. 33 A-B).

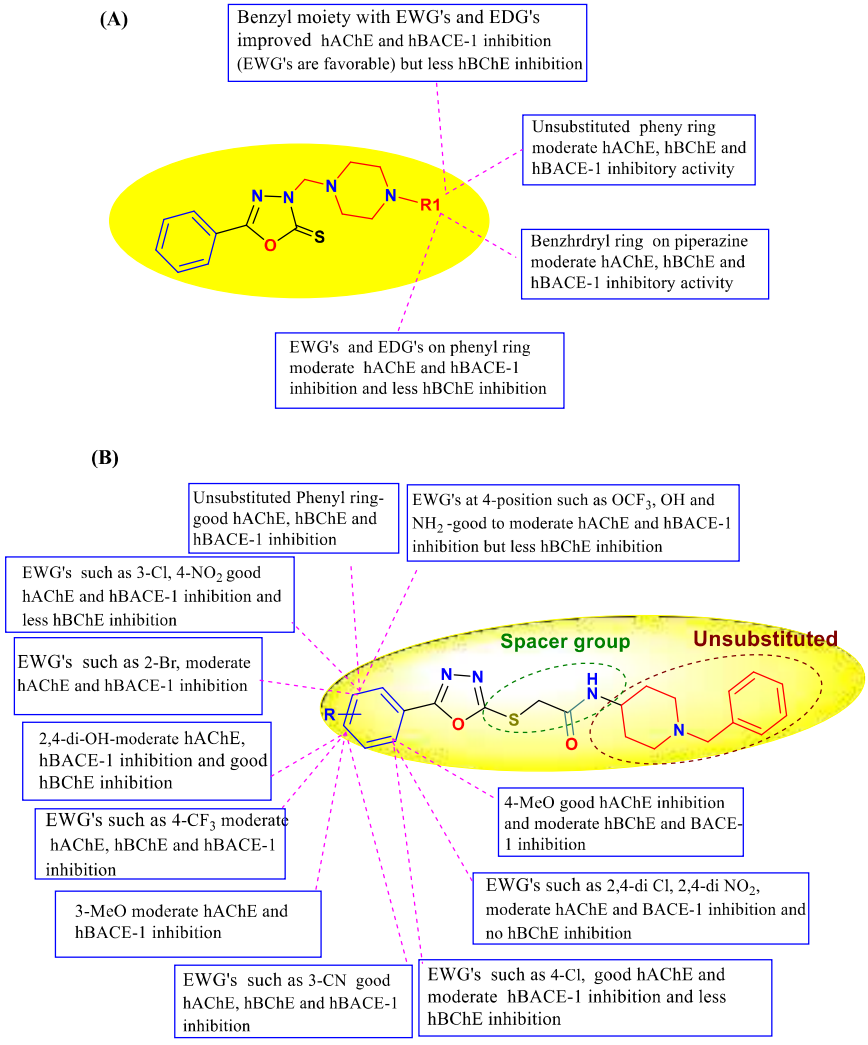

Figure 5. 33 Structure-activity relationship of the compounds **4a-j** and **5a-q**

5.2.3.1.4 Propidium Iodide Displacement assay

To investigate the potential for the selected 5-phenyl-1,3,4 oxadiazole-2-thio acetamide hAChE inhibitors to bind within the PAS region, a propidium iodide (PI) displacement assay was performed as described by Taylor et al. [TAYLOR et al. 1974]. PI is a known ligand that selectively binds with the AChE-PAS active site and shows up to 8 to 10-

fold increases in fluorescence intensity [Silva et al. 2013a]. Thus, decreases in the fluorescence intensity can measure the displacement of PI from the hAChE-PAS region. In the presence of 10 μM, 20 μM, and 50 μM concentrations of the test compounds, % PI displacement was determined. The results in Table 5. 10 indicated that compounds **5a, 5h,** and **5q** can displace ≤ PI 30%. However, for compounds **5d** and **5f** the ability to displace PI was comparable to donepezil. These findings suggest that both the compounds **5d** and **5f** have engagements of the AChE-PAS region consistent with their potencies as hAChE inhibitors.

5.2.3.1.5 PAMPA-BBB assay

The partitioning of the drugs across the Blood-brain barrier (BBB) is a major concern while developing anti-AD agents. The *in vitro* PAMPA-BBB assay method was utilized to investigate the BBB permeability of the compounds showing good *in vitro* ChE and BACE-1 inhibition [Di et al. 2003]**.**

Table 5. 10 Percentage PI displacement and PAMPA-BBB Permeability assay of selected compounds.

Compound	**PI displacement from PAS-hAChE (%)**[a]			**PAMPA-BBB permeability**	
	[I] = 10 μM	[I] = 20 μM	[I] = 50 μM	$Pe_{(exp)}$ (4.6×10^{-6} cm s^{-1})	Prediction
5a	16.459 ± 1.712	21.671± 1.254	28.358± 1.452	4.769 ± 0.029	CNS+[b]
5d	33.281 ± 1.342	40.215 ± 1.758	54.228 ± 1.282	6.137 ± 0.038	CNS+[b]
5f	29.224 ± 1.031	38.529 ± 1.317	51.331± 1.107	5.309 ± 0.021	CNS+[b]
5h	14.186 ± 1.33	19.852 ± 1.008	31.361 ± 1.563	4.929 ± 0.111	CNS+[b]
5q	10.317 ± 1.141	18.237 ± 1.271	24.775 ± 1.012	3.854 ± 0.038	CNS+[b]
donepezil	21.161 ± 1.254	28.671± 1.254	36.358± 1.752	5.928 ± 0.127	CNS+[b]

The assay involves the passive diffusion of the test compound from donor to acceptor well separated by the brain lipid membrane. The assay protocol was validated using 9 commercially available drugs to set the threshold limits (Pe > 4.7 × 10^{-6} cm s^{-1} excellent brain permeability while Pe < 1.9 × 10^{-6} cm s^{-1} poor permeability) (Figure S 5 and Table S 3). The values between threshold ranges (1.9-4.7) × 10^{-6} cm s^{-1} for particular compounds were considered to as uncertainty in BBB permeability. The PAMPA-BBB permeability results of compounds **5a**, **5d**, **5f**, **5h,** and **5q** (Table 5. 10) have suggested that all the compounds under study were excellent BBB permeable except compound **5q** which has shown uncertain BBB permeability may be due to the presence of 2-OH groups imparting hydrophilic properties to the molecule. The BBB permeability results were also co-comparable to that of the donepezil permeability.

5.2.3.1.6 Neurotoxicity studies on RA/BDNF differentiated SH-SY5Y cells

The neurotoxic liabilities of the compounds **5d** and **5f** were assessed using an MTT assay with a differentiated SH-SY5Y cell line model [Forster et al. 2016, Lingappa et al. 2021]. A two-phase differentiation methodology involving *all-trans* retinoic acid (RA) followed by brain-derived neurotrophic factor (BDNF) treatments of SH-SY5Y renders cells with more neuron-like morphology and different stressor susceptibilities. The SH-SY5Y cells were sequentially treated with RA and BDNF for 6 days to result in cell populations exhibiting long neurite networks similar to neurons. This model was deployed to assess the relative potential of **5d** and **5f** to induce cell death relative to donepezil as the standard drug in the dose range of 10- 80 μM concentration. The results of the MTT assay indicate a similar reduction in the differentiated neuroblastoma cell population at a maximum 80 μM concentration (Figure 5. 34 A). The differentiated SH-SY5Y cellular morphologies were observed by phase contrast microscopy after treatment with 80 μM donepezil, **5d,** and **5f** confirming the original

neuron-like features (Figure 5. 34 C-F). Therefore, both the compounds under investigation can be regarded as similar in safety to donepezil.

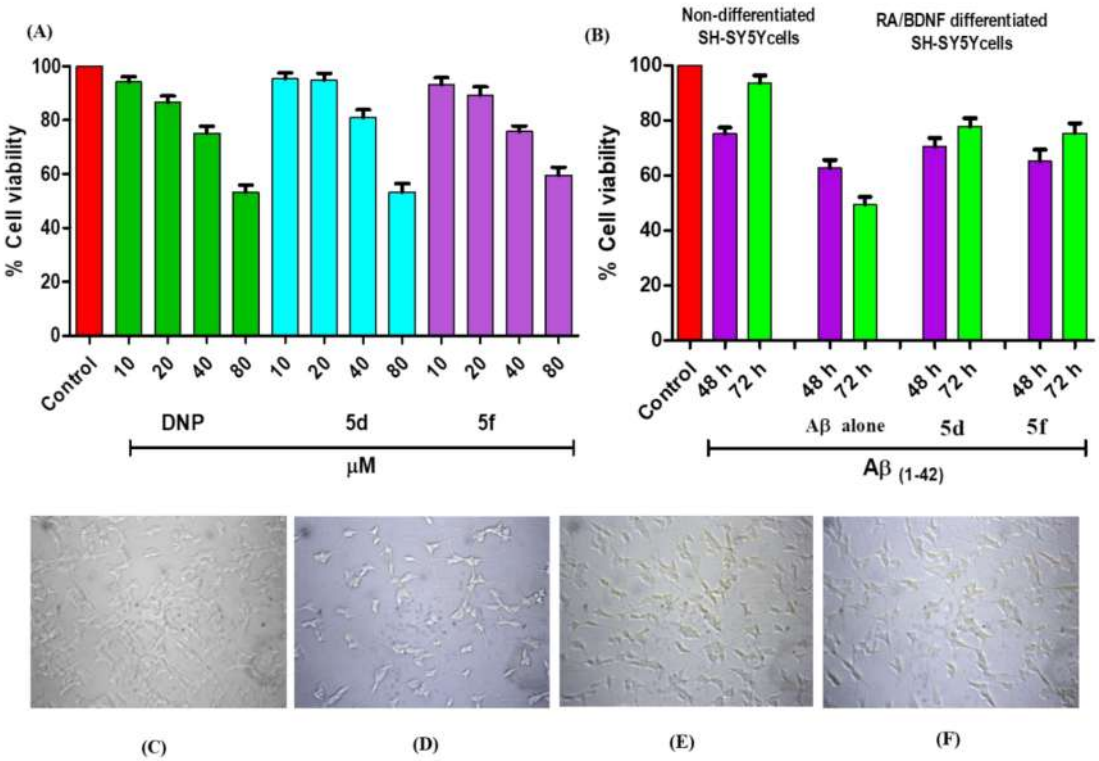

Figure 5. 34 Analysis of % cell viability and cell morphology on differentiated SH-SY5Y neuroblastoma cell lines after treatment with compounds; A) SH-SY5Y cell lines incubated with 10, 20 40, and 80 µM concentration of donepezil, **5d**, and **5f**: B) % cell viability of non-differentiated and differentiated SH-SY5Y cells incubated with $A\beta_{1\text{-}42}$ alone and **5d** and **5f** for 72 h; C) Differentiated SH-SY5Y cell lines: D) Differentiated SH-SY5Y cell lines treated with standard donepezil; E) Differentiated SH-SY5Y cell lines treated with compound **5d**; F) Differentiated SH-SY5Y cell lines treated with compound **5f.**

5.2.3.1.7 SH-SY5Y cell susceptibility to $A\beta_{1\text{-}42}$ peptides

To investigate the effect of $A\beta_{1\text{-}42}$ on the *in vitro* differentiated SH-SY5Y model, cell viability using the MTT assay was performed [More and Vince 2012]. In the presence of $A\beta_{1\text{-}42}$, the non-differentiated cells were less susceptible to a reduction in viability as compared to RA/BDNF differentiated cells [Singh et al. 2021]. The results show that $A\beta_{1\text{-}42}$ (10 µM) incubated with undifferentiated cells has a 21 % reduction in cell

viability in 48 h while after 72 h the optimum cell viability (98.83%) was observed (Figure 5. 34 B). However, A$\beta_{1\text{-}42}$ treated differentiated SH-SY5Y cells have shown a 33% reduction in cell viability after 48 h which reached to 51 % reduction after 72 h. Further, our findings suggested that the A$\beta_{1\text{-}42}$ peptide decreased the RA/BDNF differentiated SH-SY5Y cell viability as compared to non-differentiated cells in serum-free DMEM medium.

(A) (B) (C)

Figure 5. 35 Results of % cell viability assay A) SH-SY5Y cell lines incubated with 10, 20 40 and 80 µM concentration of donepezil, **5d** and **5f**: B) % cell viability of non-differentiated and differentiated SH-SY5Y cells incubated with A$\beta_{1\text{-}42}$ alone and **5d** and **5f** for 72 h; C) SH-SY5Y cells treated with A$\beta_{1\text{-}42}$; D) incubation of A$\beta_{1\text{-}42}$ treated SH-SY5Y cells with compound **5d**; E) incubation of A$\beta_{1\text{-}42}$ treated SH-SY5Y cells with **5f.** Data are displayed as mean ± SD of three independent experiments (n=3).

To explore the A$\beta_{1\text{-}42}$ treated SH-SY5Y cell rescue properties of the compounds **5d** and **5f** an MTT assay-based cell viability assay was performed. The SH-SY5Y cell lines were incubated with A$\beta_{1\text{-}42}$ (10 µM) for 24 h after which the culture medium was replaced with the medium containing compounds **5d** and **5f**. After 48 h and 72 h, an MTT assay was performed and the results suggested that the cells incubated with compounds **5d** and **5f** restored the cell viability to 70% and 65% after 48 h while the cell viability was 77% and 75 % after 72 h respectively for compounds **5d** and **5f** (Figure 5. 34 B). The morphological examination of cell viability assay suggested that the SH-SY5Y cells treated with A$\beta_{1\text{-}42}$ only have minimal neuron-like projections and enhanced cell death while the A$\beta_{1\text{-}42}$ treated SH-SY5Y cells upon incubation with

compounds **5d** and **5f** (20 μM) have an increased neuron-like projection (Figure 5. 35 A-C) and cell viability, suggesting both the compounds have anti-A$\beta_{1\text{-}42}$ aggregation potential.

5.2.3.1.8 Anti-Aβ aggregation activity

5.2.3.1.8.1 Thioflavin-T assay

Senile plaques are the important characteristics of the AD brain that result from Aβ aggregation. Aβ aggregates also disrupt molecular or cellular communication and increase memory and behavioral deficits in the AD brain [Tillement et al. 2011]. AChE-PAS active site is actively involved in the formation of Aβ aggregates and also potentiates plaque formation via large oligomer accumulation [Verma et al. 2021]. Several studies suggest that specific AChE-PAS inhibitors not only retard the AChE activity but also reduce the Aβ peptide formation. Based on the results of PI displacement assay, molecular dockings, and MD studies it was assured that **5d** and **5f** were actively bound in the AChE-PAS region; hence, they were further tested for Aβ aggregation inhibitory potential. A thioflavin-T assay based on fluorometric analysis was performed using three different ratios of the compounds **5d** and **5f**: Aβ (20:10, 10:10, and 5:10) [Levine III 1993]. Curcumin which is a known Aβ aggregation inhibitor was used as a reference standard in a self-induced experiment [Jameson et al. 2012]. The results obtained from the experiment were represented as % Aβ aggregation inhibition (Figure 5. 36 A-B) and normalized fluorescence intensity (NFI) (Figure 5. 37 A-B). Compounds **5d** and **5f** reduced Aβ aggregation in self (**5d**, 39.44-56.21% and **5f,** 36.03-59.22%) and AChE-induced (**5d**, 53.09-78.51% and **5f,** 49.15-73.98%), experiments as compared to curcumin (self 37.11-58.47%) and donepezil (self; 28.10-53.13% and AChE-induced 39.65-66.78%). The thioflavin T assay of self and AChE-induced results corroborate our *in-vitro* activity data. The self and AChE-induced anti-

Aβ aggregation experiments of both compounds exhibited anti-Aβ aggregation potential comparable to curcumin and donepezil, respectively. The Aβ aggregation inhibition potential of both compounds was also characterized through microscopic techniques.

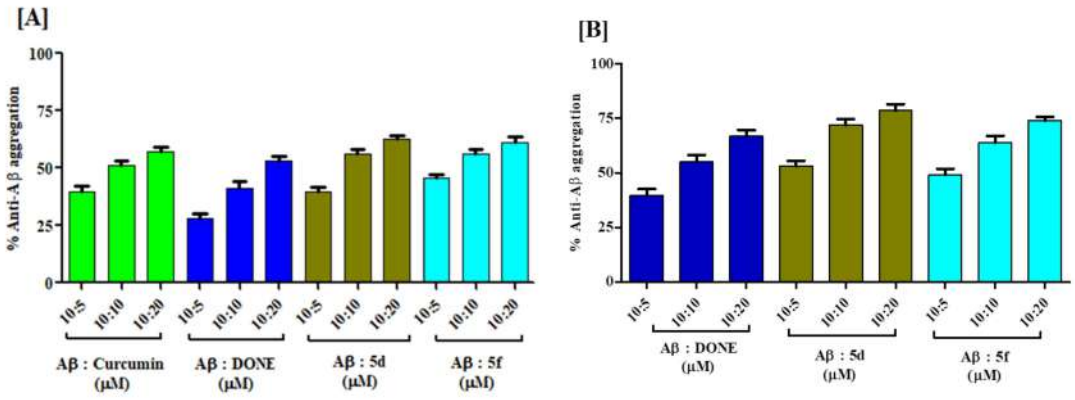

Figure 5. 36 Anti-Aβ aggregation effect of compound **5d** and **5f** compared with standard donepezil: A) self-induced % anti-Aβ aggregation experiment; B) hAChE-induced anti-Aβ aggregation experiment. Data are expressed as mean ± SEM of three independent experiments (n=3).

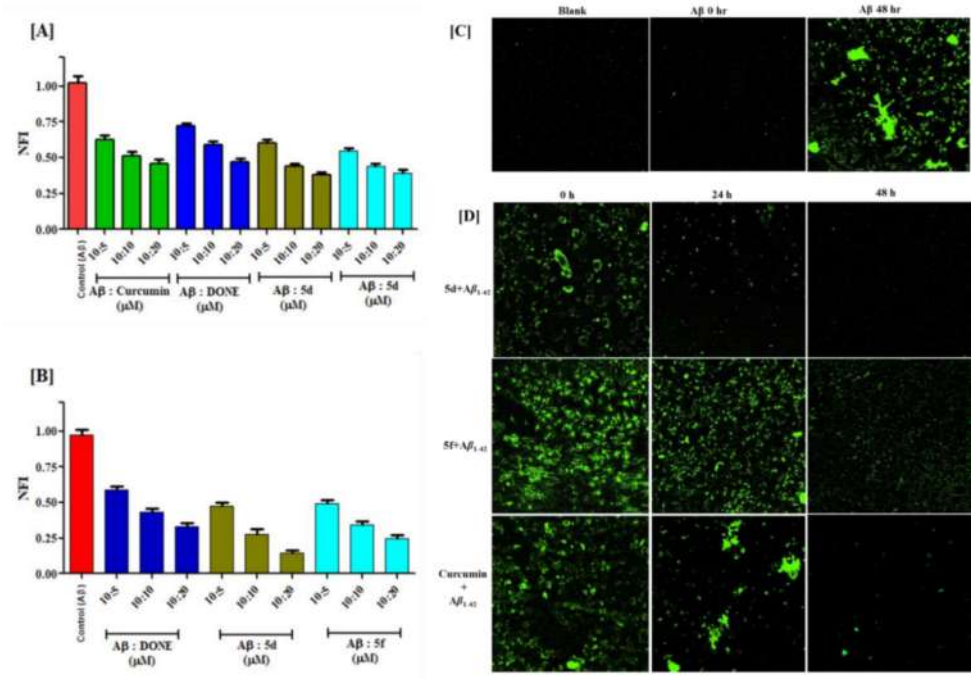

Figure 5. 37 Thioflavin T assay of compounds **5d** and **5f;** A) Self- induced Aβ aggregation B) hAChE-induced Aβ aggregation: C) Confocal microscopy images blank (PBS), Aβ (monomers) 0 h, and Aβ after 48 h (aggregates) ; D) confocal images of anti-

Aβ aggregation effects of compounds **5d**, **5f** and standard curcumin after 24 and 48 h in presence of (ThT).

The anti-Aβ aggregation properties of the compounds **5d** and **5f** were further evaluated by confocal microscopy using ThT dye. Initially, Aβ monomers treated with ThT (0 h) showed no fluorescence intensity, while Aβ aggregates (48 h incubation of Aβ monomers at room temp.) treated with ThT reached maximum fluorescence intensity (Figure 5. 37 C). Afterward, the aggregates treated with compounds **5d**, **5f,** and curcumin for 24-48 h respectively have shown a reduction in fluorescence intensity as compared to Aβ aggregates alone, suggesting that both these compounds have possibly lessened the formation of Aβ aggregates and eventually reduced the aggregates (Figure 5. 37 D) comparable to standard curcumin.

5.2.3.1.8.2 AFM and SEM anti-Aβ aggregation studies

The surface topology is a feature that can be used to determine the Aβ aggregation behavior at different time points [Sharma et al. 2019b]. To validate the inhibition of Aβ aggregation by compounds **5d** and **5f**, high-resolution topographical maps through AFM analysis were obtained. The appearances of maximum peak heights at different time intervals (days 1, 3, and 5) in the presence and absence of compounds were used to evaluate the relative effects and compared with the standard curcumin [Jiang et al. 2012, Yang et al. 2005]. The AFM images obtained suggest that the appearance of fibrils and $A\beta_{1\text{-}42}$ oligomers were highest (peak height; 1.4 μM as compared to the 800 nm of monomer) in the absence of inhibitors on day 3. Further incubation of these aggregates in the presence of compounds **5d** and **5f,** the maximum peak height of oligomers was decreased from 1.4 μM to 600 and 500 nm, respectively, while in the case of curcumin, the maximum peak height was noted from 1.4 μM to 600 nm suggesting that both compounds have comparable inhibitory effects on Aβ aggregates similar to standard curcumin (Figure 5. 38 A-B).

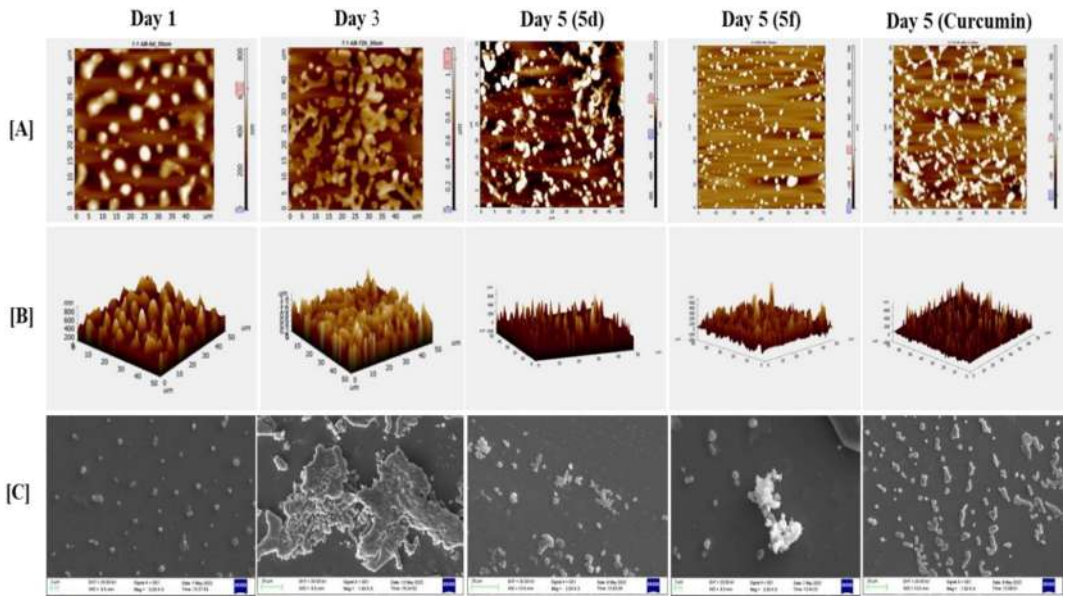

Figure 5. 38 AFM and SEM analysis of Aβ aggregation inhibition by compounds **5d, 5f,** and curcumin at different time points: A) 2D representation of AFM studies showing anti Aβ aggregation at 10 µM concentration on day 1, 3, and 5; B) 3D representation of AFM studies showing anti Aβ aggregation at 10 µM concentration on day 1, 3, and 5; C) 2D representation of SEM studies showing anti Aβ aggregation at 10 µM concentration on day 1, 3, and 5.

The morphological changes of Aβ aggregation in the presence of compounds **5d** and **5f** were also analyzed by scanning electron microscopy (SEM). The results of the SEM analysis at a 2 μM scale revealed complete A$\beta_{1\text{-}42}$ aggregation at room temperature on day 3. The Aβ aggregates after incubation with compounds **5d**, **5f,** and curcumin (10 µM) for 48 h (2 days) at room temperature showed a reduction of fibrillary aggregates into smaller size Aβ particles similar to its monomers (Figure 5. 38 C).

5.2.3.2 In vivo and ex vivo Biological studies

5.2.3.2.1 In vivo acute toxicity studies

The oral acute toxicity studies of compounds **5d** and **5f** were performed to determine their safety profile following OECD 423 guidelines in Swiss albino mice (25-30 gm). A graduated dose of up to 500 mg/kg was administered p.o. to animals in the treatment group followed by 14 days of observation for toxic or any abnormal reactions. All the

mice initially had a weight loss (5-15%) for 2-3 days which was regained thereafter and the animals also showed no signs or symptoms of toxicity over the 14 days. Subsequently, the animals were sacrificed and internal organs were subjected to histopathological examination via Hematoxylin and Eosin (H & E) staining techniques for any tissue or organ toxicity. A careful histopathological examination of the brain (hippocampus & cortex), liver, kidney, and heart was performed and suggested no tissue or organ abnormalities (Figure 5. 398). Therefore, compounds **5d** and **5f** can be regarded as safe and well-tolerated with a maximum dose of 500 mg/kg (safety margin) in the selected animal models.

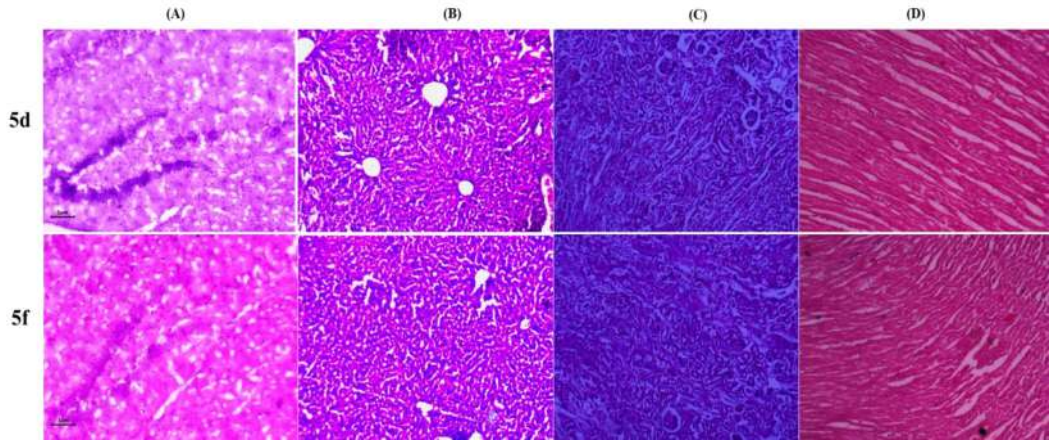

Figure 5. 39 Histopathological examination of the different animal organs via H & E staining after acute toxicity studies; A) brain tissue showing normal hippocampus and cortex; B) Liver tissue showing the presence of normal Kuepfer cells; C) Kidney tissue showing normal DCT, PCT and Glomerulus; D) Heart slice showing normal cardiac muscles.

5.2.3.2.2 Scopolamine-induced amnesia models for testing cognition enhancement in mice

Scopolamine is a cholinergic muscarinic receptor antagonist widely used drug to induce cognitive impairment in animal models [Klinkenberg and Blokland 2010]. The healthy swiss albino mice were administered oral doses of 2.5 mg, 5 mg, and 10 mg/kg of compounds **5d** and **5f**. Donepezil (5mg/kg, p.o.) was used as a positive reference, and a

scopolamine 1 mg/kg was administered to induce cognitive impairment [Uniyal et al. 2021]. Both the compounds **5d** and **5f** were assessed for learning and memory improvement in the scopolamine-induced cognitive deficit mice model.

5.2.3.2.3 Elevated plus maze test

The scopolamine-induced elevated plus maze behavioral tests were performed to assess the cognition and memory improvement in cholinergic deficit mice [Sharma and Gupta 2002]. After giving scopolamine intraperitoneally for the first three days, an elevated plus maze experiment was executed to test the mouse's spatial working memory. The 30 minutes before the scopolamine injection, treatment therapy was given, and the transfer latency and the amount of time spent in open arms were recorded. The findings were consistent with the *in vitro* investigations and indicated an anticipated reversal of dementia caused by scopolamine. In comparison to the other groups, the Naïve group (healthy control) had much lower retention transfer latency (RTL) and % initial transfer latency (% ITL) i.e. time spent on open-arm. While the scopolamine-induced (learning and memory impairment) group showed a significant (***$p < 0.001$) increased retention transfer latency (Figure 5. 40 A & D) and time spent in open arms (Figure 5. 40 B & E) as compared to the Naïve. In comparison to the scopolamine group, donepezil at a dose of 5 mg/kg showed a significant (*** $p < 0.001$) reduction in the retention transfer latency and time spent in open arms. Compounds **5d** and **5f** also significantly (***$p < 0.001$) reduced retention transfer latency and time spent in open arms (*$p < 0.05$ for 2.5 mg/kg, **$p < 0.01$ for 5 mg/kg, and ***$p < 0.001$ for 10 mg/kg) in a dose-dependent manner. Interestingly, donepezil revealed a similar statistically significant (***$p < 0.001$) change in reduced transfer latency and time spent in the open arm to that of **5d** (10 mg/kg) and **5f** (10 mg/kg) results. The time latency (in sec) results of donepezil (5 mg/kg), **5d,** and **5f** (10 mg/kg) results were also similar while both the compounds

showed significant (**p < 0.01 and ***p < 0.001) dose-dependent reduced time latency as compared to the scopolamine group (Figure 5. 40 C & F).

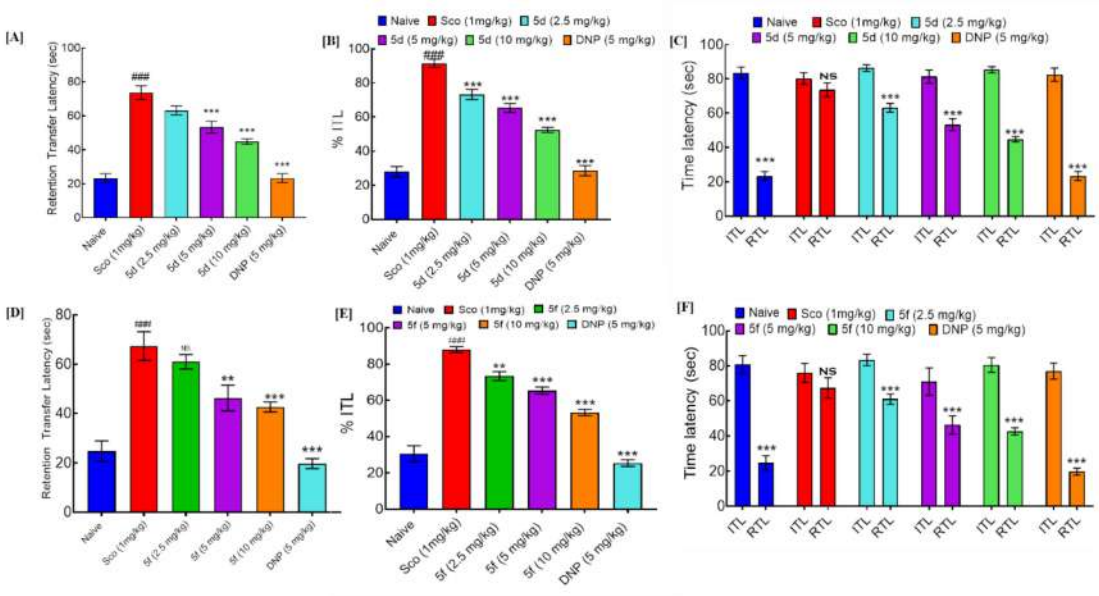

Figure 5. 40 Elevated plus maze test of compound **5d** and **5f** A) retention transfer latency of compound **5d**; B) % ITL of compound **5d;** C) Total time latency of compound **5d**; D) retention transfer latency of compound **5f**; E) % ITL of compound **5f**; F) Total time latency of compound. Data represented as mean ± SEM (n=6). ***p < 0.001, **p < 0.01, *p < 0.05 vs scopolamine; ### p < 0.001vs Naïve.

5.2.3.2.4 Ex vivo and biochemical analysis in scopolamine-induced model

The experimental animals were sacrificed via cervical dislocation post elevated plus-maze test and their brain hippocampal regions were isolated to evaluate the AChE levels and oxidative stress biomarker levels including malonaldehyde (MDA), glutathione (GSH), and nitrite.

The *ex vivo* estimation of AChE was performed using modified Ellman's method [Ellman et al. 1961]. The scopolamine-treated groups showed significantly higher rates of substrate hydrolysis or AChE levels (***p < 0.001) as compared to naïve. The animals treated with compounds **5d** and **5f** (10 mg/kg) and donepezil (5 mg/kg) had significant (***p < 0.001) decreased AChE levels or substrate hydrolysis in hippocampal and cortex brain homogenates as compared to the scopolamine-treated

group. The assay findings confirmed that the compounds **5d** and **5f** were capable to cross the BBB which resulted in reduced AChE levels. Both the compounds and donepezil have shown statistically significant (***p < 0.001) reduced AChE levels in the hippocampal and cortex brain as compared to the scopolamine-treated group (Figure 5. 41 A-B & Figure 5. 42 A-B).

The brain homogenate of the animals treated with the compounds **5d** and **5f** (10mg/kg) were used to evaluate the malonaldehyde (MDA) levels as a biomarker of lipid peroxidation which reacts under acetic conditions with thiobarbituric acid to generate a detectable thiobarbituric acid reactive substances (TBARS). Administration of scopolamine induces oxidative stress in the animals as compared to the naïve group and has shown a significant (***p < 0.001) increased level of MDA. Compound **5d** and **5f** treated group showed a gradual reduction in MDA levels in a dose-dependent manner where 10mg/kg doses showed the most significant (*** p< 0.001) decrease as compared to the scopolamine-treated group (Figure 5. 41 and Figure 5. 42 C-D). Glutathione (GSH) estimation was also performed to evaluate the generation of ROS against induced oxidative stress. The animals treated with compounds **5d** and **5f** (10 mg/kg) and donepezil (5 mg/kg) showed significant (***p < 0.001) raised in GSH levels in the brain homogenate (hippocampal and cortex) showing the reduced ROS levels as compared to scopolamine treated group, suggesting that both the compounds have the potential to engulf ROS generated in response to oxidative stress (Figure 5. 41 E-F and Figure 5. 42 E-F).

The excessive generation of NO leads to nitrite and nitrate stable products by reacting with oxygen to contribute to oxidative stress [Förstermann and Sessa 2012]. The nitrite concentrations in the brain homogenates (hippocampal and cortex) were determined using the Greiss reagent (N-(1-Napthyl) ethylenediamine) which had shown a

significant (*** $p < 0.001$) increase in NO level in the scopolamine-treated group. The animals treated with compounds **5d** and **5f** (10 mg/kg) and donepezil (5 mg/kg) have shown similar significant (***$p < 0.001$) reductions in the nitrite concentrations as compared to scopolamine treated group (Figure 5. 41 G-H and Figure 5. 42 G-H).

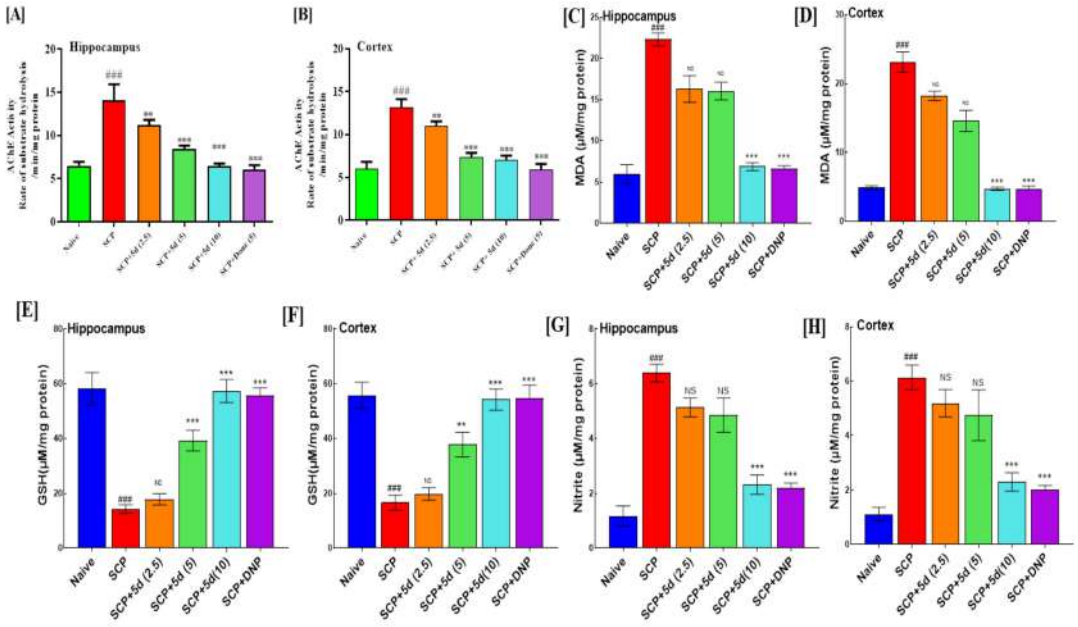

Figure 5. 41 *Ex vivo* estimation of effects of compound **5d** in scopolamine-induced mice brain hippocampus and cortex; A) & B) AChE activity estimation; C) & D) Thiobarbituric acid reactive substance (TBARS) assay to estimate MDA levels; E) & F) Glutathione (GSH) estimation to evaluate ROS generation against induced oxidative stress; G) & H) estimation of nitrite (NO) levels. Data represented as mean ± SEM (n=6). ***$p < 0.001$, **$p < 0.01$, *$p < 0.05$ vs scopolamine; $^{###}p < 0.001$vs Naïve, NS = non-significant.

The overall findings from *ex vivo* studies suggested that compounds **5d** and **5f** at 10 mg/kg doses have the potential to retard the oxidative stress induced by scopolamine. The improvement in learning and memory functions was significant (***$p < 0.001$), with promising improvements as compared to the scopolamine-treated group. Both the compounds **5d** and **5f** exhibited significant results as compared to scopolamine-treated

animals and could be regarded as equally potent as donepezil (5 mg/kg) at the described doses.

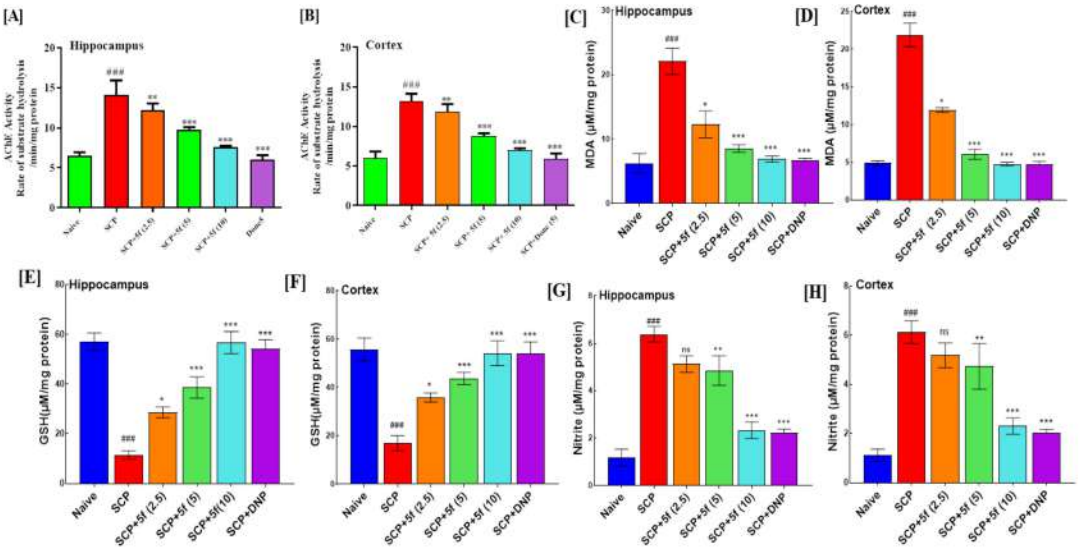

Figure 5. 42 *Ex vivo* estimation of effects of compound **5f** in scopolamine induced mice brain hippocampus and cortex; A) & B) AChE activity estimation; C) & D) Thiobarbituric acid reactive substance (TBARS) assay to estimate MDA levels; E) & F) Glutathione (GSH) estimation to evaluate ROS generation against induced oxidative stress; G) & H) estimation of nitrite (NO) levels. Data represented as mean ± SEM (n=6). ***p < 0.001, **p < 0.01, *p < 0.05 vs scopolamine; ### p < 0.001vs Naïve, ns = non-significant.

5.2.3.2.5 qRT-PCR analysis of proinflammatory cytokines (IL-1β and TNF-α)in scopolamine-induced model

The inflammatory cytokines play an important role in the development of AD. The neuroinflammatory responses as a result of Aβ-aggregation or formation of NFT trigger the microglia over-activation which results in the over-activation of proinflammatory cytokines such as IL-1β and TNF-α[Agis-Torres et al. 2014, Du et al. 2018]. The mRNA levels of IL-1β and TNF-α were measured in the hippocampal and cortex of the brain using qRT-PCR. The mRNA levels were calculated using one-way ANOVA followed by Tukey's multiple comparisons and suggested significant (***p < 0.001) effects of compounds **5d** and **5f** in comparison to the scopolamine-treated group. The

hippocampal and cortex levels of IL-1β and TNF-α suggested that both these compounds at 10 mg/kg doses are equally as potent as donepezil (5 mg/kg) dose and have shown significant (p*** < 0.001) decreased levels of proinflammatory cytokines as compared to the scopolamine control group (Figure 5. 43 A-H).

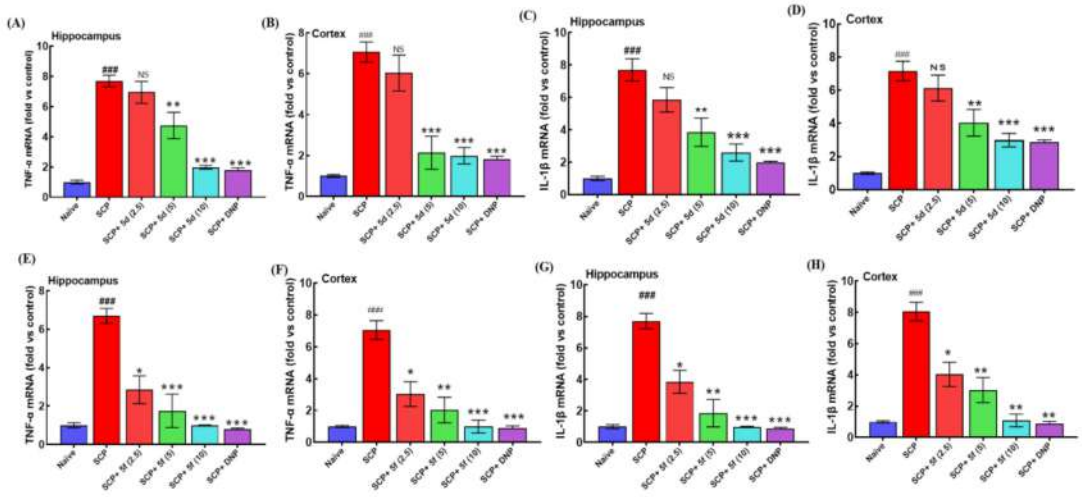

Figure 5. 43 qRT-PCR analysis of neuroinflammatory markers mRNA expression inhibition by compounds **5d** & **5f** in brain hippocampal and cortex: A) Effect of compound **5d** on TNF-α mRNA expression in the hippocampus; B) Effect of compound **5d** on TNF-α mRNA expression in Cortex: C) Effect of compound **5d** on IL-1β mRNA expression in the hippocampus: D) Effect of compound **5d** on IL-1β mRNA expression in cortex: E) Effect of compound **5f** on TNF-α mRNA expression in the hippocampus; F) Effect of compound **5f** on TNF-α mRNA expression in Cortex: G) Effect of compound **5f** on IL-1β mRNA expression in the hippocampus: H) Effect of compound **5f** on IL-1β mRNA expression in the cortex. ***p < 0.001, **p < 0.01, *p < 0.05 vs scopolamine (SCP); $^{###}$ p < 0.001vs Naïve, NS = non-significant.

5.2.3.2.6 Amyloid-β-induced water maze test

One of the most important pathophysiological processes in AD development is the aggregation and deposition of Aβ plaques. BACE-1 activity also accelerates the formation of Aβ aggregation through APP cleavage (amyloidogenic pathway)[Bloom 2014]. The Morris water maze test was used to assess anti-Aβ aggregation potential and reduction in cognitive impairment caused by compounds **5d** and **5f** in mice models after

stereotaxic intracerebrovascular (ICV) injection of Aβ (10 μM, 5 μL) to all the groups besides the sham (only surgery control group) group.

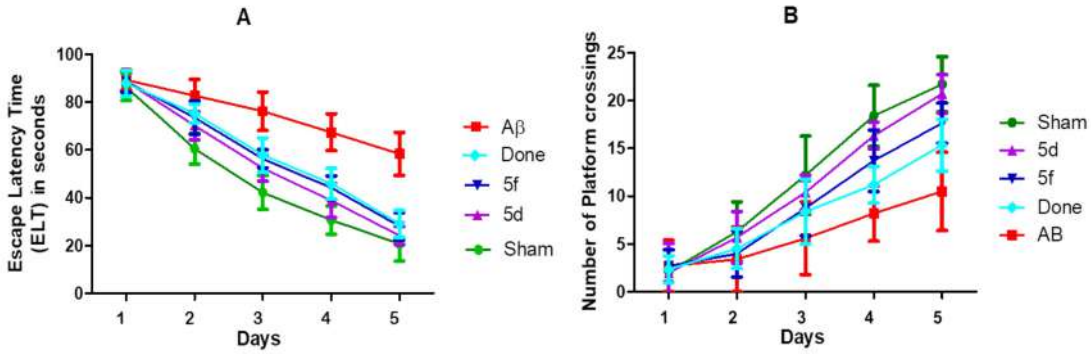

Figure 5. 44 Estimation of amelioration of Aβ-induced of cognitive deficit effects of compound **5d** and **5f** through Morris water maze test; A) escape latency time (ELT) and B) the number of total platform crossings during the last 5 days of trials. Data represented as the mean ± SEM (n=8).

The matching group of animals received treatments with **5d**, **5f,** and donepezil for nine days in a row, while the control group received vehicle. The Morris water maze test was carried out over the final five days of therapy, and the total platform crossovers were determined over 90 seconds using the escape latency time (ELT, which is the total time it takes to reach the submerged hidden platform). In the model group (Aβ diseased control) of animals during the course of 5 days, compared to the sham group, the cognitive impairment brought on by Aβ administration confirmed a large extension of ELT (Figure 5. 44 **A**), whereas total platform crossovers were noticeably decreased (Figure 5. 44 B). When compared to the model group (Aβ) of mice, the treatment with **5d** and **5f** (10 mg/kg) greatly increased total platform crossovers (Figure 5. 44 B), while it significantly decreased ELT (Figure 5. 44 **A**). Additionally, the outcomes showed that **5d** and **5f** had a marginally superior effect than donepezil (5 mg/kg) in reversing cognitive deficiency. The overall findings of behavioral investigations pointed out that

both the compounds **5d** and **5f** have anti-A*β* profiles to address learning and memory deficits at the tested dosage.

5.2.3.2.7 Western Blot Analysis of Protein expression (Aβ, Aβ/APP, BAC-1, and tau) in Aβ-induced model

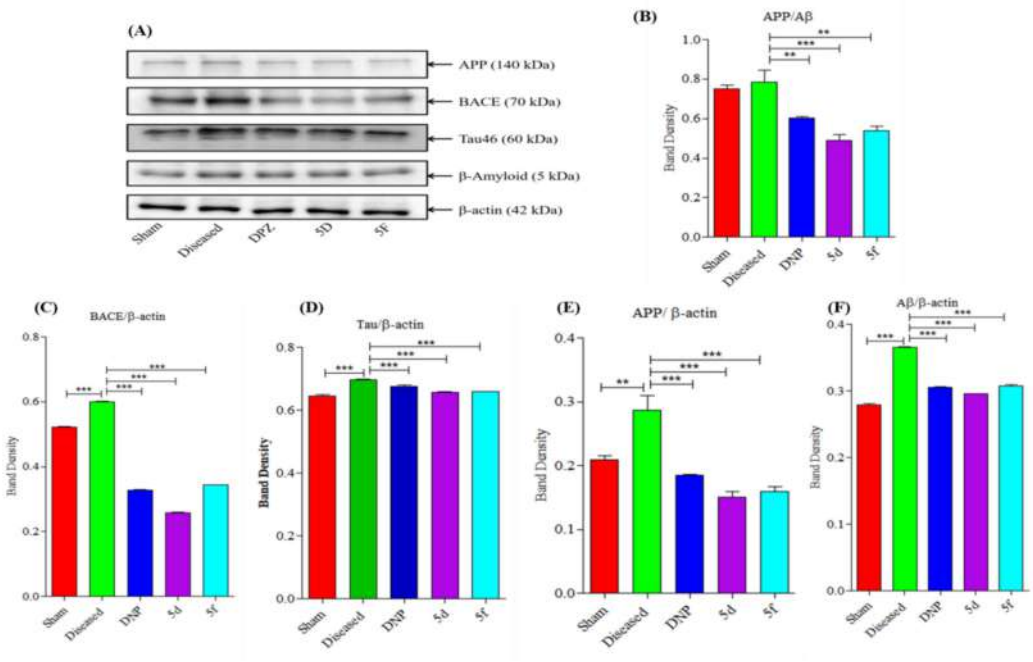

Figure 5. 45 Western blot analysis of protein expression in compound **5d** and **5f** treated mice hippocampus after ICV administration of A*β*; A) western blot representative bands, B) showing densitometric quantification APP/A*β*; C) showing densitometric quantification BACE-1; D) showing densitometric quantification tau; E) showing densitometric quantification APP; F) showing densitometric quantification A*β*. Data represented as mean ± SEM (n=3). ***p < 0.001, **p < 0.01, vs diseased.

A*β* and tau are the proteins associated with AD development and are considered to be the hallmarks of the disease progression [Tillement et al. 2011]. A*β* expression associated with the BACE-1 enzyme through APP cleavage and the expression level of tau protein in A*β* induced mice were evaluated via western blot analysis. After A*β* induced water maze tests, the mice were sacrificed and the hippocampus tissues were isolated to evaluate the BACE-1, A*β*, APP/A*β,* and tau protein expression. Our study

suggested that in the diseased group (A*β* treated group) a significant (***p <0.001) increased level of BACE-1, A*β*, APP/ A*β,* and tau were observed as compared to the sham group. The results of the treatment group for compounds **5d** and **5f** were compared with the disease (A*β)* group and found significant (**p < 0.01) attenuation in BACE-1, A*β*, APP/ A*β* and tau protein at the doses of 10 mg/kg (Figure 5. 45 A-F). The results of western blot analysis suggested that they are in accordance with our *in vitro* findings. The effects on protein expression for compounds **5d** and **5f** were also compared with the standard donepezil at 5 mg/kg dose and found significantly (p** < 0.01) better than donepezil.

5.2.3.2.8 Immunohistochemistry

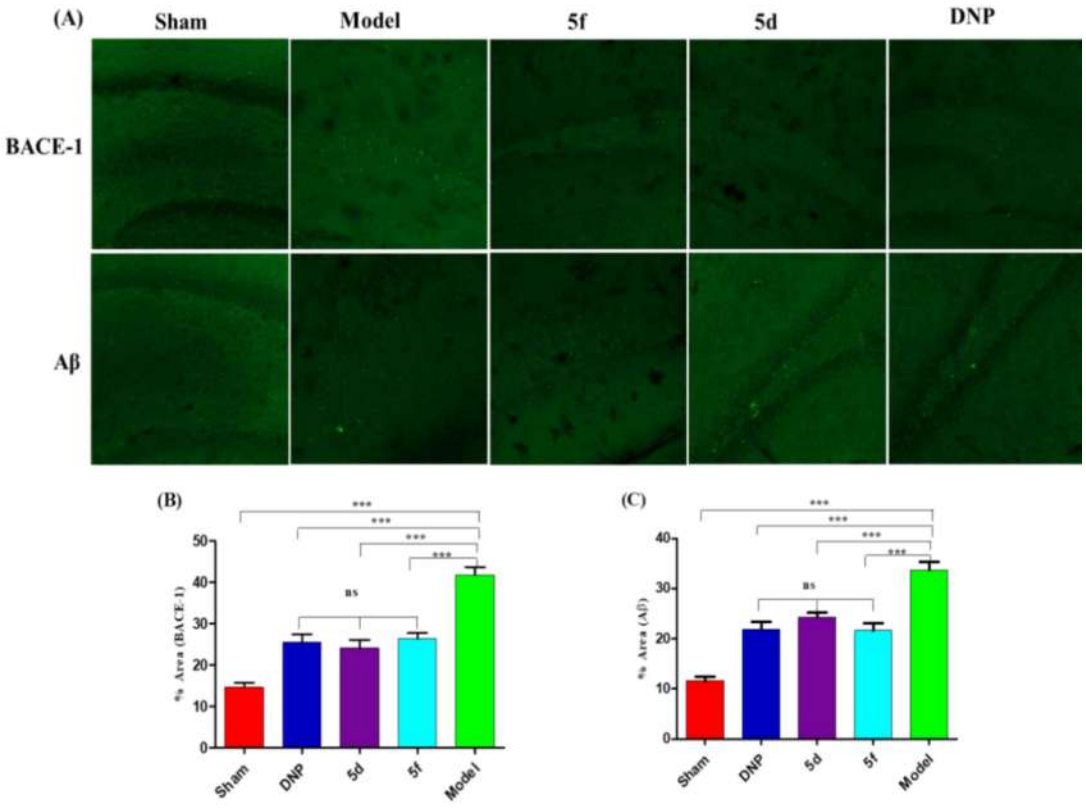

Figure 5. 46 Immunohistochemical analysis of BACE-1 and *Aβ* expression levels in the hippocampal brain; A) showing immunohistochemical expression of BACE-1 and A*β* expression effects in different animal groups; B) densitometric quantification of BACE-1 immunostains showing changes in % area (burden); C) densitometric quantification of

Aβ immunostains showing changes in % area (burden). ***p < 0.001 vs model (diseased) group, ns = nonsignificant. Data expressed as mean ± SEM (n = 3).

The expression of BACE-1 and Aβ levels in A*β* treated (ICV injection) mice was determined using the immunofluorescence method. The hippocampal region of each decapitated brain was studied to understand the expression level of the BACE-1 and Aβ in different groups of animals (Figure 5. 46 A). The results of the immunohistochemistry (IHC) suggested that the expression of both BACE-1 and A*β* was significantly (***p < 0.001) higher in the diseased (Aβ control group) group as compared to the sham group. While the expression level of both the proteins (BACE-1 and A*β*) after treatment with compounds **5d** and **5f** were significantly (***p < 0.001) lowered as compared with the diseased (model) group. The results of the IHC studies also suggested that the expression level of both BACE-1 and A*β* in **5d** and **5f** treated groups were non-significant as compared to the donepezil-treated group (Figure 5. 46 B-C).

5.2.3.2.9 Brain Tissue Histopathology in Aβ-induced model

To further examine the effects of compounds **5d** and **5f** on the histopathological changes in the mice's brain tissues, crystal violet staining was used. Histopathological examination of the animal groups of Aβ–induced water maze test revealed a significant (p < 0.001**)** reduction in neuronal population in DG, CA1 and CA3 regions (closely associated with the learning and memory functions) of A*β* treated animals as compared to the sham group of animals. While upon treatment with the compounds **5d** and **5f**, the respective group's DG, CA1, and CA3 regions have shown normal neuronal populations (non-significant (***p < 0.001**)** difference) as compared to the sham group. Similarly, the donepezil-treated group also showed a non-significant (***p < 0.001**)** difference in DG, CA1, and CA3 neuronal populations as compared to the sham group (Figure 5. 47

X-Y). The histopathological examination of the brain tissues of different animal groups suggested treatment with compounds **5d** and **5f** (10 mg/kg) and donepezil (5 mg/kg) manifests the normal structure of brain tissues and restored the Aβ-induced pathological changes as was expected. Both compounds **5d** and **5f** also protected brain tissue against Aβ-induced brain injury in different brain regions.

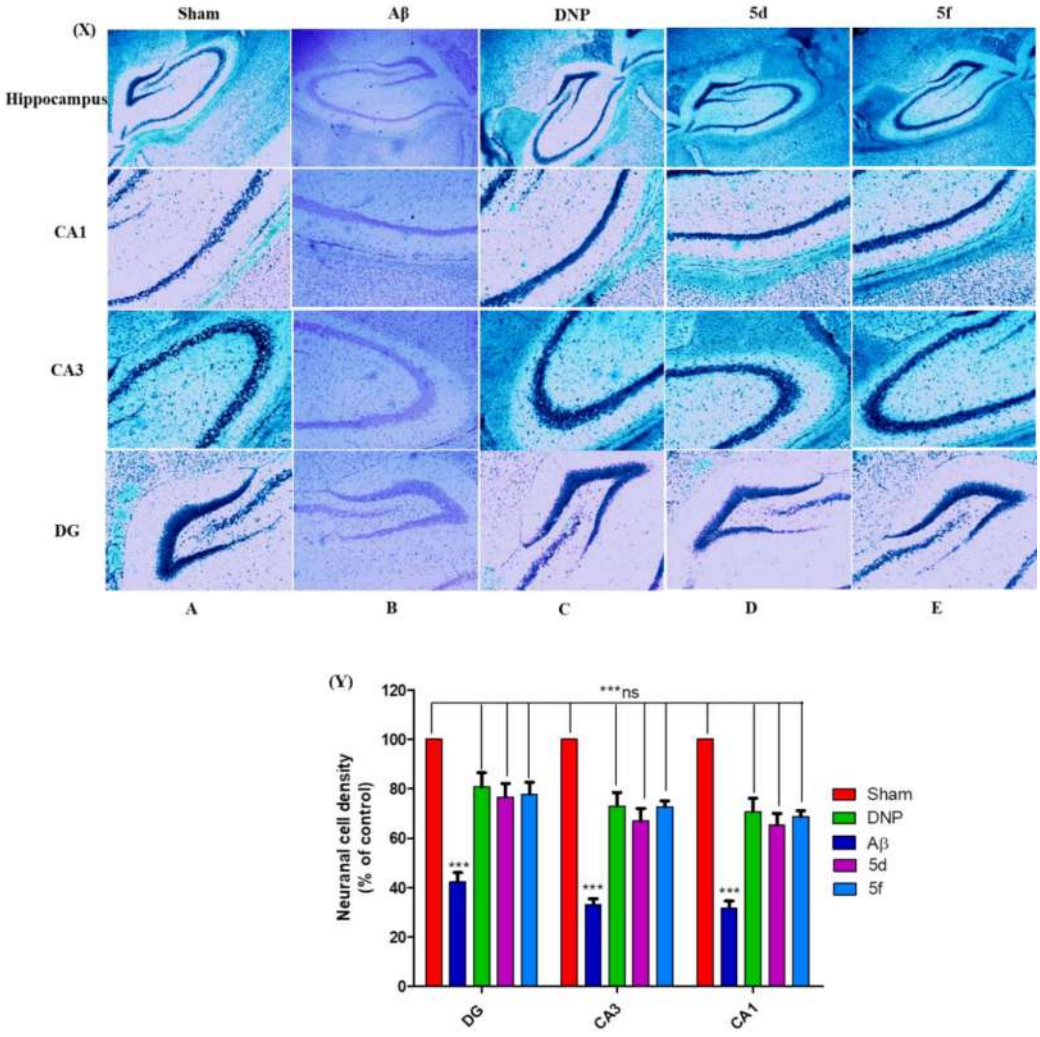

Figure 5. 47 (X) Histopathological estimation of the effects of compounds **5d** and **5f** on brain tissue via Nissl's staining after Aβ-induced Morris water maze test A) Sham group hippocampus, CA1, CA3, and DG sections; B) Aβ-induced group hippocampus, CA1, CA3, and DG sections; C) Donepezil (DNP) group hippocampus, CA1, CA3, and DG sections; D) Compound **5d** treated group hippocampus, CA1, CA3 and DG sections; E) Compound **5f** treated group hippocampus, CA1, CA3 and DG sections. (Y)

The effect of compounds **5d** and **5f** in rescuing neuronal population in Aβ-induced mice brain. The data is represented as mean ± SEM (n=3). ***p < 0.001, vs Sham, ns = non-significant.